The role of the CC chemokine CCL17 in a mouse model of Alzheimer's disease

Dissertation

zur

Erlangung des Doktorgrades (Dr. rer. nat.)

der

Mathematisch-Naturwissenschaftlichen Fakultät

der

Rheinischen Friedrich-Wilhelms-Universität, Bonn

vorgelegt von

Kim Anke Neitzert

aus

Neuwied

Bonn

Dezember 2012

Angefertigt mit Genehmigung der Mathematisch-Naturwissenschaftlichen Fakultät der Rheinischen Friedrich-Wilhelms-Universität Bonn

1. Gutachter: Prof. Dr. Andreas Zimmer
2. Gutachter: Prof. Dr. Waldemar Kolanus

Tag der Promotion: 07.05.2013
Erscheinungsjahr: 2013

Disclosure statement:

I hereby declare that I prepared this thesis entitled: "The role of the CC chemokine CCL17 in a mouse model of Alzheimer's disease" entirely by myself except where otherwise stated. All text passages that are literally or correspondingly taken from published or unpublished papers are indicated as such. All materials or services provided by other people are equally indicated.

Bremen, December, 13th 2012

Kim Neitzert

Die Vernunft drückt das Gesetz der Notwendigkeit aus, das Bewusstsein das Wesen der Freiheit.

Leo N. Tolstoi, Krieg und Frieden

Abbreviations

Aβ	Amyloid beta
AD	Alzheimer's disease
AF	AlexaFluor
APC	Allophycocyanin
APP	Amyloid precursor protein
Arg1	Arginase-1
BACE	β-site APP cleaving enzyme
BCA	Bicinchoninic acid
BDNF	Brain-derived neurotrophic factor
BM	Bone marrow
BSA	Bovine serum albumine
CD	Cluster of differentiation
CNS	Central nervous system
CR	Chemokine receptor
Ct	Cycle threshold
Cy3	Cyanine 3
DAPI	4',6-Diamino-2-phenylindole
DC	Dendritic cell
DMEM	Dulbecco's modified eagle medium
EDTA	Ethylenediaminetetraacetate

EEA-1	Early endosome antigen-1
ELISA	Enzyme-linked immunosorbent assay
FACS	Fluorescence activated cell sorter
FCS	Fetal calf serum
HRP	Horse radish peroxidase
ICL	Intracerebral leukocytes
IL	Interleukin
iNOS	Inducible nitric oxide synthetase
LN	Lymph node
LPS	Lipopolysaccharide
MARCO	Macrophage receptor with collagenous structure
M-CSF	Macrophage colony stimulating factor
MEM	Minimum essential medium
mM	Millimolar (millimol/l)
MMP-9	Matrix metalloproteinase-9
MMR	Macrophage mannose receptor
NEP	Neprilysin
PBMC	Peripheral blood mononuclear cells
PBS	Phosphate buffered saline
PCR	Polymerase chain reaction
PE	Phycoerythrin

PerCP-Cy5.5	Peridinin-chlorophyll-cyanine 5.5
PFA	Paraformaldehyde
PS1, PSEN1	Presenilin-1
RIPA	Radioimmunoprecipitation assay
RAGE	Receptor for advanced glycation end products
RPMI	Roswell Park Memorial Institute
SDS	Sodium dodecyle sulphate
SEM	Standard error of the mean
TAE	Tris acetate
TARC	Thymus and activated-regulated chemokine
TCR	T cell receptor
TE	Tris EDTA
TGF-β	Transforming growth factor
TMB	3,3',5,5'-Tetramethylbenzidine
TNE	Tris NaCl EDTA
TNF	Tumor necrosis factor
Tris	Tris(hydroxymethyl)aminomethane
qRT-PCR	Quantitative real-time PCR
v/v	Percent by volume
w/v	Percent by weight
WT	Wildtype

Contents

1 Introduction

1.1 Alzheimer's disease

Alzheimer's disease (AD) is a neurodegenerative disorder and one of the most common forms of dementia in elderly humans (50-70 % of all cases) [1]. In 1907 the german psychiatrist Alois Alzheimer published a case study about the 51 year-old woman Auguste Deter in "On an Unusual Illness of the Cerebral Cortex" ("Ueber eine eigenartige Erkrankung der Hirnrinde") [2]. In this article, he described cognitive and behavioral impairments of the patient and related these deficits with postmortem identified neurofibrils, "miliary foci" (today: amyloid plaques), and a general atrophy of the brain. Today, considered clinical symptoms are episodic memory deficits at an earlier stage, followed by an increasing confusion and memory loss during disease progression. In the later stages psychological and behavioral problems occur, such as hallucination, agitation, wandering, up to loss of body function control in the latest stage [3].

The neuropathology of AD is characterized by a severe synapse and neuronal loss, extracellular aggregated amyloid beta (Aβ) peptides (amyloid or senile plaques), and intracellular neurofibrillary tangles, which consist of hyperphosphorylated tau protein (a microtubule-associated transport protein). In Fig.1.1.a, a representative image of the typical look and distribution of plaques (brownish spots) and tangles (black tri-angled shapes) within an AD brain tissue is shown. The hippocampus is the most affected brain area by these neuropathological lesions, followed by cortical regions and others (e.g. amygdala) [1, 4]. This gradual process is accompanied by a shrinkage of cerebral cortex and an enlargement of ventricles (Fig.1.1.b) [3].

Depending on the disease onset, one can differentiate between two forms of AD. One of those is an early-onset genetically-dominated form, whereas the other one is a so-called sporadic or late-onset form. The early-onset (meaning disease onset before 60-65 years of age) is caused by autosomal-dominant mutations in Aβ generation-related genes, why it is also known as familial AD (FAD) [5]. While this form of AD is relatively rare (1 %) [1], the sporadic AD forms the majority of all cases [6]. The greatest risk factor developing AD is age, although genetic factors, e.g. mutation in APOE4 gene [6], or environmental factors are thought to play a substantial role. Several epidemiological studies considered also depression, traumatic head injury, lower education level, and risk factors associated with heart disease and stroke such as cigarette smoking, obesity, high blood pressure and high cholesterol as promotive factors [4].

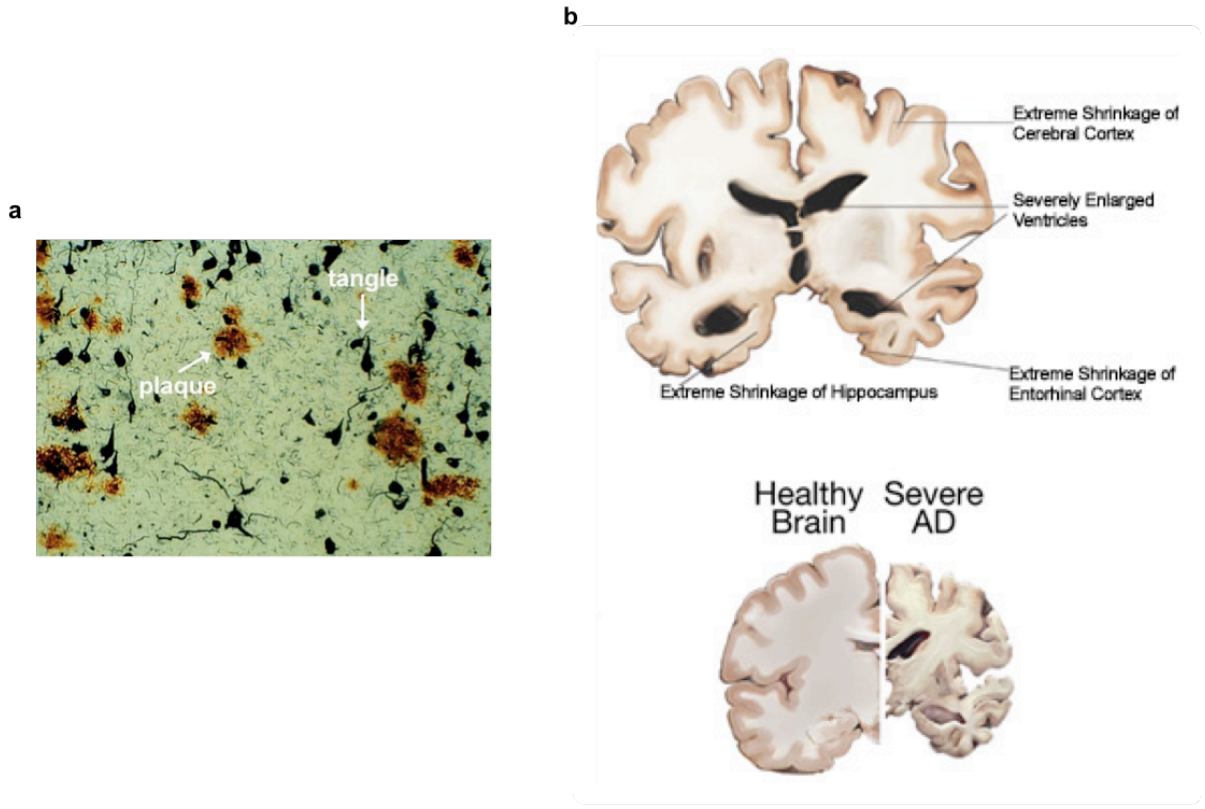

Figure 1.1: **Histopathological hallmarks of AD**
(a) Amyloid plaques (brownish spots) and neurofibrillary tangles (black triangled shapes) in a AD brain tissue. (b) Schematic view of an atrophic AD brain compared to a healthy control. Remarks are shrinking of cortex and enlargement of ventricles. Image (a) from [7] and (b) from [3].

1.1.1 APP processing and amyloid beta generation

Amyloid plaques rise from the aggregation of a proteolytic cleavage product of the amyloid precursor protein (APP). APP is a single-pass transmembrane protein of cell plasma membranes, containing a short cytoplasmic domain and a large extracellular domain. Its actual function is unknown, although studies about protein functional domain mapping considered metal binding, protease inhibition, or neurotrophic and adhesion function [8, 9]. Two different competitive degradation pathways for APP metabolism exist. At the site of plasma membrane, APP is predominantly proteolysed by α-secretases. Processing of APP by α-secretase competes with β-secretase, thus preventing the production of toxic Aβ peptides and therefore called the non-amyloidogenic cascade. Here, the proteolytic processing leads to the production of sAPPα protein and CTFα peptides (C83), as intermediates. CTFα in turn is further cleaved by γ-secretase. End products of this pathway are small non-toxic protein fragments p3 and APP intracellular domain (AICD) that do not aggregate (Fig.1.2).

Internalization of plasma membrane-bound APP into early endosomes activates the amyloidogenic pathway of APP cleavage. In early endosomes, APP is proteolytically processed by β-secretase or BACE1 (β-site APP-cleaving enzyme-1) leading to a soluble

form of APP (sAPPβ) and a membrane-fixed CTFβ (C99). This fragment is now cleaved by presenilin, the catalytic subunit of the multiprotein complex γ-secretase, releasing Aβ monomers (length 36-43 amino acids) and an AICD fragment (Fig.1.2) [8, 10, 11].

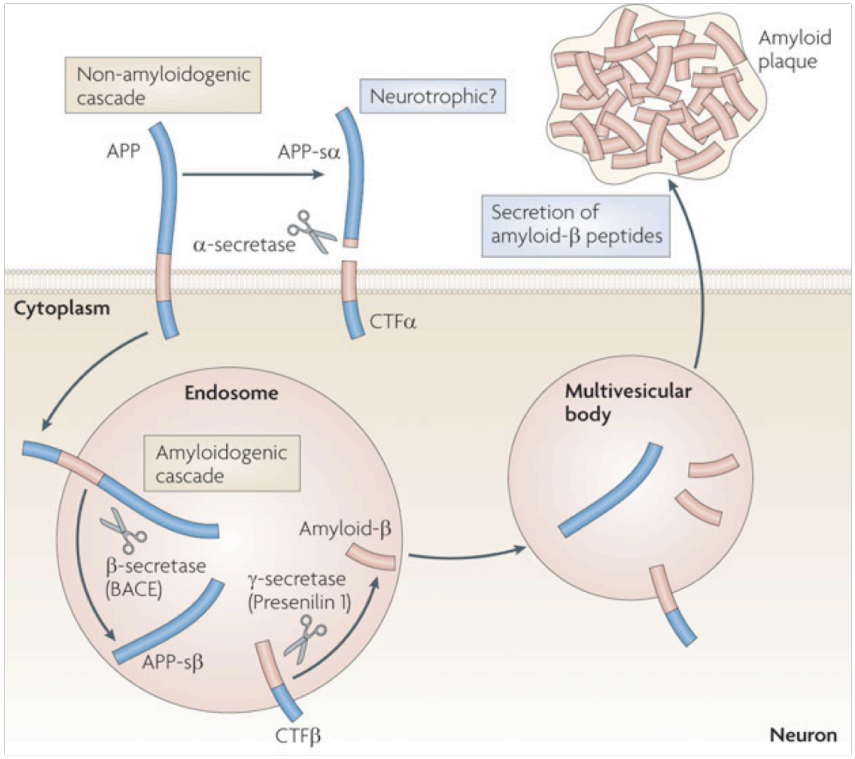

Figure 1.2: **APP processing**
Non-amyloidogenic cascade: APP processing by α-secretase produces soluble APP-sα protein and CTFα fragment. Amyloidogenic cascade: Cleavage of APP by β-secretase (BACE) results in soluble APP-sβ protein and CTFβ fragment, which is then processed by γ-secretase to toxic Amyloid-β petides. These are secreted into the extracellular space and form extracellular amyloid plaques. Image from [10].

Most of the Aβ isoforms have a length of 40 or 42 amino acids with Aβ_{42} showing the highest tendency to aggregate [12]. The aggregation is a kinetic process which starts by dimerization of Aβ monomers, formation of meta-stable oligomers (lag or nucleation phase) and protofibrils, and at last the extracellular deposition of insoluble, thermodynamically stable fibrils (elongation phase) as so-called senile plaques (Fig.1.3) [8, 10, 13].

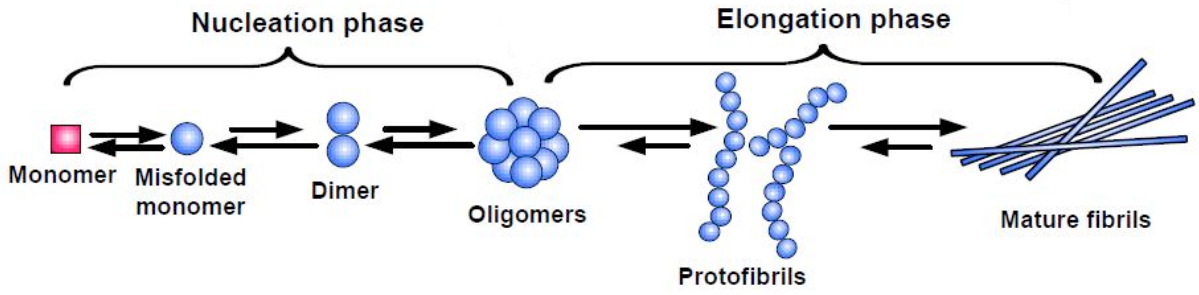

Figure 1.3: **Kinetic model of Aβ polymerization**
Formation of mature Aβ fibrils can be divided into two processes: Dimerization of misfolded Aβ monomers and formation of metastable oligomers as aggregation nuclei (nucleation phase), followed by the thermodynamically-driven formation of stable mature fibrils (elongation phase). Illustration adapted from [14].

1.1.2 Mouse models of AD

In FAD three different genes, *APP*, *PSEN1*, and *PSEN2* (which both are genes for presenilin protein), have been identified bearing autosomal mutations leading to a massive overproduction of toxic amyloid beta peptides in these patients. All commonly used transgenic mouse models of AD overexpress mutated forms of either one or more genes found in patients with FAD. In *APP*, more than 20 pathogenic mutations have been identified, most of them caused by amino acid exchange, e.g. K670D/M671L (so-called swedish mutation) or V717F (Indiana mutation). However, more than 130 mutations have been found in *PSEN1* or *PSEN2* genes, causing the majority of FAD cases [1]. Expression of different human APP mutations or PSEN1, alone or as double transgenic mouse strain, results in different phenotypes (see table 1.1). For example, the intensity of plaque development differs between 5 to 14-fold of endogenous amyloid beta expression, depending on the mutation or the promotor used in the mouse model [15, 16, 17]. Additionally, some show a higher pre-mature death rate and epileptic seizures, while others do not [1]. However, most of all existing APP/Aβ overexpressing mice show AD-like pathologies as cognitive impairment and amyloid deposition. Although apparent neuronal loss is not visible in all strains, several mouse models exhibit neuritic injuries or synaptic dysfunction [18]. Table 1.1 lists the most common mouse models for AD and their AD-like pathologies.

Table 1.1: **Expression of different APP mutations in AD mouse models and related phenotypes**
Aβ: Aβ pathology, NL: neuronal loss, SD: synaptic dysfunction, MD: memory deficits, †: pre-mature death. Table adapted from [1]

Strain	Gene	Phenotype	Reference
APP23	hAPP695swe (K670D/M671L)	Aβ, NL, MD, †	[1, 18]
Tg2576	hAPPswe	Aβ, MD, †	[1]
PDAPP	hAPPV717F	Aβ, MD	[1]
PS1 M146L	hPSEN1M146L	Aβ	[1]
APPswe(K594N/M595L) /PSEN1dE9	hAPP695swe and PSENdE9	Aβ, SD, MD, †	[17, 19]
5xFAD	APP$_{swe,Florida,London}$/ PS1(M146L,L286V)	Aβ, NL, SD, MD	[18]
3xTg	APPswe/Tau/ PS1M146L	Aβ, SD, MD	[1, 18]

1.2 Inflammatory processes in AD

The old dogma that the brain is isolated from the immune system was totally reversed after growing evidence indicated that instead there is a complex connection between both, essential for maintaining homeostasis and defense against pathogens [10, 20]. Beside the classical neuropathological hallmarks such as amyloid plaques and neurofibrillary tangles,

the presence of inflammatory response is characteristic for the AD brain. This includes the localization of complement factors in AD brains, production of pro-inflammatory cytokines or MHC class II molecules by microglia, and a general activation of microglial cells and astrocytes [21, 22]. Furthermore, long-term consuments of some non-steroidal anti-inflammatory drugs (NSAIDs) have a lower risk to develop AD [20, 23, 24]. Microglia show on the one hand a promoting effect on neurodegeneration by releasing neurotoxic factors, but on the other hand they can phagocytose Aβ, thus preventing accumulation of extracellular deposits [10, 22, 25]. Although these are inconsistent findings, it obviously strengthens the notion of an important role of the immune system in the development of AD [20].

1.2.1 Immune cells of the CNS - microglia

Physiological function of microglial cells

More than 25 years ago, it was found that microglia in an AD brain could be stained with the use of a major histocompatibility complex (MHC) class II antibody, indicating microglial cells are part of the immune system and negating the theory of an immunopriviliged status of the brain [26, 27, 28]. The term "microglia" was coined by Rio-Hortega, a student of Ramón y Cajal (nobel prize winner for physiology or medicine 1906), who classified as the first microglial cells as a third cell population within the CNS [29]. Microglial cells derive from mesenchymal myeloid progenitor cells, that migrate into the developing brain during embryogenesis, where they proliferate and develop into central nervous system (CNS)-resident microglial cells [28]. In Fig.1.4, the hematopoietic lineage of microglial precursors is depicted. Microglia originate from common myeloid progenitor cells rather than neuroectodermal or neuroepithelial progenitor cells [30]. Microglial cells, as mononuclear phagocytes of the CNS, are close related to adult tissue macrophages, such as perivascular, meningeal, or choroid plexus macrophages (Fig.1.4). As the CNS-resident macrophages, microglia are responsible for immune surveillance and debris removal during homeostasis [31]. Under physiological conditions microglia survey the environment for necrotic or apoptotic cells, pathogens, or debris of misfolded proteins and other cellular components. Encountering pathogens or other detrimental factors like Aβ peptides, microglia can undergo a morphology change, from ramified to ameboid, and possess an reactive phenotype [29].

Phagocytosis of amyloid β

In AD brains, microglia are found close to amyloid plaques [32, 33], where they present a highly activated phenotype [34]. It has been demonstrated in *in vitro* and *in vivo* studies that microglia show Aβ uptake [35, 36, 37], and that they express several Aβ receptors, such as scavenger receptors CD36 and scavenger receptor A (SRA), receptor for advanced-glycosylation end products (RAGE), as well as Aβ degrading enzymes

(matrix metalloproteinase-9 (MMP9), insulin-degrading enzyme (IDE), and neprilysin (NEP)), indicating a promoting effect in Aβ clearance [38]. Furthermore, increased microglia accumulation in some mouse [39, 40] or rat [41] models of AD reduces AD-like pathology, whereas impaired microglial accumulation accelerates Aβ deposition [42, 43]. Additionally, it was shown that cultured microglial cells on AD brain section lead to an accumulation on amyloid plaques [44].

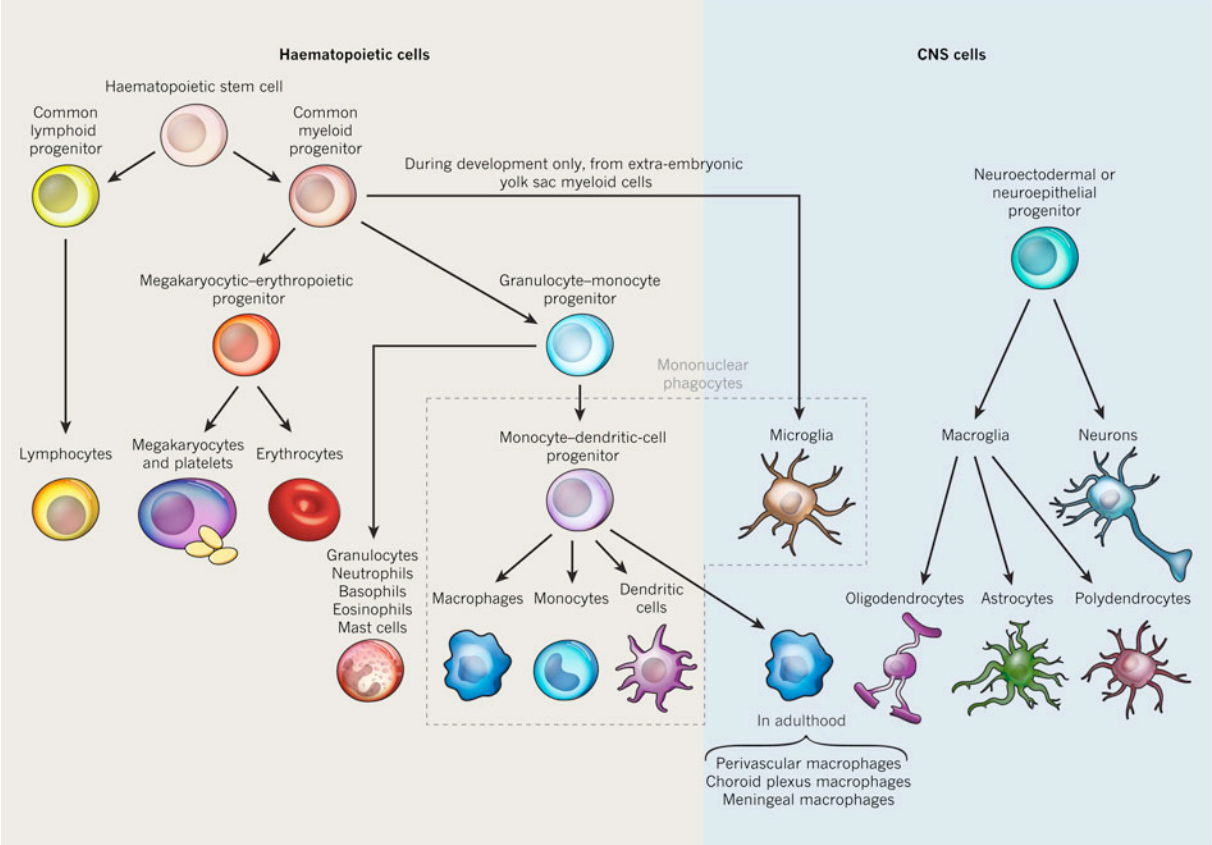

Figure 1.4: **Hematopoietic origin of microglial cells**
Shown are hematopoietic cell lineages of lymphocytes, platelets, erythrocytes, granulocytes, neutrophils, etc., and mononuclear phagocytes. CNS cells, such as neurons, oligodendrocytes, and astrocytes derive from neuroectodermal progenitor cells. Microglia, macrophages, monocytes, and DCs derive from common myeloid progenitor cells, although microglia originate only from extra-embryonic yolk sac myeloid cells during development. Image from [30].

In contrast, complete ablation of microglia in a mouse model of AD did not influence amyloid plaque progression [45], and several studies showed that microglia were unable to degrade internalized Aβ peptides, and Aβ accumulates within the cells for days or weeks [46, 47, 48]. Moreover, there is evidence that the ability of microglial Aβ clearance depends on the inflammatory phenotype of these cells. Stimulation of BV-2 microglial cells with pro-inflammatory cytokines results in a significantly decreased Aβ_{42} phagocytosis rate [49]. A reduced Aβ uptake and decreased expression of SRA and CD36 by mouse microglia after stimulation with TNF-α was also demonstrated [38]. The authors could also show that microglia isolated from old APP/PS1 mice express higher levels of IL-1β and TNF-α than young APP/PS1 mice, together with a decreased expression of Aβ degrading enzymes and receptors [38]. It has been suggested, and is called "frustrated

phagocytosis" [34, 50, 51, 52], that the inability of microglia to degrade Aβ results in a pro-inflammatory, highly reactive phenotype that eventually contributes to AD progression.

On the other hand, stimulation of microglial cells via Toll-like receptors (TLRs) 2, 4 or its co-receptor CD14, and TLR9 enhances their ability to internalize Aβ [34, 53]. TLRs are pattern recognition receptors (PRRs), that basically recognize pathogen-associated molecular patterns, e.g. lipopolysaccharides (LPS) found on bacterial cell surfaces. Cultured microglial cells lacking TLR2, TLR4, or CD14 exhibit a reduced pro-inflammatory response to Aβ stimulation [54, 55, 56]. In addition, the deficiency of TLR2 or CD14 in AD mouse models attenuates plaque deposition by modulating the inflammatory milieu [57, 58, 59]. In contrast, a loss-of-function mutation for TLR4 in APP/PS1 mice due to a C3H background, increases Aβ deposition and cognitive deficits, but reduces microglial activation in these mice [53, 60].

Activation states

Stimulation of microglia with Aβ, isolated post-mortem from AD and non-demented subjects, leads to an increased expression of IL-1β, TNF-α, IL-6, and IL-12, indicating a pro-inflammatory phenotype [61]. Combs *et al.* showed that treatment of neonatal murine microglia with Aβ, co-cultured with embryonic neurons, results in neuronal death induced by secreted TNF-α and enhanced production of reactive oxygen species (ROS) [62]. However, in analogy to macrophages, microglia exhibit different activation phenotypes possessing pro- or anti-inflammatory phenotypes [10, 20, 29, 63]. Stimulation with LPS, TNF-α, IFN-γ or IL-1β results in a classical activation or M1 phenotype, whereas stimulation with IL-4 or IL-13 leads to an alternative activation or M2 phenotype. A more precise classification also suggests a third type (acquired activation) [63] or subtypes of M2 type (M2a-c) [64, 65] activated by TGF-β and/or IL-10 stimulation.

M1 phenotype is characterized by the expression of pro-inflammatory cytokines, such as IL-12, TNF-α, IL-1β or IL-6, and Th2 cell response mediators, like MHC II, CD86, inducible nitric oxide synthase (iNOS). M2 type microglia or macrophages are characterized by enhanced expression of anti-inflammatory cytokines (IL-10) and phenotypic markers, such as macrophage mannose receptor (MMR), arginase-1 (Arg1), found in inflammatory zone-1 (Fizz1), and a reduced expression of iNOS (Fig.1.5) [64, 65, 66]. These different inflammatory phenotypes of microglia are related to either release of pro-inflammatory cytokines and production of ROS leading to neuronal cell damage or phagocytosis of Aβ and release of neurotrophic factors supporting neuronal protection [10, 67].

1.2.2 CNS-invading macrophages

Although microglia are the main mononuclear phagocyte population in the healthy CNS, since they have a slow turnover it is suggested that peripheral monocytes infiltrate the CNS by crossing the blood brain barrier (BBB) and renew the resident microglia popula-

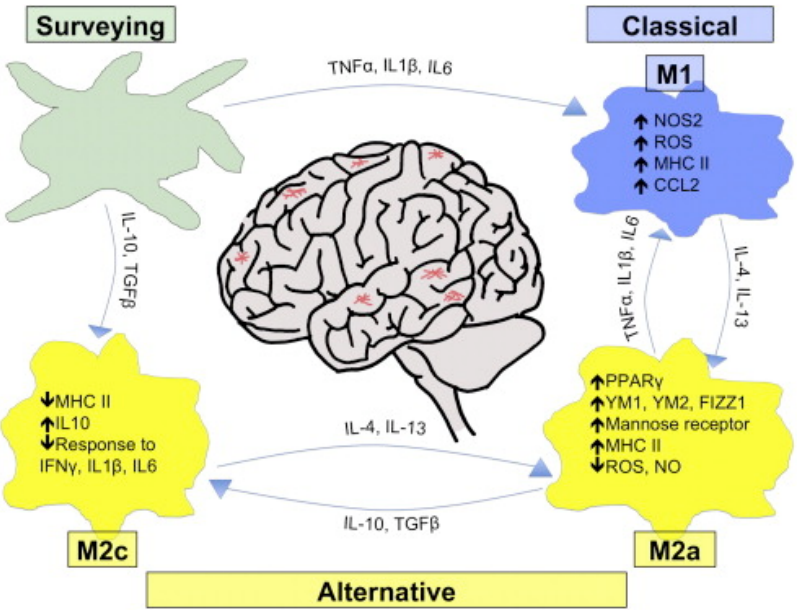

Figure 1.5: **Microglial heterogenity**
microglial cells can undergo different activation states after encountering Aβ peptides or plaques (shown in red). The surveying microglia can be stimulated with either pro-inflammatory cytokines (TNF-α, IL-1β, IL-6) leading to classical activated M1 phenotype (blue), or with anti-inflammatory cytokines (IL-10, TGFβ) resulting in alternative activated phenotypes (M2a-c, yellow). M1 cells upregulate NOS2, CCL2, and ROS production, while M2 types show reduced pro-inflammatory responsiveness, and upregulate FIZZ1, YM-1, mannose receptor or IL-10. Phenotype switching between these different states can be performed using appropriate cytokines. Image from [64].

tion [20, 34, 68]. In AD, repopulation of CNS-resident micrcoglia cells, which are potentially ineffective in Aβ clearance, by infiltrating monocytes/macrophages can contribute to a better Aβ degradation. It was shown that stimulation of cultured microglia with macrophage colony stimulating factor (M-CSF) decreases the lysosomal pH value comparable to macrophages and results in a better Aβ degradation [48]. Using GFP-expressing transplanted bone marrow (BM)-derived cells in irradiated APP mice, enhanced immigration and differentation of BM-derived microglia in response to Aβ deposits could be demonstrated [69, 70]. Further, it was shown that BM-derived microglia are essential in restricting plaque progression [40, 43, 70]. Depletion of CD11b$^+$ thymidine kinase transgenic CNS-resident microglia in APP/PS1 mice by intracerebral administration of ganciclovir shows that blood-derived microglia phagocytose Aβ [70]. The blockade of TGF-β signaling *in vitro* and *in vivo* demonstrates enhanced phagocytic ability of peripheral macrophages but not microglia, and results in the attenuation of AD-like pathology in Tg2576 mice by increased peripheral macrophage infiltration [40]. The deficiency of CD45, an important immune regulatory protein expressed by all hematopoietic cells, but not or only to a small extent by microglia, significantly increases neuronal loss and Aβ burden in an AD mouse model [43].

One major source for tissue-infiltrating specialized macrophages are BM-derived blood circulating monocytes [71]. These monocytes are characterized by and can be divided into two subclasses of either Ly6C^{high}CCR2$^+$CX3CR1$^-$ or Ly6C^{low}CCR2$^-$CX3CR1$^+$ ex-

pression [71, 72, 73]. Ly6C is possibly involved in cell differentiation [74], whereas CCR2 and CX3CR1 are classical chemokine receptors mediating cell migration [75]. Ly6C^{high} monocytes are so-called inflammatory monocytes, that infiltrate and differentiate into short-lived macrophages in inflamed tissues responsible for pathogen defense and wound healing, whereas Ly6C^{low} monocytes are thought to renew tissue-resident macrophages like Kupffer cells or microglia under physiological conditions [71]. Interestingly, El Khoury *et al.* found by using CCR2$^{-/-}$ deficient Tg2576 mice a CCR2 dosage-dependent impaired microglial accumulation and enhanced Aβ deposition in these mice [42]. Although it has been shown, that BBB leakage caused by whole body irradition prior to BM transplantion is crucial for CNS-infiltration [76], several studies demonstrated that CCR2^{+} cells are essential in Aβ clearance [77, 78] and improved cognitive impairment in APP/PS1/CCR2$^{-/-}$ non-irradiated mice [78].

1.2.3 Astrocytes, neurons, and oligodendrocytes

The most abundant cells in the CNS are astrocytes and beside microglia, they are considered to be a major source for inflammatory mediators in AD. Astrocytes accumulate in the plaque periphery [79, 80] and express high levels of glial fibrillary acidic protein (GFAP), a marker for reactive astrocytes. High expression of GFAP is linked to an increased expression of insulin-degrading enzyme (IDE), which is one of the main Aβ degrading factors [28]. Furthermore, astrocytes express several receptors, that interact with Aβ, such as RAGE, scavenger receptors (MARCO, SRA), and complement receptor C1q. High levels of CCL2, which is a chemoattractant for adult astrocytes, are found within plaques [61]. *In vitro* studies of Aβ stimulated astrocytes showed increased expression of IL-1β, TNF-α, and NO [81] as well as neuronal degeneration in co-cultures [82].

Neurons can express a number of molecules that mediate regulatory signals to microglial cells. Some of these molecules are ligands of microglia surface receptors, e.g. loss of CX3CL1 (fractalkine) - CX3CR1 (fractalkine receptor) signaling causes extensive neuronal damage due to microglia hyperactivity [83]. Likewise, interactions of CD200 - CD200R and CD47 - SIRPα downregulate microglia reactivity. Furthermore, several neuropeptides and transmitters downregulate microglial production of pro-inflammatory cytokines to prevent neuronal damage [20].

Oligodendrocytes are involved in neuronal transmission by producing myelin sheats of axons and neuroprotection. Myelin lesions have been observed in AD patients and mouse models for AD, and *in vitro* studies demonstrated Aβ toxicity for oligodendrocytes in cell culture [84].

1.3 Chemokines and chemokine receptors

Chemokines are important modulators of the innate and adaptive immune response. They were originally named by abbreviating "chemoattractant cytokines", although today they are counted as their own protein superfamily independent of the cytokine classification. Chemokines are small secreted proteins with a molecular weight between 8-14 kDa. Primarily found to be involved in cell attraction during inflammation and regulate also cell trafficking in homeostasis, they can also modulate cell activation, proliferation, adhesion and other cell processes [75]. Chemokines can be divided into four subclasses CXC, CC, XC, and CX3C depending on their primary amino acid structur. CXC, CC, and CX3C chemokines have four cysteine residues, which are either adjacent to each other (the first two in CC subclass), separated by one amino acid (CXC) or by three amino acids (CX3C). Chemokines of the XC subclass contain only two cysteine residues, that are the second and the fourth ones in the other subclasses. The cysteine residues create disulfide bonds, between the first and the third and the second and the fourth cystein residue, that are responsible for a highly conserved tertiary structure [85]. They also contain a C-terminal helix, three-stranded β-sheets (both are binding determinants), and a disordered N-terminus with 6-10 amino acids, which is the key-signaling domain.

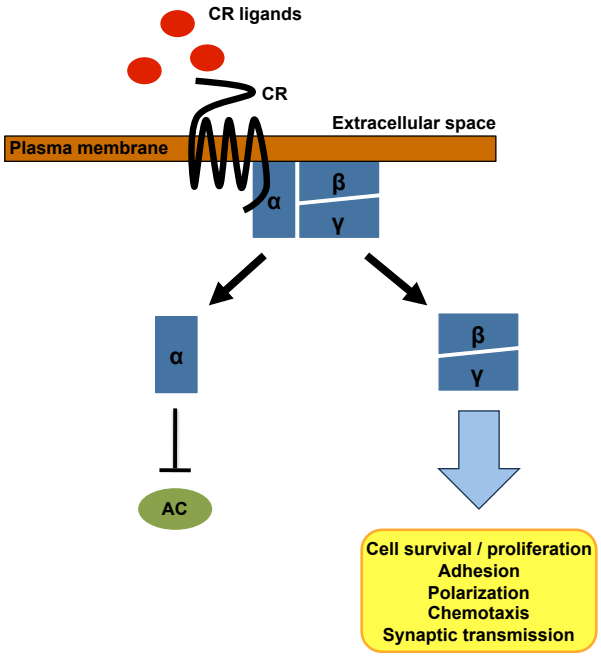

Figure 1.6: **Chemokine signaling**
After chemokine binding, the active G protein dissociates from the CR and into the subunits α and $\beta\gamma$. Activation of G proteins leads the inhibition of adenylyl cyclase and cell proliferation, survival, adhesion, chemotaxis, etc. AC: adenylyl cyclase, CR: chemokine receptor. Illustration adapted from [75].

Chemokines signal through G protein-coupled receptors (GPCR), belonging to the seven-transmembrane domain receptor superfamily. The nomenclature of chemokine receptors refers to the subclass of their chemokine ligand (e.g. CCR). Up to now, around 50 chemokines and 20 chemokine receptors are known in humans [85]. In general, GPCR

contain an extracellular N-terminal domain and an intracellular C-terminal domain and inbetween seven transmembrane domains, which are connected by three extra- and three intracellular loops. Signal transduction is mediated after a conformation change upon ligand binding via a heterotrimeric $G_{\alpha i}$ protein. After ligand-binding and receptor activation, G protein switches from an inactive GDP-bound ground state to an active GTP-bound state by nucleotide exchange. The active G protein dissociates into an α and a $\beta\gamma$ subunit leading to the initiation of several parallel running signal cascades. Gα·GTP blocks cAMP production by the inhibition of adenylyl cyclase. Cellular effects of $\beta\gamma$ signaling are proliferation, synaptic transmission, cell adhesion, chemotaxis, etc. (Fig.1.6) [75].

1.3.1 Chemokines in AD

Chemokines and their receptors are expressed in the fetal, neonatal and adult brain, so that they are involved in developing processes and homeostasis of the brain. Under physiological conditions, chemokines and their receptors can induce migration and proliferation of neuronal progenitor cells, e.g. CCL5 and CXCL12 [75]. For example, disturbances in CXCL12-CXCR4 interaction cause severe neurodevelopmental effects in mice [86].

Furthermore, chemokines are specifically up- or downregulated during pathological conditions [75]. In AD brains, several chemokines and chemokine receptors are present. CCR3, CCR5, CXCR2 and CXCR3 were found post-mortem in cortex and hippocampus of AD patients by immunohistochemical analysis [75]. CCR3 and CCR5 showed a higher expression on reactive microglia derived from AD brains in contrast to healthy controls, while CCL3 and CCL4 were found on neurons, microglia and in a subpopulation of reactive astrocytes [75]. In the cerebrospinal fluid (CSF) of some AD patients CCL2, CXCL8, and CXCL10 have been found to be increased [87, 88]. Serum CCL2 levels were also increased in patients with mild cognitive imapirments (MCI) and mild AD [89]. *In vitro* studies on astrocytes and oligodendrocytes showed that Aβ is capable to induce CCL2 (also known as MCP-1) and CCL5 (RANTES), whereas human microglia isolated from old AD and non-AD subjects express CXCL8, CCL2, CCL3, and CCL4 in presence of Aβ dose-dependently [90]. In mouse models of AD, several studies were conducted to unravel the role of chemokines and their receptors in the neuroinflammatory aspect of AD development. Using CCR5 knock out mice ($CCR5^{-/-}$), Lee *et al.* found that a deficiency in CCR5 in aged (12-18 months old) mice caused astrocytic activation, increased endogenous Aβ deposit, and severe memory functions [91]. Additionally, CCR5 ligand CCL5 activates rat microglia *in vitro* to produce nitric oxide (NO) [92]. The chemokine receptor CCR6 was found to be increased in the CNS of a triple transgenic 3xTg mouse model, but also in peripheral immune organs, such as spleen and blood [93]. Since the authors found the elevation of CCR6 in both, pre-symptomatic and symptomatic mice, they suggested a possible role of CCR6 as biomarker for AD.

Table 1.2: **Chemokine receptors and ligands found in AD**
AD: Alzheimer's disease, CR: chemokine receptor, MD: Memory deficits, PBMC: peripheral blood mononuclear cells, ↑: upregulated, ↓: downregulated.

CR or chemokine	**Site of expression**	**Effect in AD mouse models**
CCR2	microglia, astrocytes, BM-derived microglia [75, 42]	deficiency: plaques ↑, MD ↑ [42, 78]
CCR3	AD brain tissue [75]	unknown
CCR5	AD brain tissue, microglia [75]	deficiency: reactive astrocytes ↑, endogenous Aβ ↑, MD ↑
CCR6	brain, spleen, PBMC in 3xTg mice [93]	unknown
CXCR2	AD brain tissue [75]	unknown
CXCR3	AD brain tissue [75]	unknown
CX3CR1	microglia [75]	contradictory [94, 95, 96]
CCL2	CSF, serum, microglia [87, 75]	overexpression: plaques ↑, MD ↑ [97]
CCL3	neurons, microglia, astrocytes [75]	unknown
CCL4	neurons, microglia, astrocytes [75]	unknown
CCL5	astrocytes, oligodendrocytes [92]	unknown
CXCL8	CSF [88], microglia [75]	unknown
CXCL10	CSF [88]	unknown
CX3CL1	neurons [98, 99]	unknown

In contrast, investigation of CX3CL1 (fractalkine)-CX3CR1 signaling revealed a more complex role of chemokines during AD progression. Recently, it was shown that CX3CR1 deficiency reduces Aβ load in two mouse models of AD while altering microglia cytokine expression [94]. Furthermore, others showed at the same time the specific CX3CR1 knock-out in microglial cells in a mouse model of AD protects against neuronal loss [95]. However, earlier findings of *in vitro* stimulation studies of microglia activation by Aβ or LPS indicate a protective role of the CX3CR1 ligand fractalkine during microglia-mediated neuroinflammation by blocking the production of IL-6, TNF-α, and NO [98, 99]. In a different mouse model of AD it was shown that CX3CR1 knock out increases cortical IL-6 level, which correlates with cognitive deficits in these mice [96]. Chemokines and their receptors can also show opposite effects in AD pathogenesis. Overexpression of CCL2 in Tg2576 mice enhances cognitive dysfunction and accelerates Aβ deposition [97], whereas its receptor CCR2 leads to recruitment of peripheral macrophages with protective effects in an AD mouse model [42]. Table 1.2 gives an overview of chemokine receptors and their ligands found to be involved in AD.

1.4 The CC chemokine CCL17

CCL17, originally named as TARC (thymus and activation-regulated chemokine), belongs to the CC chemokine subclass. It was found in 1996 to be constitutively expressed in thymus and highly selective for T cells [100]. CCL17 is mainly expressed by mature DCs found in several lymphoid and non-lymphoid tissues [101], but it was also found in alternative activated macrophages *in vitro* upon IL-4 stimulation [102, 103], human keratinocytes and fibroblasts [104]. The chemokine receptor for CCL17 is CCR4 [105], which is expressed by Th2 cells, regulatory T cells (Treg), NK cells, DCs, basophils, and platelets, but also by macrophages [106]. An interaction of CCL17 with CCR8 has been discussed also [107], although others excluded CCL17 as chemoattractant and modulator for $CCR8^{high}$ expressing $CD4^+$ Th2 cells [108]. CCL17 is critically involved in recruitment of Th2 cells in asthma [109], and regulation of mast cell [110] and cutaneous DC migration [111] in skin diseases [112]. Further, it plays important roles in alternative cross-presentation by DCs [113], control of Treg cell homeostasis in atherosclerosis [114], and regulation of IL-23 production by $CCR4^+$ DCs causing experimental autoimmune encephalomyelitis (EAE), a mouse model for multiple sclerosis [115]. In a mouse model for HIV-1-induced neurodegeneration *ccl17* mRNA was found to be upregulated in the frontal cortex of APPswe mice after chronic Tat exposure, suggesting a potential role in neuroinflammation [116].

2 Aim of this study

The majority of people over 70 years of age in the industrial countries are affected by any dementia, and in most cases they received the diagnosis Alzheimer's disease. Up to now, no drug or other medication is available to stop this neurodegenerative process, even less to reverse this process. Inflammatory processes are critically involved by cells releasing neurotoxic or neurotrophic factors influencing survival of neurons and synapses, and thereby cognitive behavior. Several chemokines and their receptors have been shown to be upregulated in AD and play a crucial role in plaque deposition, microglia and astrocyte activation, and cognitive behavior in AD mouse models. A deeper understanding of the inflammatory mechanisms, regulated by chemokines and their receptors could give raise for potential new targets for drug development. CCL17 is an inducible chemokine, found to be upregulated under neuroinflammatory conditions in humans [117, 118] and mice [116]. By the usage of a CCL17-deficient APPswe/PS1dE9 mouse strain (APP/PS1-CCL17$^{E/E}$) a potential role of CCL17 in the pathogenesis of AD should be investigated. In the first part of the project, the behavioral phenotype of cognitive abilities and plaque progression of APP/PS1-CCL17$^{E/E}$ was assessed. In the second part of the project, the influence of APP/PS1 transgenity on CCL17 expression and the cellular source of CCL17 was analyzed. In the third part, a potential mechanism underlying the altered phenotype of APP/PS1-CCL17$^{E/E}$ was investigated. Finally, the question was addressed, whether CCL17 levels in the cerebrospinal fluid or the plasma of individuals could be used as a biomarker for AD.

3 Materials

3.1 Materials, chemicals, and buffers

3.1.1 Equipment

Analytical Balance	Sartorius BP 2100, Elk Grove, IL, USA
Apotome	ApoTome2, Zeiss, Jena, Germany
CCD camera	Axiocam MRm, Zeiss, Jena, Germany
Cell count chamber	Neubauer, CarlRoth GmbH, Karlsruhe, Germany
Cell culture dishes	Greiner Bio-one, Frickenhausen, Germany
Centrifuge	Fresco17 Zentrifuge, Heraeus and Multifuge 3SR, Heraeus, Thermo Scientific, Langenselbold, Germany
Cryostate	CM3050 S, Leica, Wetzlar, Germany
Electrophoresis apparatus	PowerPac supply, BioRad, München, Germany
Flow cytometer	FACS-Canto I, FACS-Canto II, BD Bioscience, Heidelberg, Germany
Homogenizers	Precellys® 24, Bertin Technologies, Erlangen, Germany Ultra-Turrex®, IKA Werke, Staufen, Germany Ultrasound homogenizer, Bandelin Sonoplus, Berlin, Germany
Incubator	CB210, Binder, Tuttlingen, Germany

Magnetic stirrer	MR3001, Heidolph, Schwabach, Germany
Microscope	Axioplan 2, Zeiss, Jena, Germany
PCR Cycler	7900 HAT Fast Realt-Time PCR System, Applied Biosystem, Carlsbad, CA, USA
Photometer	NanoDrop ND-1000 Spectraphotometer, Wilmington, DE, USA
Petri dishes	Greiner, Bio-one, Frickenhausen, Germany
Polyamide mesh (40 μm)	VWR International, Darmstadt, Germany
Polypropylene vials (15, 50 ml)	BD Bioscience, Pharmingen, San Diego, CA, USA
Polystyrene vials (5 ml)	BD Bioscience, Pharmingen, San Diego, CA, USA
Safe-lock vials (0.5, 1.5, 2 ml)	Eppendorf, Hamburg, Germany
SlideA-Lyzer mini dialysis cassette (3.5 kD)	Pierce, ThermoFisher Scientific, Rockford, IL, USA
Superfrost Plus® slides	Menzel-Gläser, Braunschweig, Germany
Thermo mixer	Eppendorf, Hamburg, Germany
Thermo cycler	ICycler, BioRAD, München, Germany
Tissue culture hood	HERsafe, Thermo Scientific, Langenselbold, Germany
Plate photometer	MRX TC II, Dynex Technologies, Denkendorf, Germany
24-well-plate	BD Bioscience, Pharmingen, San Diego, CA, USA

96-well-plate	Greiner, Bio-one, Frickenhausen, Germany
384-well-plate	Applied Biosystems, Carlsbad, CA, USA

3.1.2 Antibodies, chemicals, and primers

Antibodies

Table 3.1: **List of antibodies used in this study.** Abcam, Cambridge, UK; AbD Serotec, Düsseldorf, Germany; BD Pharmingen, San Diego, IL, USA; Biozol, Eching, Germany; eBioscience, Frankfurt, Germany; Invitrogen, Darmstadt, Germany; Millipore, Schwalbach, Germany; Santa Cruz Biotechnol., Heidelberg, Germany; SIGMA-Aldrich, Steinheim, Germany; Signet Laboratories, Dedham, MA; USA

1st Antibody	**Species**	**Host**	**Dilution**	**Company**
amyloid beta 6E10	human	mouse	1:1000	Signet Laboratories
β-actin	mouse	mouse	1:1000	SIGMA-Aldrich
CCR2	mouse	goat	1:20	AbD serotec
CD11b-APC	mouse	rat	1:100	eBioscience
CD11b-bio	mouse	rat	1:100	BD Pharmingen
CD11b-eFluor450	mouse	rat	1:100	eBioscience
CD11b-PE	mouse	rat	1:100	BD Pharmingen
CD11c-AlexaFluor647	mouse	hamster	1:200	Biozol
CD16/32	mouse	rat	1:300	Biozol
CD40-PE	mouse	rat	1:100	eBioscience
CD45.2-AlexaFluor647	mouse	mouse	1:100	Biozol
CD45-eFluor450	mouse	rat	1:100	eBioscience
EEA1	mouse	rabbit	1:200	Abcam
GFAP-bio	mouse	rabbit	1:100	Santa Cruz Biotechnol.
Ly6C-bio	mouse	rat	1:100	BD Pharmingen
MMR-bio	mouse	rat	1:100	Biozol
NeuN-bio	mouse	rabbit	1:100	Millipore
TCR-bio	mouse	hamster	1:200	eBioscience
2nd Antibody				
anti-goat-AlexaFluor647	goat	rabbit	1:200	Invitrogen
anti-rabbit-bio	rabbit	goat	1:200	Invitrogen
anti-rabbit-Cy3	rabbit	goat	1:300	Invitrogen
Streptavidin-APC	-	-	1:200	Biozol
Streptavidin-Cy3	-	-	1:200	Invitrogen
Streptavidin-PerCP-Cy5.5	-	-	1:200	BD Pharmingen

Cell culture stimulants & enzymes

Table 3.2: **List of cell culture stimulants & enzymes used in this study.** Peptide Specialty Companies, Heidelberg, Germany; Roche, Grenzach, Germany; R&D systems, Wiesbaden-Nordenstadt, Germany; SIGMA-Aldrich, Steinheim, Germany

Stimulant or enzyme	End concentration or dilution	Company
Amyloid beta peptide	515 nM	Peptide Specialty Companies
Collegenase (CNS)	1:10	Roche
Collegenase (LN, spleen)	1:100	SIGMA-Aldrich
DNase (CNS)	1:10	Roche
DNase (LN, spleen)	1:100	SIGMA-Aldrich
IFNγ	20 ng/ml	R&D systems
LPS	100 ng/ml	SIGMA-Aldrich
Proteinase K	0.6 % (v/v)	Roche

ELISA and assay kits

Table 3.3: **ELISA and assay kits used in this study.** BD Pharmingen, San Diego, CA, USA; eBioscience, Frankfurt, Germany; Invitrogen, Darmstadt, Germany; Linaris, Dossenheim, Germany; PerkinElmer, Rodgau, Germany; R&D systems, Wiesbaden-Nordenstadt, Germany; ThermoFisher, Rockford, IL, USA

Kit	Company
Peptide labeling kit	ThermoFisher
BCA assay	ThermoFisher
Cytofix/Cytoperm	BD bioscience
human Aβ1-40	Invitrogen
human Aβ1-42	Invitrogen
mouse CCL2 ELISA	eBioscience
human CCL17 ELISA	R&D systems
mouse IL-6 ELISA	eBioscience
mouse IL-10 ELISA	eBioscience
Perm/Wash buffer	BD bioscience
TSA Enhancer System	PerkinElmer
VectaShield DAPI	Linaris

PCR primers

Table 3.4: **Primersequences for PCR.** All PCR primers were purchased from TIBMolBiol, Berlin, Germany

Primer	Sequence
PSEN-1 (forward)	ggT CCA CTT CgT ATg CTg
PSEN-1 (reverse)	AAA CAA gCC CAA Agg TgA T
control (forward)	gTT TAA ACg TTT TCg Cgg ggg CCT gCg gTg CAT CAA g
control (reverse)	gTT TAA ACC CgC CAA TgC CCA AgA A

Taqman assays

Table 3.5: **List of Taqman gene assays used in this study.** All Taqman primer were purchased from Applied Biostystems, Carlsbad, CA, USA

Target gene	Assay ID	Cycle steps
arg1	Mm00475988_m1	40
ccl17	Mm00516136_m1	40
ccl22	Mm00436439_m1	40
ccr2	Mm00438270_m1	40
ccr4	Mm00438271_ml	45
gapdh	Mm99999915_gl	40, 45
ide	Mm00473077_m1	40
il-1β	Mm01336189_m1	40
il-6	Mm00446190_m1	40
il-10	Mm99999012_m1	40
inos	Mm00440485_m1	40
mmp-9	Mm00442991_m1	40
marco	Mm00440265_m1	40
nep	Mm00485028_m1	40
rage	Mm01134790_g1	40
tgf-β1	Mm00441724_m1	40
tnf-α	Mm00443258_m1	40
ym-1	Mm00657889_mH	40

3.1.3 Buffers and solutions

All reagents used in this work were purchased from Carl Roth (Karlsruhe, Germany), Invitrogen (Darmstadt, Germany), Merck (Darmstadt, Germany), or SIGMA-Aldrich (Steinheim, Germany). Exceptions are noted seperately.

Cell culture medium	DMEM (4.5 g/l glucose) 10 % (v/v) FCS
Digestion solutions for CNS	1:10 Collagenase (in cell culture medium) and 1:10 DNase (in cell culture medium)
Digestion solution for peripheral lymphoid tissues	Collagenase (1:100) and DNase (1:16) (in cell culture medium)
ELISA washing buffer	1x PBS 0.05 % (v/v) Tween-20
ELISA stop solution	1 M H_3PO_4
FACS buffer	1x PBS (pH = 7.2) 2 % (v/v) FCS (inactivated)
Lysis buffer	450 μl TNE buffer 50 μl 10 % (w/v) SDS 3 μl Proteinase K
Macrophage culture medium	RPMI 1640 15 % (v/v) M-CSF 10 % (v/v) FCS (inactivated) 1 % (v/v) Penicillin / Streptomycin 0.1 % (v/v) β-Mercaptoethanol
Microglia culture medium	DMEM (4.5 g/l glucose) 10 % (v/v) FCS (inactivated) 1 % (v/v) Penicillin / Streptomycin 1 % (v/v) MEM 0.1 % (v/v) β-Mercaptoethanol

Narcotic solution	5 ml Xylariem 2.5 ml Ketamin 52.5 ml 0.9 % (w/v) NaCl
Percoll gradient solutions	70 % (v/v) percoll (in cell culture medium) 30 % (v/v) percoll (in FACS buffer)
RIPA buffer	100 mM Tris (pH = 8) 150 mM NaCl 0.5 % (w/v) IPEGAL 0.2 % (w/v) SDS (prior to use: 1 tablet Complete Mini Protease Inhibitor per 10 ml buffer)
10 % SDS	100 g SDS per 1 l pH = 7.2
TAE buffer	40 mM Tris acetate 1 mM EDTA
TE buffer	10 mM Tris-HCl 1 mM EDTA pH = 7.6
TNE buffer	10 ml 1 M Tris (pH 8.0) 20 ml 5 M EDTA 2 ml 0.5 M EDTA make up to 1 l with H_2O_{milliQ}

3.1.4 Statistics

All data represent mean ± standard error of the mean (SEM). If not otherwise stated, statistical data analysis with Student's t-test or 1-way-ANOVA with Bonferroni *post-hoc* test was performed using GraphPad Prism (Version 4.0a or 5.0a, GraphPad Software Inc.). All data were analyzed by KS normality test (alpha = 0.05).

4 Methods

4.1 Mouse strains and animal housing

The APP/PS1-CCL17$^{E/E}$ mouse strain were generated by breeding APPswe (K594N/M595L)/PS1dE9 mice (C57BL/6J background, Charles River Laboratories) with CCL17-deficient mice (CCL17$^{E/E}$). CCL17$^{E/E}$ mice are homozygous for a knock-in of an enhanced green fluorescent protein (EGFP) cassette into the gene encoding region of the *ccl17* locus under the endogenous mouse *ccl17* promoter [101].

Animals were group-housed under temperature-controlled conditions with a 12 h light-dark cycle and had free access to food and water. All experiments were performed according to the German national animal care guidelines (Tierschutzgesetz Deutschland) and approved by the local committee for animal studies (Landesamt für Natur, Umwelt und Verbraucherschutz NRW).

4.2 APP/PS1 genotyping

APP/PS1 mice were bred heterozygous, for this genotyping for wt or transgene expression was needed. Tail tissue was obtained from mice 3-4 weeks after birth and incubated in 500 μl lysis buffer at 56°C overnight. DNA was extracted by adding 500 μl of phenol/chloroform/isoamylalcohol (25:24:1). After centrifugation at 13,000 rpm for 5 min the supernatant was taken and the DNA was precipitated by adding 900 μl ethanol$_{abs.}$. After centrifugation at 13,000 rpm for 5 min, the supernatant was discarded and the pellet was washed with 500 μl 70 % (v/v) ethanol and dried for 20 min. The pellet was resuspended in 200 μl TE buffer. The DNA concentration was measured at λ = 260 nm using NanoDrop spectralphotometer. Purity of DNA sample was given by a ratio of $A_{260/280nm} = 1.8$ and a ratio of $A_{260/230nm} = 2.0$. The APP/PS1 genotype was determined by polymerase chain reaction (PCR). DNA concentration was diluted to 50 - 100 ng/ml. For each sample following concentrations were used:

1 μl sample
9.5 μl H_2O
12.5 μl 2x GoTaq Green Master Mix
1 μl PSEN-1 (forward primer)
1 μl PSEN-1 (reverse primer)

The PCR product has a size of 536 base pairs (bp). DNA from wildtype mice did not produce a band, for this an internal DNA control was needed:

1 μl sample
9.5 μl H_2O
12.5 μl 2x GoTaq Green Master Mix
1 μl DNA control (forward primer)
1 μl DNA control (reverse primer)

Both reaction mixtures were run under following conditions:

Cycle 1 (1x):	Denaturation:	95°C, 5 min
Cycle 2 (40x):	I. Denaturation:	95°C, 1 min
	II. Annealing:	63°C, 1min
	III. Elongation:	72°C, 1 min
Cycle 3(1x):	Final Denaturation:	72°C, 10 min
		15°C, ∞

The samples were load on a 1 % (w/v) agarose gel, run with 120 V for 50 min, and incubated in a 0.16 % (w/v) EtBr bath for 20 min.

4.3 Behavioral phenotyping

Survival

Survival of animals was controlled every week for 6 months starting at age of 3 months. Data were analyzed using Kaplan-Meier survival curves.

Morris water maze

Performing the Morris water maze (MWM) spatial learning and memory abilities of mice can be assessed. The test consists of two tasks, the acquisition phase and the probe trial. Mice were first tested for four consecutive sessions per day over seven days (acquisition phase), and on day 8 mice were tested in one session (probe trial). During the acquisition phase a platform was hidden in a milky water bath suspension at a fixed spatial location in a target quadrant (T). All quadrants (T = target, O = opposite, L = left, R = right) were marked with four points equally distributed along the wall. On day one and two animals were placed in quadrant O for each session. From day 3 to day 7, mice were placed in O, L, R, and T in the four sessions. Escape latency for all sessions was measured. During the probe trial, the platform was removed and the time to reach the target quadrant and time spent in the target quadrant was measured.

4.4 Organ withdrawal and isolation methods

Brain removal for protein isolation and immunohistochemistry
Mice were anesthetized by i.p. injection of 500-1,000 μl narcotic solution, and afterwards fixed on a polystyrene plate lying on the back. Abdomen and thorax were opened, and the mice were transcardially perfused with 20 ml of ice-cold PBS. The skull was opened, brain was removed and cut into the hemispheres. For protein isolation, the left hemisphere was immediately snap-frozen in $N_{2(liq.)}$ and stored at -80°C. For histochemistry, the right hemisphere was fixed in 4 % (w/v) PFA overnight at 4°C, followed by an incubation in 20 % (w/v) sucrose for 4-5 h, embedded in TissueTek, and stored at -80°C.

Isolation of cortex and hippocampus
After cervical dislocation, cortex was isolated and snap-frozened in an isopentan/dry ice mixture. After the removal of the cortex the hippocampus became visible and could also be isolated and snap-frozened. Samples were stored at -80°C.

Serum preparation
Blood samples were taken from living animals by a single cut of the tail vein. Mice were pre-warmed by an infrared lamp, fixed in a small tube, and the tail vein was cut. A volume of up to 500 μl blood from each mouse was collected. The samples were stored at room temperatur for 30-60 min. After clotting the serum was clearly separated and centrifuged with 13,000 rpm for 30 min at 4°C. The supernatant was stored at -20°C.

Isolation of intracerebral leukocytes
Mice were anesthetized and perfused as described above. Brains were removed and placed in 5 cm^2 Petri dishes. Per brain, 1 ml of collagenase digestion solution was added and the brains were further minced by pipetting up and down with a syringe containing 4 ml cell culture medium. Brains were incubated at 37°C and 5 % CO_2 for 45 minutes. One ml of DNase digestion solution per dish was added and the brains were incubated again for 45 min (37°C, 5 % CO_2). After the digestion the single cell suspension was pipetted through a 100 μm filter, and the digestion solution was inhibited by diluting with cell culture medium up to 50 ml. The cell suspension was centrifuged with 15000 rpm for 7 min at 4°C and the pellet was dissolved in 20 ml of 70 % (v/v) percoll solution. 20 ml of 30 % (v/v) percoll solution was carefully added to get a two-phase density gradient system. The samples were centrifuged with 2,100 rpm for 25 min at room temperature without brake. Intracerebral leukocytes are located at the interface of the two phases and can be seen (depending on the number of cells) as a white ring. 10 ml of the interphase were placed into a fresh tube and 40 ml of cell culture medium were added. After centrifugation with 1,800 rpm for 10 min at 4°C, the pellet was dissolved in 1 ml FACS buffer for flow cytometric analysis. Cells were counted manually using a Neubauer chamber.

Isolation of peripheral blood mononuclear cells

Blood samples were taken as described above (serum preparation), but to avoid blood clotting a volume of around 500 μl blood from each mouse was collected in a 1.5 ml vial containing 20 μl heparin. 4 ml of ficoll were covered with 450 μl of blood and centrifuged with 2,000 rpm for 20 min at room temperatur without brake. Isolated mononuclear cells appeared as a white ring in the upper part of the gradient solution. 1 ml of the cell suspension was placed into a fresh tube, filled with FACS buffer up to 1.5 ml and centrifuged with 6,000 rpm for 5 min at 4°C. The pellet was resuspended in 500 μl FACS buffer, cells were counted and stained for flow cytometric analysis. Cells were counted manually using a Neubauer chamber.

Isolation of cells from spleen or lymph nodes

Mice were perfused as described above. Spleen and mesenterial lymph nodes (LN_{mes}) were isolated first. Then, parietal peritoneum was carefully separated from the abdominal wall and inguinal LN_{ing} were isolated. Axillary LN_{ax} and cervical LN_{cerv} were isolated after removal of the ambient tissue. Spleen and LN were placed into 10 and 5 cm^2 Petri dishes, minced and digested in 10 and 5 ml collagenase/DNase solution for 45 min at 37°C and 5% CO_2. Single cell suspension was made by pipetting up and down and filtering through a 100 μm filter. Cells were washed by adding ice-cold PBS up to a final volume of 50 ml, counted, and centrifuged with 1500 rpm for 7 min at 4°C. The pellet was resuspended in 1 ml FACS buffer. Cells were counted manually using a Neubauer chamber. Then, cells were stained for flow cytometric analysis.

4.5 Generation of primary mouse cell cultures

Generation of bone marrow-derived macrophages

After cervical dislocation, skin-free femur and tibia were separated and opened under cell culture-sterile conditions. Bone-marrow was flushed out with ice-cold PBS using a 10 ml-syringe, collected per mouse in a 10 cm^2 Petri dish and resuspended using a glas pipette. The single cell suspension was filtered through a 100 μm filter, cells were washed by adding ice-cold PBS up to an end volume of 50 ml, counted, and centrifuged with 1,500 rpm for 10 min at 4°C. The cell pellet was resuspended in macrophage culture medium, and placed into an uncoated 10 cm^2 Petri dish to yield a cell concentration of $1.5x10^5$/ml in 10 ml of total medium. Cells were incubated for 6 days at 37°C and 5 % CO_2. On day 3, 5 ml of freshly prepared medium were added. On day 6 cells were used for either stimulation or phagocytosis assays.

Generation of primary microglial cell cultures

Brains of 0-5 days old pups ($CCL17^{E/E}$ and WT) were dissected out, placed in ice-cold Hanks' buffer while meninges were removed. Isolated cortices were mechanically minced

to a single-cell suspension using a pipette. After centrifuging for 1,500 UpM for 5 min at 4°, cell pellets were resuspended in 1 ml neonatal microglia cell culture medium and 2-3 pups of each genotype were cultured in one cell culture flask. Cells were cultured overnight at 37°C and 8 % CO_2. On the next day, medium was changed and cells were further cultured for 2-3 weeks until a specific cell density was reached. Medium was changed every 3rd day.

4.6 Amyloid-β peptide labeling

Synthetic Aβ1-42 was labeled with DyLight^{TM}649 prior to phagocytosis assay according to manufacturer's recommendations. Afterwards, purification of Aβ-DyLight649 (4.5 kDa) from unlabeled peptide was performed by using Slide-A-Lyzer mini dialysis cassette for petides > 3.5 kDa. The Aβ-DyLight649 solution was placed into the dialysis cassette and incubated for 2 h in HBSS on a stirrer (RT, dark). Purified Aβ-DyLight649 solution was stored at -20°C before use.

4.7 Phagocytosis and stimulation assays

Cells were stimulated with LPS (100 ng/ml) for 16 h either in culture flasks or dishes. For phagocytosis, cells were seeded in 24-wells-plate (2 x 105 cells/well) and settled overnight in fresh medium before experiments. AlexaFluor649-labeled Amyloid beta (1-42) (515 nM) was let to be phagocytosed for 1 h, afterwards medium was replaced by Aβ-free medium. Chasing of Aβ degradation was done, starting from medium change at 0 h, 1 h, 3 h, and 6 h or up to 24h. Internalization of AlexaFluor649-labeled Amyloid beta (1-42) was performed within 15 min. Cells were harvested, stained, and analyzed either by flow cytometry or microscopy.

4.8 Protein isolation and quantification

Protein isolation

Frozen brains were weighed and 1 ml RIPA buffer per 150 mg brain was added. Brains were homogenized with the Ultra-Turrax for 10 s on ice, sonicated first with 1x 20 s, 30 % cycles, 100 % power, second with 1x 20 s, 60 % cycles, 100 % power, and chilled on ice for 20 min. Then the samples were centrifuged with 13,300 g for 30 min at 4°C. The supernatant was collected aliquoted in 200 μl aliquotes and stored at -80°C.

Protein quantification by BCA assay

For total protein concentration a commercial available kit was used. The BCA assay based on the biuret reaction. Bicinchoninic acid (BCA) forms in the presence of proteins and copper ions a color-intense stable complex with light-sensitivity at $\lambda = 562$ nm.

Samples were diluted 1:50 and the total protein concentration was measured following manufacturer's instructions.

Enzyme-linked immunosorbent assays (ELISA)
ELISA based on the principle of antibody-mediated detection of a specific protein in a complex matrix such as plasma, cell culture supernatants, or tissue homogenates. The concentration of the target protein is directly correlated to a light-sensitive detection signal given by enzymatically oxidized 3,3',5,5'-tetramethylbenzidine (TMB). Detection signal is measured at $\lambda = 450$ nm. Human amyloid beta 42 and 40 (hAβ42, hAβ40) were detected in brain homogenates and mouse serum following manufacturer's instructions. Serum samples were assayed undiluted, whereas for brain homogenates the dilution factor was determined individually for each aging group. For the determination of cytokines or chemokines the samples were diluted individually for each target protein and the concentration was determined according to the manufacturer's instructions.

Western blot
Right hemispheres were homogenized in 0.325 M sucrose (in PBS with phosphatase/protease inhibitor) by sonification: 20x 70 %, 20s on ice, repeated 5x, 30 min on ice inbetween. Samples were centrifuged (13.000 rpm, 45 min, 4°C) and supernatants stored at -80°C until analysis. Samples, gel electrophoresis, and western blot were performed according to manufacturer's instructions for reduced samples. For SDS-PAGE following materials or chemicals were used: 4-12 % NuPAGE Novex Bis-Tris gel, NuPAGE MES SDS running buffer and Novex Sharp Prestain Standard. Anti-human amyloid beta 6E10 (1:1000 in PBS-T (0.02 % NaN_3)) was incubated overnight at 4°C and the signal was developed using enhanced chemiluminescence (ECL). Data were analyzed by BioRad QuantityOne software.

4.9 RNA isolation and qRT-PCR

RNA isolation
RNA from organ tissue (cortex, hippocampus) was isolated using TRIzol protocoll. Samples were transferred into MagNA Lyser tubes, 800 μl TRIzol were added, and for the homogenization the Precellys homogenizator (program 2) was used. Samples were centrifuged with 11,400 rpm for 5 min at 4°C, the supernatant was transferred into a new tube, 160 μl BCP were added, and both solutions were roughly mixed for 30 s. After incubation at room temperature for 3 min, samples were centrifuged with 11,400 rpm for 10 min at 4°C. The RNA-containing phase (aqueous) was transferred into a new tube and 400 μl isopropyl alcohol were added. Samples were mixed, incubated for 10 min at 4°C, and centrifuged with 11,400 rpm for 10 min at 4°C. The RNA pellet was washed with 1 ml 75 % ethanol and centrifuged with 11,400 rpm for 5 min at 4°C three times. Pellets

were dried at 50°C for 10 min and dissolved in 20 μl RNase-free water by incubation for 20 min at room temperature. RNA concentration was measured at $\lambda_{nm} = 260$ nm using a NanoDrop spectralphotometer and samples stored at -80°C. Purity of RNA sample was given by a ratio of $A_{260/280nm} = 2$ and a ratio of $A_{260/230nm} = 2.0$.

For RNA isolation from cell culture (neonatal microglia), cells were harvested, centrifuged with 4,500 rpm for 5 min 4°C, pellets were resuspended in 800 μl TRIzol and mechanically homogenized using a pipette. Further protocol steps were similar to as described above.

Reverse transcriptase polymerase chain reaction (RT-PCR)

Complementary DNA (cDNA) from isolated RNA was made using the RT-PCR method, based on the enzymatic ability of reverse transcriptase to transcribe RNA into single-strand DNA. For the reaction mixture following conditions were used:
Starting reaction solution:

x μl RNA (= 5 μg)
y μl (= 11 - xμl) RNase-free water
1 μl OligodT
1 μl dNTP

Samples were pre-heated in a cycler using the follwing program:

65°C, 5 min	
4°C, ∞	$\Rightarrow$ add 6 μl 5x First-Strand buffer/DTT per samples
42°C, 2 min	
4°C, ∞	$\Rightarrow$ add 1 μl SuperScript II Reverse Transcriptase
42°C, 50 min	
70°C, 15 min	
4°C, 2 min	

After the reaction was completed, samples were diluted 1:6 with RNase-free H_2O to a final concentration of 42 ng/μl cDNA and stored at -20°C.

Quantitative real-time polymerase chain reaction (qRT-PCR)

Quantitative real-time PCR is a widely used method for detection of mRNA expression levels within tissues or cells. Based on the principle of common PCR, e.g. amplification of a DNA sequence by an active DNA polymerase, the amount of DNA products is tracked by a fluoresence signal. During the PCR, fluorescence-labeled gene-specific primers are degraded at their 5' end by the Taq DNA polymerase, which leads to a release of the fluorochrome from a quencher molecule. The emitted fluorescence signal is directly correlated to the initial mRNA expression level and the target cDNA within the sample. Following conditions for the reaction mixture were used:

Reaction solution:

2 μl cDNA (= 84 ng)
7 μl RNase-free water
10 μl 2x Taqman Gene Expression Master Mix
1 μl 20x Taqman Gene Expression Assay

2 μl cDNA of each sample were pipetted into a well of a 384-well plate, 18 μl of master mix were added and the plate was read in a PCR cycler by the program SDS 2.2 for relative quantification. Each sample was run in triplicates and for each gene one water control was run. Standard program conditions were as follows:

Step 1: 95°C (10 min)
Step 2 (40 cycles): 95°C (15 s), 60°C (1 min)

ΔCT values were calculated by substracting the CT values of the internal standard gene (GAPDH) and $2^{-\Delta CT}$ values were calculated.

4.10 Histochemistry and immunofluorescence

Cryo section
TissueTek-embedded frozen brains were sagitally sliced into 12 μm slices. Starting from a lateral depth of 1.92 mm to a lateral depth of 0.24 mm every second slice was taken on Superfrost microscope slides (three slices / slide). Slides were stored at -20° until staining.

Thioflavin S staining
Fibrillary proteins, such as amyloid aggregates, containing β-sheet-rich structures can be stained by either Thioflavin T (Fig. 4.1) or Thioflavin S. Thioflavin S is a mixture of benzothiazol dye isoforms. These chemical compounds exhibit a red shift of fluorescence emission by binding to amyloid fibrils [119, 120].

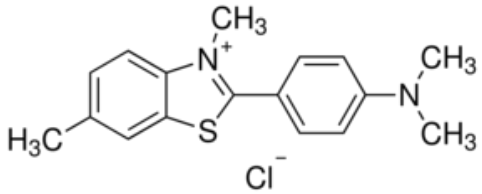

Figure 4.1: **Molecular structure of Thioflavin T**
Binding to amyloid fibrils results in enhanced fluorescent emission.

Brain slices were thawed for 5 min at 4°, washed for 5 min in PBS, and incubated in 280 ml of 0.025 % (w/v) Thioflavin S solution (1:2 EtOH/PBS). Slices were washed twice with PBS for 5 min and subsequently embedded in Fluoromount G (Southern BioTech, Birmingham, AL, USA). Cover slips were fixed with nail polish.

Immunohistochemistry

Brain slices were stained with fluorophore-labeled secondary reagents (strepatividin-Cy3 or streptavidin-APC). As primary antibodies were used: anti-GFAP-bio, or anti-NeuN-bio. Signal enhancement was performed using TSA tyramide signal amplification system in accordance with manufacturer's instructions. Endogenous peroxidases were neutralized by incubating with 1 % H_2O_2 solution (in PBS, 0.1 % NaN_3) for 30 min at RT on a stirrer. Blocking solution was incubated for 2 h at RT, followed by sequential blocking steps for avidin and biotin for 20 min each (RT, dark). Biotinylated primary antibody was incubated overnight (1:100, 4°C, dark). After incubation with streptavidin-HRP for 30 min (1:200, RT, dark), signal enhancement was performed by adding HRP substrate solution (bio-tyramide, 1:100) to slices for 8 min. Afterwards, slices were incubated with secondary antibody (streptavidin-Cy3 or -APC) for 30 min (RT, dark). Slices were washed twice with PBS for 5 min and subsequently embedded in VectaShield DAPI. Cover slips were fixed with nail polish.

Immunocytochemistry

Staining of cells from phagocytosis assay was performed in 24-well plates. Cells were fixed by incubating with 500 μl cytofix/cytoperm for 20 min on ice in the dark. After a washing step (500 μl perm/wash buffer, 5 min, on ice, dark), cells were incubated in 300 μl blocking solution (1:100 CD16/32, 10 % goat serum in perm/wash buffer) for 15 min on ice in the dark. Cells were washed and incubated in primary antibody solution (1:100 EEA1 in perm/wash buffer) for 30 min on ice in the dark. After washing, cells were incubated in a secondary antibody solution (1:300 anti-rabbit-Cy3 in perm/wash buffer) for 30 min on ice in the dark. Cells were embedded in VectaShield DAPI. Cover slips were fixed with nail polish.

Quantitative fluorescence analysis

Images of cortex (frontal, parietal, occipital) or hippocampus were taken (20x magnification) and analyzed by ImageJ 1.42q. Background was substracted, same threshold was set for all images and area fraction or mean size of particles was measured. 3-5 mice per group and 5 slices per mouse were analyzed. Z-stack pictures (63x magnification) of cells were taken and amyloid beta-positive particles within the cells were analyzed by ImageJ 1.42q. Three images of the center of cells were analyzed by ImageJ 1.42q using analyze particles mode (triplicates / mouse, three mice / group).

4.11 Flow cytometry

Sample preparation

Cells from isolation procedure (as described above) or phagocytosis assay were washed in 1 ml of FACS buffer by centrifuging with 4,500 rpm for 5 min at 4°C. The cell pellet was

resuspended in 45 μl blocking buffer (CD16/32 in FACS buffer, 1:300), and incubated for 15 min on ice. Cells were washed by adding 500 μl FACS buffer and centrifuged with 4,500 rpm for 5 min at 4°C. Cells were resuspended in 45 μl mixed primary antibody solution (1:100) and stained for cell surface markers by incubating for 15 min in the dark on ice. After a subsequent washing step, cells were incubated in 45 μl secondary antibody solution (1:200) for 15 min in the dark on ice. Cells were washed, centrifuged and resuspended in either 300 μl (intracerebral leukocytes), 500 μl (peripheral blood mononuclear cells), or 1 ml (cells from spleen or lymph nodes). Cell suspensions were filtered through a 40 μm filter into FACS tubes and measured immediately. Data analysis were performed using FlowJo 887. Absolut numbers of cell populations were calculated by multiplying the percentages with total cell numbers divided by 100.

4.12 Human samples

Cerebrospinal fluid (CSF) and plasma samples were kindly provided and collected by the Department of Psychiatry and the Department of Neurology of the University Medical Center Bonn (UKB). Samples were stored at -80°C and -20°C, respectively until measurement, thawed on ice, and human CCL17 protein concentration was determined using human CCL17/TARC ELISA following manufacturer's instructions. 50 μl of undiluted sample, standard or control were add per well. All samples were run in triplicates. Protein concentration was measured at $\lambda = 450$ nm, wavelength correction was performed at $\lambda = 570$ nm.

4.13 Integrated projects and cooperation partners

Christina Müller and Ramona Göhrs were supervised during this thesis for their medical and diploma thesis, respectively. Experiments involving NeuN staining, GFAP and CD11b immunofluorescence staining were performed by Christina Müller in the context of her medical thesis. Ramona Göhrs performed during her diploma thesis the phagocytosis assay, IL-6 and IL-10 ELISA of neonatal microglial cells. The behavioral analysis for learning and memory was performed in cooperation with Önder Albayram and PD Dr. Andras Bilkei-Gorzo. The western blot analysis of Aβ oligomers and APP expression was done in a cooperation with Ilker Karaca and Prof. Dr. Jochen Walter from the Department of Neurology, University of Bonn.

5 Results

5.1 Analysis of CCL17-deficient APP/PS1 mice

Investigation of the role of CCL17 in Alzheimer's disease was performed by crossing APPswe (K594N/M595L)/PS1dE9 mice, a common mouse model for AD [19], with CCL17-deficient mice (CCL17$^{E/E}$). Behavioral analysis was conducted in APP/PS1-CCL17$^{E/E}$ and APP/PS1 mice at 12-14 months of age (hereafter referred to as "aged" mice). Aβ progression was followed in young (four to six months), middle-aged (nine months), and aged APP/PS1-CCL17$^{E/E}$ and APP/PS1 mice. Characterization of the neuroinflammatory response was performed in aged mice, when plaque load and cognitive deficits were fully developed in APP/PS1 mice [17, 129, 130]. WT and CCL17$^{E/E}$ mice were used as AD-negative controls ("non-tg").

5.1.1 APP/PS1-CCL17$^{E/E}$ mice exhibit WT-like survival and behavioral phenotype

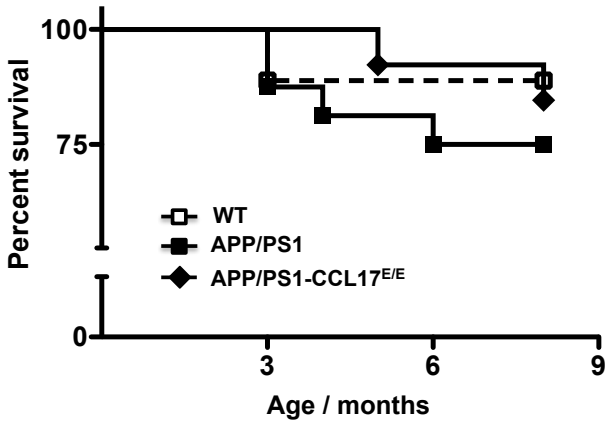

Figure 5.1: **Survival analysis of APP/PS1-CCL17$^{E/E}$, APP/PS1, and WT mice**
Diagram shows survival curves of APP/PS1-CCL17$^{E/E}$ (black squares), APP/PS1 (black quadrants), and WT (open quadrants). Each data point represents an occasion of death. Survival was controlled each week between 3 and 9 months of age. Given are Kaplan-Meier survival curves for each group. Data analysis: Log-rank (Mantel-Cox) Test. (n = 9-16 mice/-group)

It has been shown that transgenic APPswe(K594N/M595L)/PS1dE9 mice have a 35 % higher pre-mature death rate before six months of age than age-matched WT mice [129].

To test whether the defiency of CCL17 leads to an altered mortality, the survival of APP/PS1-CCL17$^{E/E}$, APP/PS1 controls and WT mice from three months to nine months of age was evaluated. As shown in Fig.5.1, APP/PS1 mice had a death rate of 25 % within this time, whereas WT mice showed a mortality rate of 11 %. Interestingly, APP/PS1-CCL17$^{E/E}$ mice had a similar (15 %) death rate like WT mice in contrast to APP/PS1 controls.

Next, the cognitive abilities of aged APP/PS1-CCL17$^{E/E}$ mice were assessed. To test whether the defiency of CCL17 in a mouse model of AD leads to an altered behavioral phenotype in cognitive performance, aged APP/PS1-CCL17$^{E/E}$, APP/PS1 as AD control, and WT controls were analyzed in Morris water maze (MWM) paradigm, a commonly used behavioral task for learning and memory [91, 131]. The MWM consists of two trials, the acquisition phase and the probe trial. During the acquisition trial mice were trained to find a hidden platform in a milky water bath (Fig.5.2.a), whereas the platform was removed from the target quadrant T (Fig.5.2.c) during the probe trial to test the memory strength. Statistical analysis revealed differences in both the acquisition task (genotype effect: $F_{2,161} = 32.13$; $p < 0.001$) and in the probe trial (quadrant-genotype interaction: $F_{6,92} = 5.028$; $p < 0.001$). In Fig.5.2.a, learning curves of APP/PS1-CCL17$^{E/E}$, APP/PS1, and WT are shown. On seven consecutive days WT mice showed an increasing learning ability as given by a continuously decreasing curve for escape latency. As expected, APP/PS1 mice had a significantly increased escape latency during this task when compared to WT. Interestingly, APP/PS1-CCL17$^{E/E}$ showed a significantly better performance in this task when compared to APP/PS1 mice , and a similar learning ability like WT mice. During the probe trial the memory strength is given by the time spent by the mouse in the target quadrant. As shown in Fig.5.2.c, WT mice spent significant more time in the target quadrant T than in the others (O = opposite, L = left, R = right). APP/PS1-CCL17$^{E/E}$ mice showed a comparable memory strength like WT, whereas normal APP/PS1 mice had no preference to any quadrant. Differences in swim speed could not be detected in all mouse groups, indicating differences in escape latency and time per quadrant is not interfered by swim impairments (acquisition phase: $F_{2,161} = 0.723$; N.S. and probe trial: $F_{2,26} = 0.252$, N.S.) (Fig.5.2.b, d).

Altogether, these data clearly show an WT-like behavioral phenotype and survival rate of aged APP/PS1-CCL17$^{E/E}$ mice compared to their age-matched APP/PS1 controls.

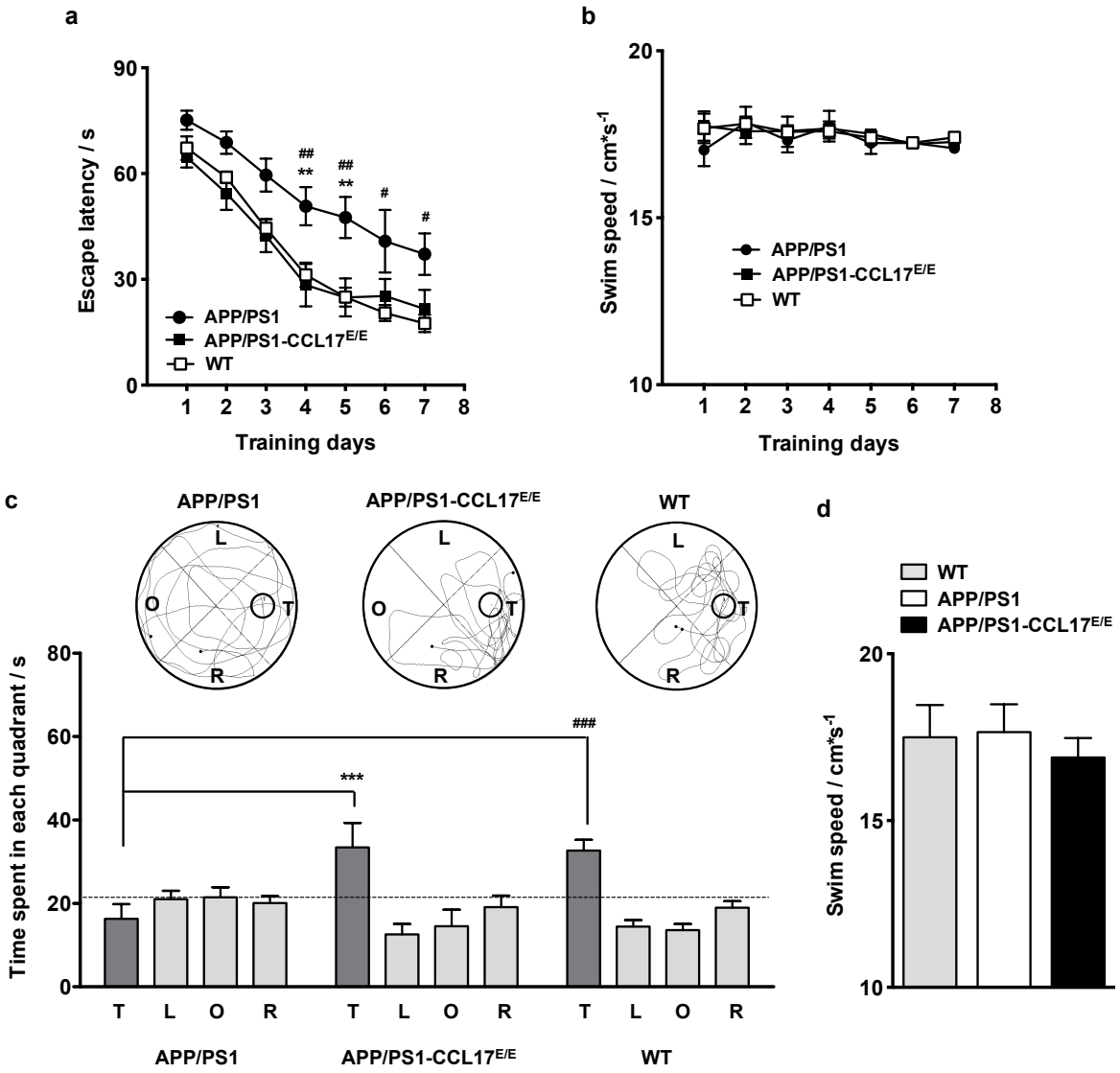

Figure 5.2: **APP/PS1-CCL17$^{E/E}$ mice showed WT-like learning and memory performance in a Morris water maze task**

(a) Shown are learning curves of APP/PS1 (black circles), APP/PS1-CCL17$^{E/E}$ (black quadrants), and WT (open quadrants) mice during the acquisition trial. The curves present average escape latencies ± SEM to the hidden platform on each of seven days of acquisition trials. APP/PS1-CCL17$^{E/E}$ and WT mice exhibit a similar learning ability within 7 days, while APP/PS1 mice had a significant higher escape latency. (b) Diagram shows the curves of swim speed during the acquisition trial. (c) A schematic view of the Morris Water Maze pool visualizes representative swimming patterns of APP/PS1 (left), APP/PS1-CCL17$^{E/E}$ (middle) and WT (right) mice in the water maze. The diagram shows the mean ± SEM of time spent in each quadrant (T, target; L, left; O, opposite; and R, right) of the Morris water maze during the probe trial. APP/PS1-CCL17$^{E/E}$ and WT spent significant more time in the target quadrant than in the other quadrants. Both mouse strains showed a better performance than APP/PS1 mice. (d) Diagram shows the mean ± SEM of swim speed during the probe trial. The analysis of swim speed during acquisition trial (b) and probe trial (d) revealed no differences in swimming performance in APP/PS1, APP/PS1-CCL17$^{E/E}$, and WT mice. Data analysis: (a), (b), (d): repeated measurement 2-way ANOVA with Bonferroni *post-hoc*, $^{**}p < 0.01$, and $^{***}p < 0.001$ for APP/PS1-CCL17$^{E/E}$ *vs.* APP/PS1, $^{\#}p < 0.05$, $^{\#\#}p < 0.01$, and $^{\#\#\#}p < 0.001$ for WT *vs.* APP/PS1. (c): 1-way-ANOVA with Bonferroni *post-hoc*, $^{***}p < 0.001$ for APP/PS1-CCL17E/E *vs.* APP/PS1, $^{\#\#\#}p < 0.001$ for WT *vs.* APP/PS1. (n = 8-9 mice / group); (Fig.5.2: Önder Albayram)

5.1.2 Reduced sAβ level in aged APP/PS1-CCL17$^{E/E}$ mice

The expression of the human amyloid precursor protein (APP) together with human presenilin-1 (PSEN-1), part of the γ-secretase APP-cleaving complex, in mice (APP-swe(K594N/M595L)/PS1dE9) results in a strong amyloid-beta plaque burden starting at four to six months of age [17, 129]. To investigate whether CCL17 deficiency results in an altered amyloid-beta load, the amount of soluble Aβ monomers and oligomers, as well as deposited Aβ fibrils was assayed. First, the amount of extracellular deposits in aged mice was determined to test whether the reduced cognitive decline is accompanied by a reduced Aβ aggregation. For this, the percentage of occupied area and the size of Thioflavine S-stained Aβ plaques in cortex and hippocampus (HC) was evaluated. In Fig.5.3.a, representative immunofluorescence images of brain tissue slices of APP/PS1 (upper panel) and APP/PS1-CCL17$^{E/E}$ (lower panel) mice are shown. Equivalent plaque size (Fig.5.3.b, right) and occupied area (Fig.5.3.b, left) were found in both groups.

Recent data suggested that soluble Aβ peptides are neurotoxic and the primary cause of neuronal loss and cognitive decline rather than extracellular deposits [132]. Soluble Aβ peptides were isolated by mild homogenization in sucrose buffer and a western blot analysis was performed. In Fig.5.3.c, a representative picture of a western blot shows soluble oligomeric and proto-fibrillic Aβ (oAβ) (top panel) as slightly diffuse bands due to different oligomerization states. Monomeric Aβ is seen as sharp bands with a size of 3 kDa, whereas dimeric Aβ shows relatively weak bands at 6 kDa. Interestingly, although a similar expression of oAβ in middle-aged mice (lane 1-3 APP/PS1, 4-6 APP/PS1-CCL17$^{E/E}$) was found, the aged mice exhibit a marked reduction of soluble Aβ oligomers in APP/PS1-CCL17$^{E/E}$ (lane 10-12) compared to APP/PS1 controls (lane 7-9). To exclude whether the reduction of Aβ peptides is a result of reduced APP expression, western blotting of sAPP in APP/PS1 and APP/PS1-CCL17$^{E/E}$ mice in both groups was assessed. However, sAPP bands (62 kDa) present equivalent expression (Fig.5.3.c).

Enzymatic cleavage of APP by γ-secretase results in the production of several monomeric Aβ isoforms with 36-43 amino acid residues. Aβ_{40} is the most common isoform produced in the CNS, but Aβ_{42} is supposed to be the most toxic compound as it shows the highest aggregation tendency and is more abundant in plaques [9]. The amount of both Aβ isoforms in the CNS of middle-aged and aged APP/PS1-CCL17$^{E/E}$ and APP/PS1 mice were determined using ELISA. Since Aβ production and plaque deposition is reported to start at around four to six months of age [17, 129], the amount of soluble Aβ_{40} and Aβ_{42} was analyzed in young mice as well. First, in order to control the isolation procedure for protein analysis, the total amount of proteins in the CNS of young, middle-aged, and aged mouse groups were determined by using BCA assay. The total protein content is equivalent between all age groups, and between APP/PS1-CCL17$^{E/E}$ and age-matched APP/PS1 mice (Fig.5.4).

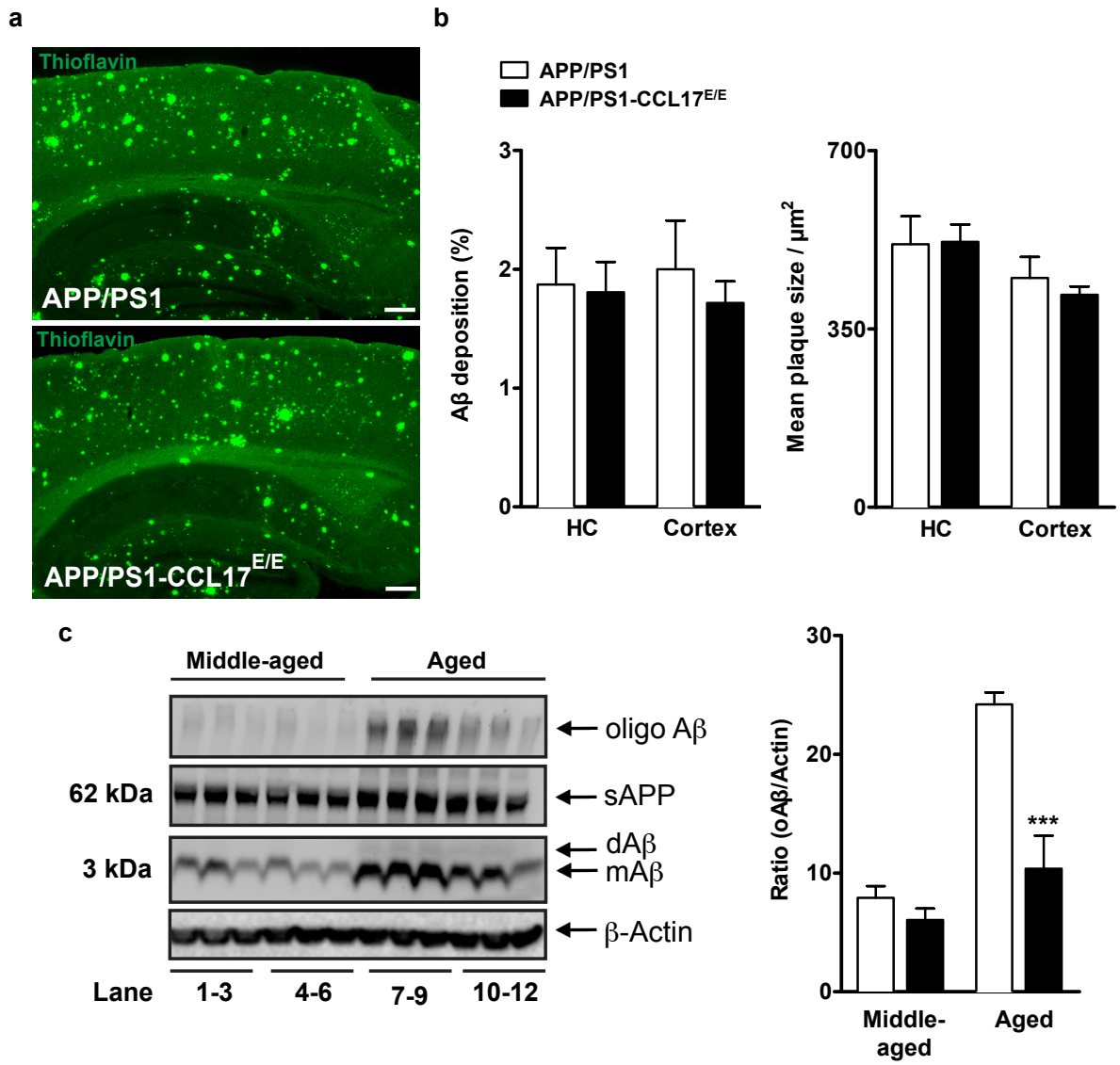

Figure 5.3: **Equivalent plaque deposition, but reduced soluble Aβ oligomers in aged APP/PS1-CCL17$^{E/E}$ mice**
(a) Representative immunofluorescence images of brain tissue slices of APP/PS1-CCL17$^{E/E}$ (lower) and APP/PS1 (upper) mice are shown (scale bar = 200 μm). (b) Diagrams show mean ± SEM of area fraction (%) occupied by plaques (left) and mean plaque size (right) in cortex and HC. APP/PS1-CCL17$^{E/E}$ (black bars) showed similar plaque deposition like APP/PS1 (white bars) mice. (c) Western blot analysis of soluble Aβ oligomers (>188 kDa), sAPP (66 kDa), and dimeric and monomeric Aβ (3 and 6 kDa) revealed reduced oAβ in aged APP/PS1-CCL17$^{E/E}$ mice compared to age-matched APP/PS1 mice, but not in middle-aged mice. Diagram shows mean ± SEM of oAβ/Actin ratio. Data analysis: Student's t-test, ***p $<$ 0.001 for APP/PS1-CCL17$^{E/E}$ *vs.* APP/PS1. (n = 5 mice/group (b); 3 mice/group (c)); (Fig.5.3.c: Ilker Karaca)

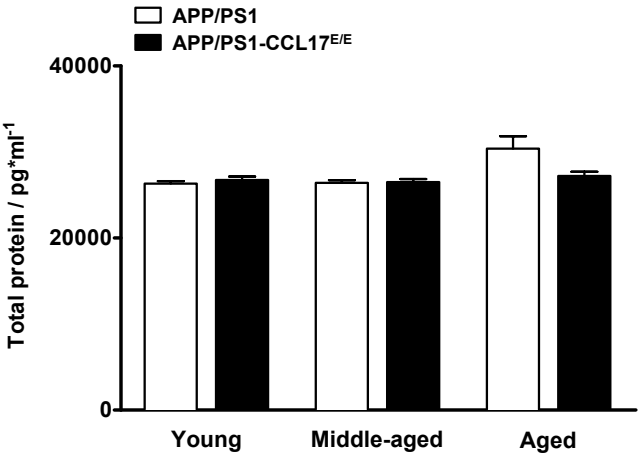

Figure 5.4: **Equivalent total protein amount in the CNS of APP/PS1-CCL17$^{E/E}$ and APP/PS1 mice**
Diagram shows mean ± SEM of total protein concentration of one hemisphere of young, middle-aged and aged APP/PS1-CCL17$^{E/E}$ and APP/PS1 mice. Data analysis: Student's t-test. (n = 7-14 APP/PS1, 11-13 APP/PS1-CCL17$^{E/E}$)

Next, the determination of sAβ isoforms within the CNS and serum of APP/PS1-CCL17$^{E/E}$ and APP/PS1 mice was carried out. Fig.5.5 shows diagrams of Aβ protein expression level in the serum, and in the CNS of young APP/PS1-CCL17$^{E/E}$ and APP/PS1 mice. Interestingly, in young mice enhanced levels of both, intracerebral Aβ_{40} (Fig.5.5.b) and Aβ_{42} (Fig.5.5.c) isoforms respectively, were increased in APPPS1-CCL17$^{E/E}$ mice compared to APP/PS1 controls. Furthermore, the serum Aβ concentration is reduced in young APP/PS1-CCL17$^{E/E}$ mice compared to age-matched APP/PS1 mice (Fig.5.5.a).

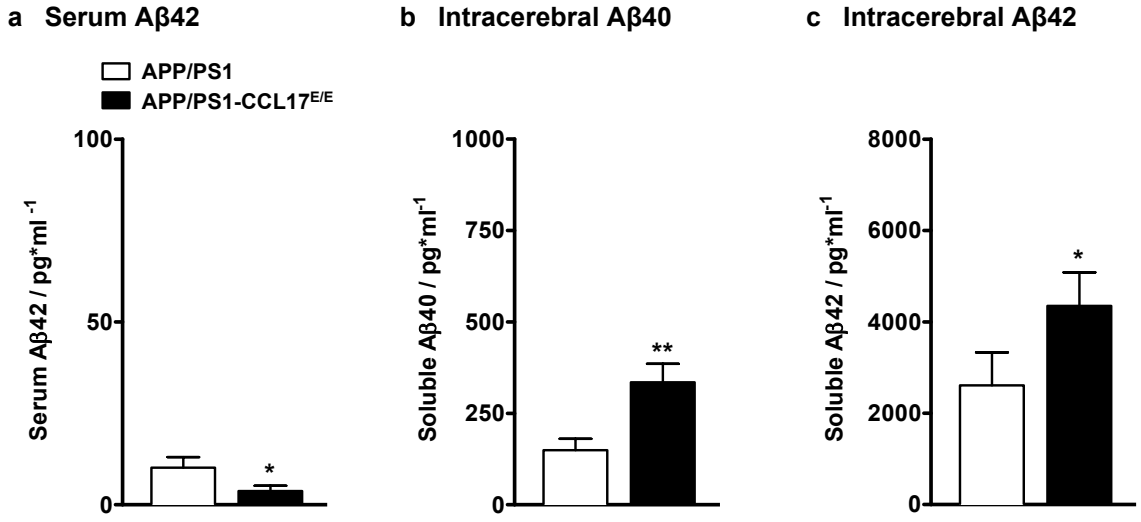

Figure 5.5: **Increased Aβ levels in the CNS of young APP/PS1-CCL17$^{E/E}$ mice**
(a-c) Diagrams show mean protein concentration ± SEM of serum Aβ_{42} (a) and intracerebral sAβ_{40} (b) and sAβ_{42} (c) of young APP/PS1-CCL17$^{E/E}$ and APP/PS1 mice measured by ELISA. Significant higher sAβ_{40} and sAβ_{42} levels, together with reduced serum Aβ_{42} were found in young APP/PS1-CCL17$^{E/E}$ compared to age-matched APP/PS1 controls (a). Data analysis: Student's t-test, *p $<$ 0.05, **p $<$ 0.01 for APP/PS1-CCL17$^{E/E}$ *vs.* APP/PS1. (Serum: n = 7-9 mice/group; CNS: 12-14 mice/group)

However, as shown in Fig.5.6, in middle-aged mice equivalent levels of intracerebral soluble Aβ_{40} and Aβ_{42} level, as well as serum Aβ_{42} concentrations were found.

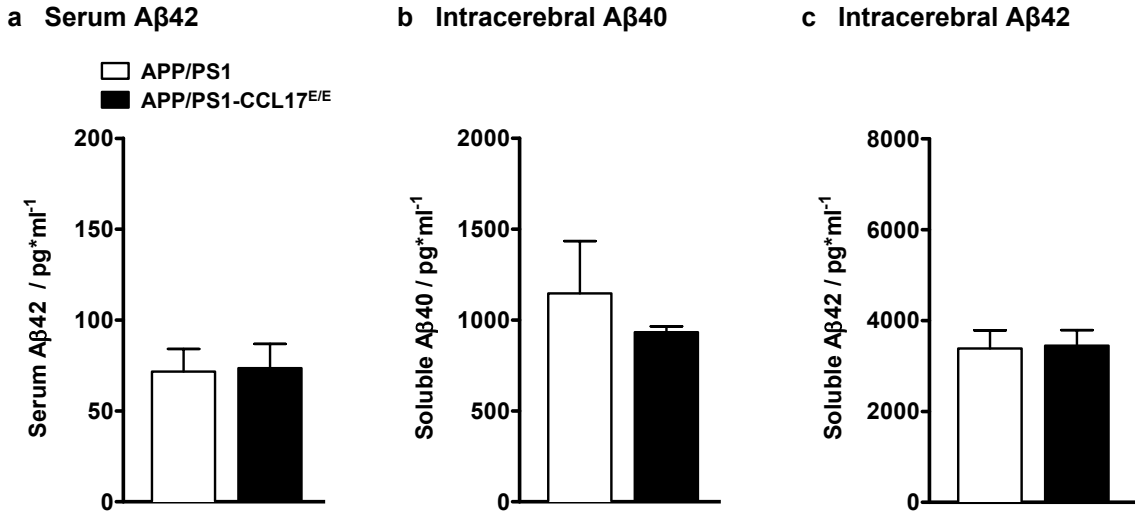

Figure 5.6: **Equivalent Aβ in the CNS of middle-aged APP/PS1-CCL17$^{E/E}$ and APP/PS1 mice**
(a-c) Diagrams show mean protein concentration ± SEM of serum Aβ_{42} (a) and intracerebral sAβ_{40} (b) and sAβ_{42} (c) of middle-aged APP/PS1-CCL17$^{E/E}$ and APP/PS1 mice measured by ELISA. In middle-aged mice all Aβ levels were found to be equivalent between both mouse groups. Data analysis: Student's t-test. (Serum: n = 11-12 mice/group; CNS: 11-12 mice/-group)

Fig.5.7 shows diagrams of Aβ protein expression level in the serum and in the CNS of aged APP/PS1-CCL17$^{E/E}$ and APP/PS1 mice. WT samples were assayed as controls. Although the measurement of sAβ_{40} in the CNS of WT mice revealed a high background, Aβ_{42} levels in the CNS and serum of WT mice were at a low background level as expected (Fig.5.7). Similar to the results of middle-aged mice, serum Aβ_{42} levels and intracerebral Aβ_{40} levels were found to be equivalent in aged APP/PS1-CCL17$^{E/E}$ and APP/PS1 mice (Fig.5.7.a, b). However, the sAβ_{42} level in the CNS of aged APP/PS1-CCL17$^{E/E}$ mice was significantly reduced compared to APP/PS1 mice (Fig.5.7.c).

Altogether, measurement of Aβ_{42} levels in young, middle-aged and aged APP/PS1-CCL17$^{E/E}$ and APP/PS1 mice revealed an increase of Aβ concentration from $<$ 20 pg/ml in the young mouse group to $\sim$ 100 pg/ml in the aged mouse group (age effect: $F_{2,2}$= 114,444; p $<$0.01). Furthermore, intracerebral sAβ_{40} levels rise from $<$ 400 pg/ml to $\sim$ 1500 pg/ml. Interestingly, in APP/PS1 mice the intracerebral sAβ_{42} concentration showed a strong increase from $<$ 3000 pg/ml in young mice to $\sim$ 6000 pg/ml in aged mice ($F_{2,30}$= 6.232; p $<$0.01), while in contrast the intracerebral sAβ_{42} concentrations of APP/PS1-CCL17$^{E/E}$ mice in all three age groups were found to be $\sim$ 4000 pg/ml ($F_{2,33}$= 0.8555; N.S.).

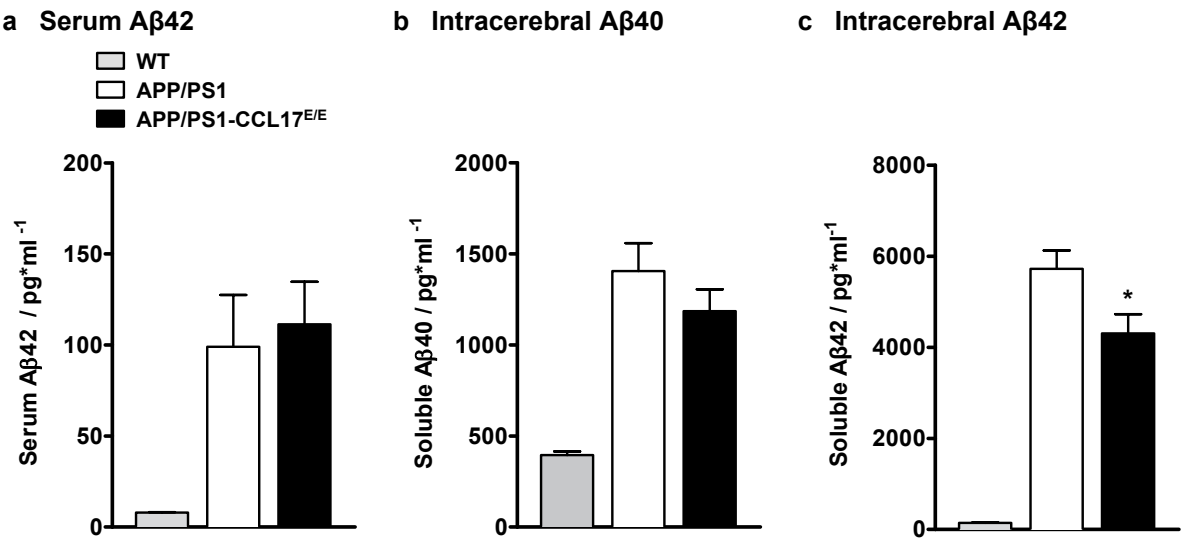

Figure 5.7: **Reduced sAβ_{42} in the CNS of aged APP/PS1-CCL17$^{E/E}$ mice**
(a-c) Diagrams show mean protein concentration ± SEM of serum Aβ_{42} (a) and intracerebral sAβ_{40} (b) and sAβ_{42} (c) of aged APP/PS1-CCL17$^{E/E}$ (black bars), APP/PS1 (white bars), and WT (light grey bars) mice measured by ELISA. While serum Aβ_{42} and intracerebral sAβ_{40} level were found to be equivalent in aged mice, sAβ_{42} level was significant reduced in APP/PS1-CCL17$^{E/E}$ mice compared to APP/PS1 controls. WT mice show small amounts of Aβ_{40} and Aβ_{42} levels (c). Data analysis: Student's t-test, *p < 0.05, **p < 0.01 for APP/PS1-CCL17$^{E/E}$ *vs.* APP/PS1. (Serum: n = 6-10 mice/group, 5 WT; CNS: 7-11 mice/group, 5 WT)

5.1.3 Reduced NeuN$^+$ neurons in the hippocampus of APP/PS1 mice, but not in APP/PS1-CCL17$^{E/E}$ mice

The overproduction of Aβ peptides and plaque deposition is often related to cognitive impairment and neuronal loss [43, 130, 133]. In order to evaluate the neuronal integrity of hippocampal neurons, a neuronal nuclei (NeuN) immunofluorescence staining for mature neurons [133, 134] was assessed in brain tissue slices of aged APP/PS1-CCL17$^{E/E}$, APP/PS1, and WT mice. In Fig.5.8, representative immunofluorescence images of the hippocampal CA3 region of brain tissue slices of WT (left panel), APP/PS1 (middle), and APP/PS1-CCL17$^{E/E}$ (right) mice are shown. APP/PS1-CCL17$^{E/E}$ exhibit a NeuN staining pattern comparable to WT mice. In contrast, APP/PS1 mice showed a marked reduction in NeuN$^+$ neurons, indicating a loss of mature neurons in the hippocampus. Quantification of NeuN immunoreactive cells as area fraction (% of area) revealed a significant reduction of NeuN staining pattern in the hippocampus of brain tissue slices of aged APP/PS1 mice compared to age-matched APP/PS1-CCL17$^{E/E}$ and WT mice. Survival of neurons is multifactory-dependent, one major component discussed to play a potential role in AD is the brain-derived neurotrophic factor BDNF [9, 123]. The expression level of *bdnf* mRNA in the hippocampus of aged APP/PS1-CCL17$^{E/E}$ mice was assayed using qRT-PCR. Equivalent *bdnf* level was found in the HC of APP/PS1-CCL17$^{E/E}$ mice compared to WT and CCL17$^{E/E}$ control, whereas the *bdnf* expression is increased in APP/PS1 mice (Fig.5.8.c).

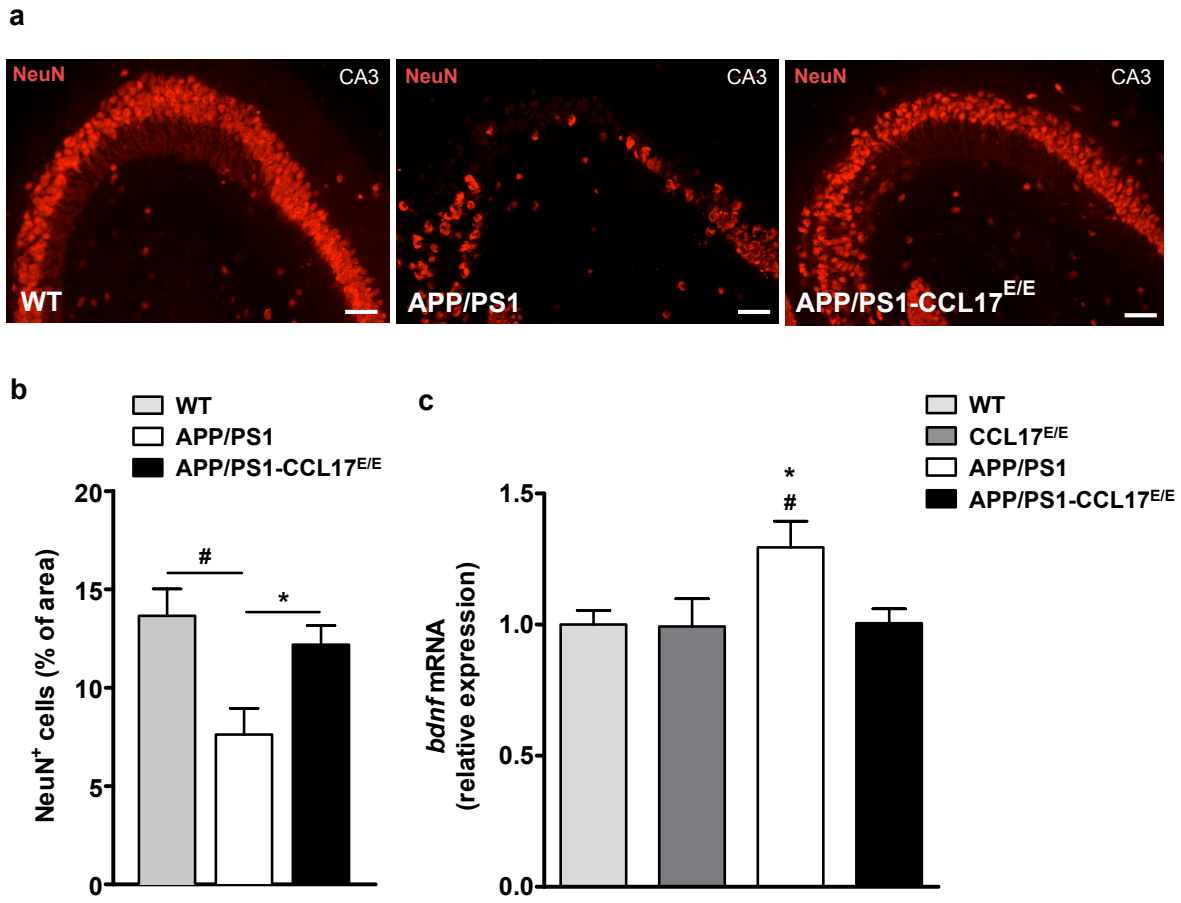

Figure 5.8: **Reduced NeuN immunoreactivity in the hippocampus of APP/PS1 mice, but not in APP/PS1-CCL17$^{E/E}$ mice**
(a) Representative sagittal sections of hippocampal CA3 region of WT (left), APP/PS1 (middle), and APP/PS1-CCL17$^{E/E}$ (right) (scale bar = 50 μm). (b) Diagram shows mean area fraction ± SEM of NeuN immunoreactive tissue slices. APP/PS1-CCL17$^{E/E}$ (black bar) and WT (light grey bar) exhibit a similar NeuN staining pattern in contrast to APP/PS1 mice (white bar), which showed a marked reduction of NeuN immunoreactivity. (c) qRT-PCR analysis of *bdnf* mRNA in the hippocampus of aged APP/PS1-CCL17$^{E/E}$ (black bar), APP/PS1 (white bar), CCL17$^{E/E}$ (dark grey bar), and WT (light grey bar) mice. Diagram shows mean ± SEM. Data analysis: 1-way-ANOVA and Student's t-test, *p < 0.05 for APP/PS1-CCL17$^{E/E}$ *vs.* APP/PS1, and $^{\#}$p < 0.05 for APP/PS1 *vs.* WT. (b: n = 3-4 mice/group, c: 4-6 non-tg, 8-9 tg); (Fig.5.8.a, b: Christina Müller)

These data show a reduced soluble Aβ concentration, but not of insoluble Thioflavin-positive plaques, within the CNS of aged APP/PS1-CCL17$^{E/E}$ mice, which is accompanied by a reduced loss of mature neurons in the hippocampal region.

5.1.4 Analysis of APP/PS1-CCL17$^{E/+}$ reporter mice

Investigation of eGFP expressing cells in the periphery and the CNS of APP/PS1-CCL17$^{E/+}$ and CCL17$^{E/+}$ reporter mice

Alferink *et al.* showed that CCL17 is mainly expressed by mature DCs in various lymphoid and non-lymphoid organs using a CCL17 reporter mouse model [101]. In this study an eGFP (enhanced green fluorescent product) cassette was inserted via homologous recombination into the murine *ccl17* locus under the control of the *ccl17* promotor. After blastocyste injection chimeric mice were backcrossed to a C57BL/6 background and heterozygous CCL17$^{E/+}$ mice expressed wildetype CCL17 and eGFP reporter protein. Homozygous CCL17$^{E/E}$ mice, carrying the eGFP construct on both alleles, are deficient for murine CCL17. CCL17$^{E/+}$ and CCL17$^{E/E}$ cells are visualized by their green fluorescence. The dominant cellular producers of CCL17 are CD11c^{+} DCs. eGFP^{+} DCs can be identified in the LN in CCL17$^{E/+}$ heterozygous mice under physiological and inflammatory conditions [101], and in spleen only after NKT (natural killer T) cell ligand induction [113]. To investigate whether the amount of CCL17^{+} DCs is altered in the periphery of APP/PS1-CCL17$^{E/+}$ due to APP/PS1 expression, flow cytometric analysis of green-fluorescent DCs in LN$_{cerv}$, LN$_{ax,mes}$, spleen, and blood was performed. Additionally, it was asked whether eGFP^{+} cells can be detected in the CNS of APP/PS1-CCL17$^{E/+}$ mice or their healthy controls.

However, in LN$_{ax,mes}$ and LN$_{cerv}$ of APP/PS1-CCL17$^{E/+}$ and CCL17$^{E/+}$ reporter mice equivalent levels of eGFP^{+}CD11c^{+} cells were found (Fig.5.9.b, c). Analysis of PBMC and spleen revealed relatively low percentages of eGFP^{+}CD11c^{+} cells (Fig.5.9.c). In the spleens of these mice less than 1 % of isolated cells present eGFP expression, whereas in blood and in brain tissue eGFP^{+} cells could not be detected. This result fits to previous observations in which the investigation of brain tissue slices of APP/PS1-CCL17$^{E/+}$ revealed no eGFP^{+} cells, although green-fluorescent cells could be found in LN of APP/PS1-CCL17$^{E/+}$ mice [127].

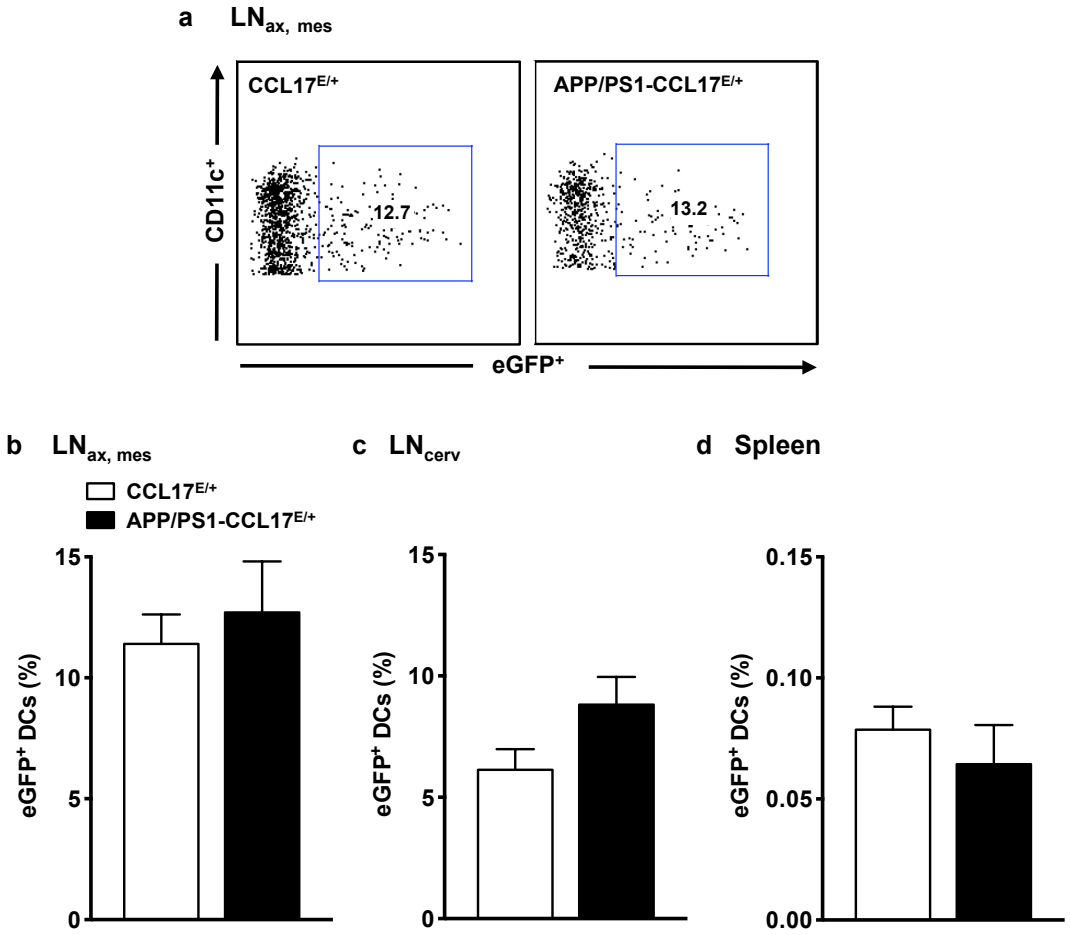

Figure 5.9: **Equivalent percentages of eGFP$^+$DCs in LN$_{ax,mes}$, LN$_{cerv}$, and spleen of APP/PS1-CCL17$^{E/+}$ and CCL17$^{E/+}$ reporter mice**
(a) Representative dot plots of CD11c$^+$eGFP$^+$ cells isolated from LN$_{cerv}$ of APP/PS1-CCL17$^{E/+}$ (right) and CCL17$^{E/+}$ (left) mice. Blue gates: CD11c$^+$eGFP$^+$ cells. Numbers are frequencies (in %). (b-d) Equivalent percentages of eGFP$^+$CD11c$^+$ cells in LN$_{ax,mes}$ (b), LN$_{cerv}$ (c), and spleen (d) in APP/PS1-CCL17$^{E/+}$ and CCL17$^{E/+}$ mice. Diagrams show mean ± SEM. Data analysis: Student's t-test. (n = 3-4 mice/group)

Quantification of peripheral myeloid and lymphoid cells in APP/PS1-CCL17$^{E/+}$ and CCL17$^{E/+}$ reporter mice

Several studies showed an AD-related alteration of peripheral biomarkers or a modulated Aβ reactivity of peripheral immune cells in humans [121, 122, 123, 124]. To investigate whether the overexpression of APP/PS1 in a mouse model of AD leads to an alteration in the numbers of peripheral immune cells, the analysis of heterozygous APP/PS1-CCL17$^{E/+}$ reporter mice was conducted.

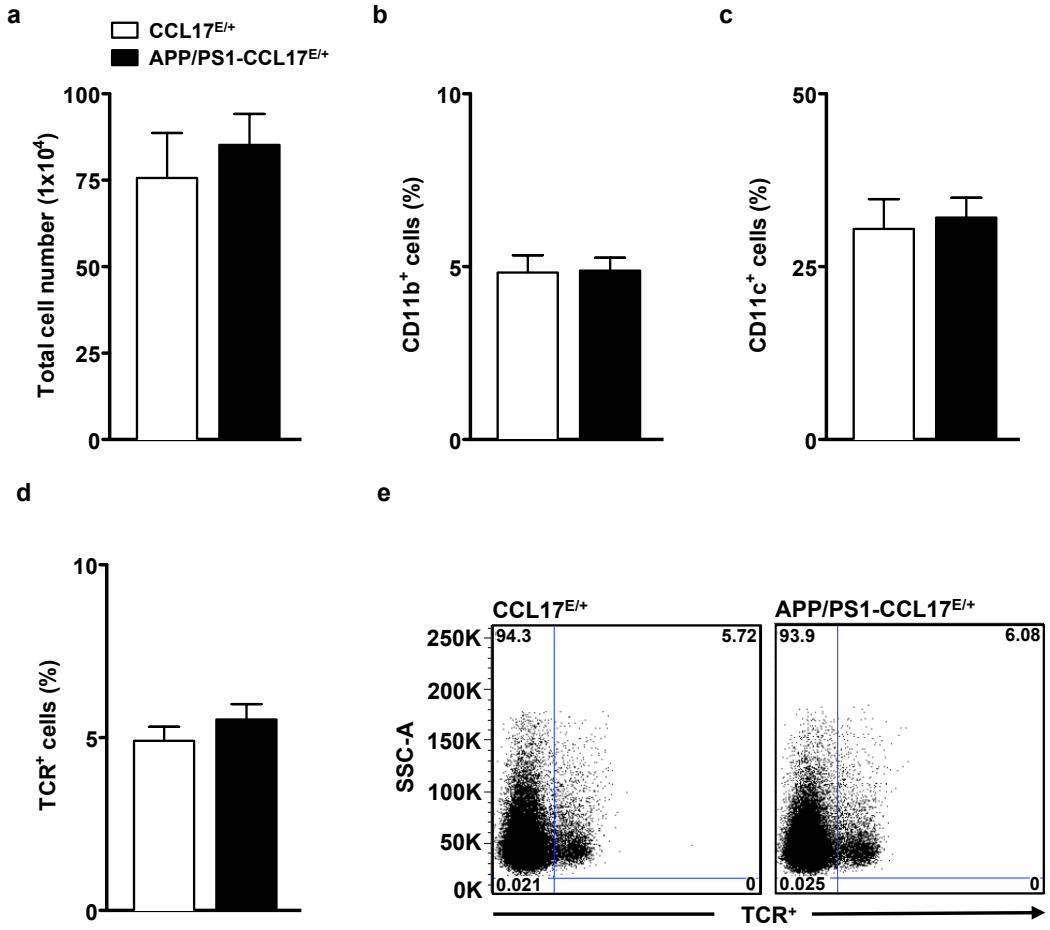

Figure 5.10: **Equivalent percentages of LN-derived CD11b$^+$, CD11c$^+$, and TCR$^+$ cells in APP/PS1-CCL17$^{E/+}$ and CCL17$^{E/+}$ reporter mice**
(a-d) Diagrams show mean ± SEM of equivalent total cell numbers (a) and percentages of CD11b$^+$ (b), CD11c$^+$ (c), and TCR$^+$ cells (d) isolated from pooled axillary, inguinal, and mesenterial lymph nodes of APP/PS1-CCL17$^{E/+}$ (black bars) and CCL17$^{E/+}$ (white bars) mice. (e) Representative dot plots of LN-derived TCR$^+$ T cells. Numbers in blue quadrant gates are the frequencies of events (in %). Data analysis: Student's t-test. (n = 5 mice/group)

First, cells from pooled axillary, inguinal, and mesenterial lymph nodes (LN$_{ax,mes}$) and from the spleen of 10-12 months-old APP/PS1-CCL17$^{E/+}$ and CCL17$^{E/+}$ reporter mice were isolated and the amount of myeloid and lymphoid cells were determined using flow cytometry. For this, total cell numbers were counted and cells were stained for CD11b (monocytes / macrophages), CD11c (dendritic cells) and T-cell receptor TCR (T cells) surface expression.

As shown in Fig.5.10.a, cell counting revealed equivalent total cell numbers in lymph nodes of APP/PS1-CCL17$^{E/+}$ and CCL17$^{E/+}$ reporter mice. Flow cytometric analysis of CD11b$^+$ (Fig.5.10.b), CD11c$^+$ (Fig.5.10.c), and TCR$^+$ (Fig.5.10.d) LN-derived cells revealed also no differences between the two mouse groups. In Fig.5.10.e, representative dot plots of TCR$^+$ cells (SSC *vs.* TCR PerCP-Cy5.5) isolated from LN$_{ax,mes}$ of APP/PS1-CCL17$^{E/+}$ (right) and CCL17$^{E/+}$ (left) are depicted. Furthermore, flow cytometric analysis of splenic cells of APP/PS1-CCL17$^{E/+}$ and CCL17$^{E/+}$ reporter mice revealed equivalent total cell numbers (Fig.5.11.a), CD11b$^+$ (Fig.5.11.b), CD11c$^+$ (Fig.5.11.c), and TCR$^+$ (Fig.5.11.d) cells.

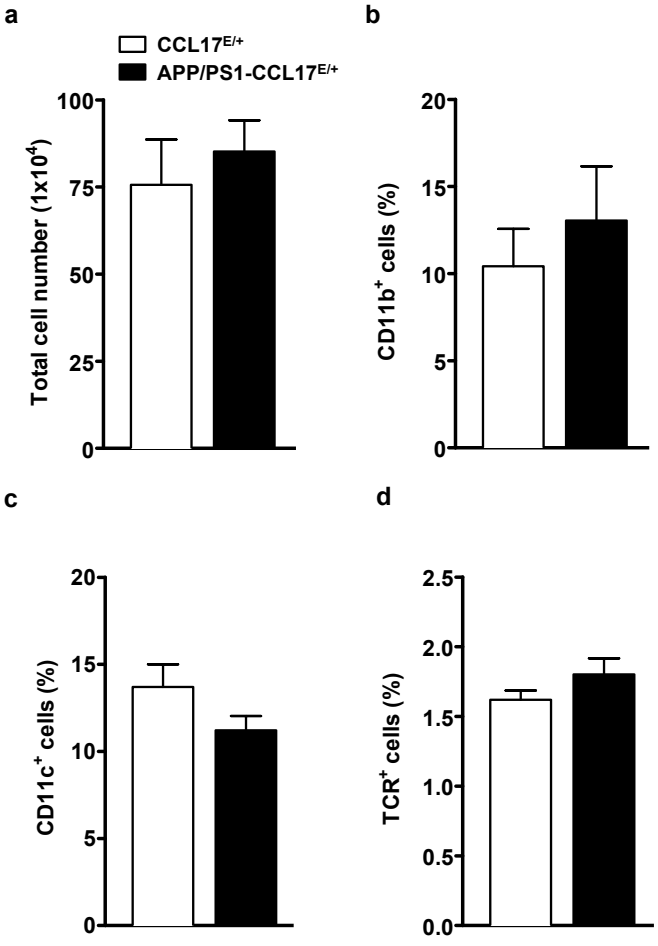

Figure 5.11: **Equivalent percentages of CD11b$^+$, CD11c$^+$ and TCR$^+$ cells in the spleen of APP/PS1-CCL17$^{E/+}$ and CCL17$^{E/+}$ reporter mice**
(a-d) APP/PS1-CCL17$^{E/+}$ and CCL17$^{E/+}$ mice present equivalent total cell numbers (a) and percentages of CD11b$^+$ (b), CD11c$^+$ (c), and TCR$^+$ cells (d). Diagrams show mean ± SEM. Data analysis: Student's t-test. (n = 5 mice/group)

It was reported that drainage of Aβ from the CNS to cervical lymph nodes (LN$_{cerv}$) can occur [125, 126]. Since own data showed that CD11c$^+$ DCs are able to phagocytose Aβ peptides *in vitro* [127], the amount of CD11c$^+$ DCs in cervical LN and blood (peripheral blood mononuclear cells (PBMC)) of APP/PS1-CCL17$^{E/+}$ mice was determined. In Fig.5.12.a, representative dot plots of LN$_{cerv}$-derived CD11c$^+$ cells (SSC *vs.* CD11c AF647) are shown. However, the determination of total cell numbers and CD11c$^+$

cells revealed no differences between APP/PS1-CCL17$^{E/+}$ and CCL17$^{E/+}$ reporter mice neither in LN$_{cerv}$ (Fig.5.12.b) nor in PBMC (Fig.5.12.c).

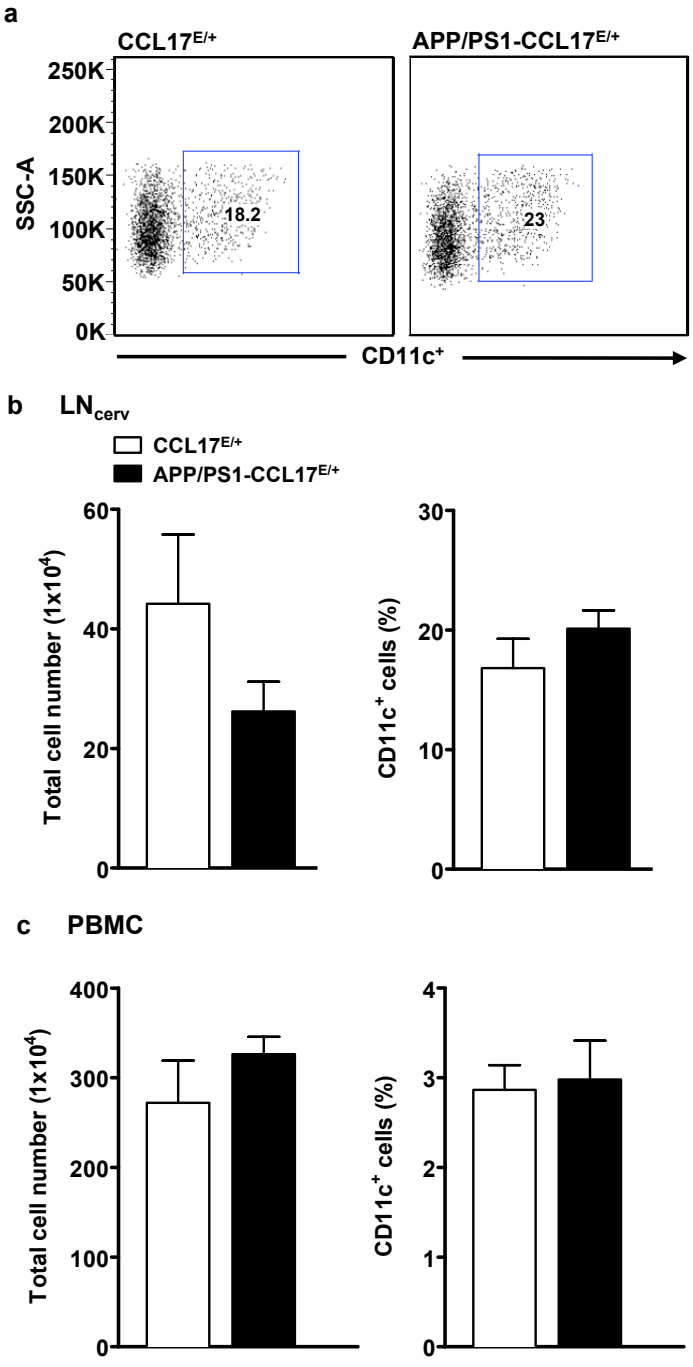

Figure 5.12: **Equivalent total cell numbers and CD11c$^+$ cells in LN$_{cerv}$ of APP/PS1-CCL17$^{E/+}$ and CCL17$^{E/+}$**
(a) Representative dot plots of CD11c$^+$ cells isolated from LN$_{cerv}$ of APP/PS1-CCL17$^{E/+}$ (right) and CCL17$^{E/+}$ (left) mice. (b-c) Diagrams show mean ± SEM of total cell numbers and percentages of CD11c$^+$ cells of LN$_{cerv}$ (b) and PBMC (c). Data analysis: Student's t-test. (n = 5 mice/group)

Characterization of intracerebral leukocytes of APP/PS1-CCL17$^{E/+}$ and CCL17$^{E/+}$ reporter mice

To determine the amount of invading and resident mononuclear cells in the CNS of APP/PS1-CCL17$^{E/+}$ reporter mice, isolated intracerebral leukocytes (ICL) from the CNS were analyzed by flow cytometry using CD11b and CD45 double staining. CD11b is expressed by several cell types within the CNS such as invading monocytes / macrophages and CNS-resident microglial cells. In contrast, CD45 is expressed by CNS-infiltrating cells such as lymphocytes and monocytes / macrophages. In Fig.5.13.b, a representative dot plot of CD45$^+$ CD11b$^+$ cells, pre-gated for life cells, is given.

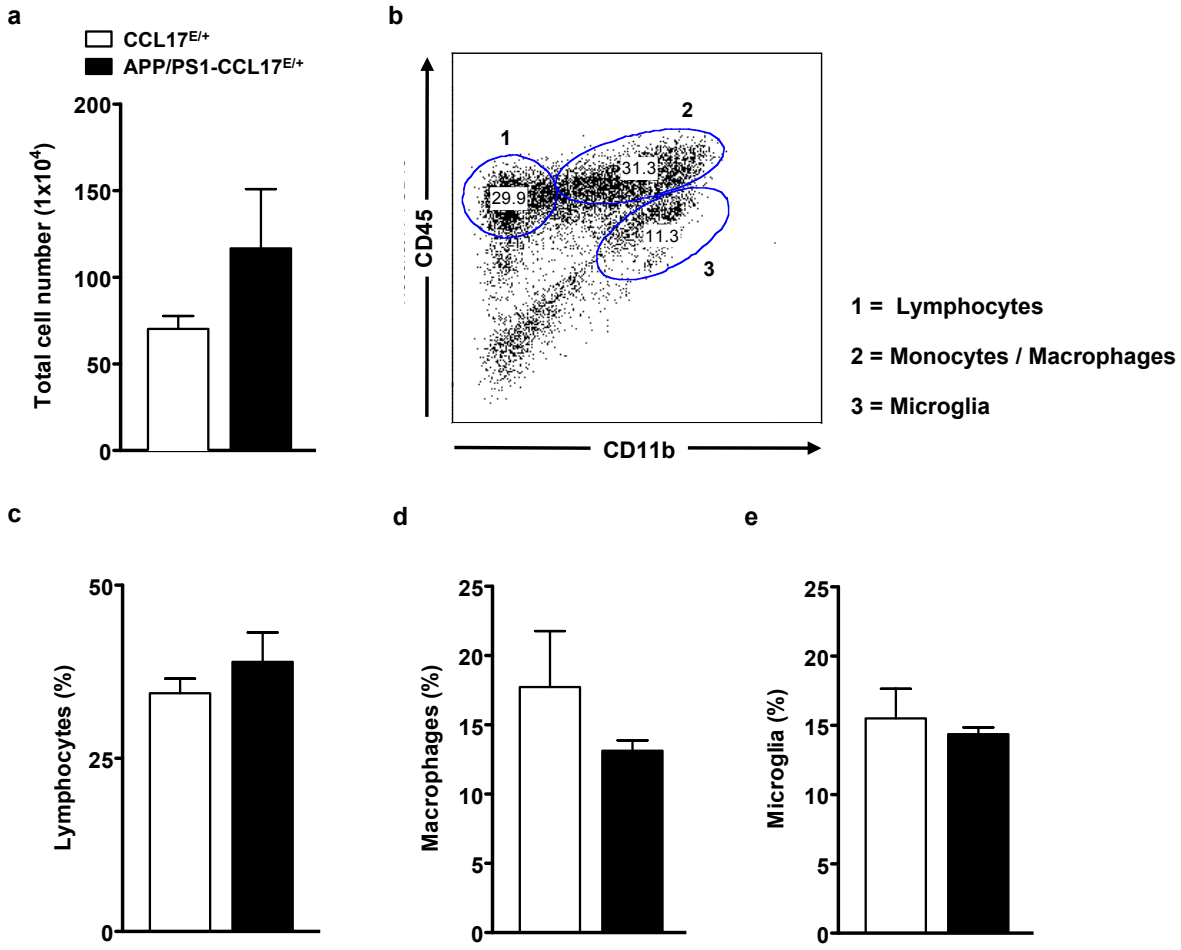

Figure 5.13: **Equivalent numbers of intracerebral leukocytes in APP/PS1-CCL17$^{E/+}$ and CCL17$^{E/+}$ reporter mice**
(a) Diagram shows mean ± SEM of total cell numbers of intracerebral leukocytes (ICL) of APP/PS1-CCL17$^{E/+}$ and CCL17$^{E/+}$ mice. (b) Representative dot plot of CD45$^+$CD11b$^+$ ICL. Gates are indicated in blue ovals. Numbers are frequencies of events (in %). (c-e) Flow cytometric analysis of ICL of APP/PS1-CCL17$^{E/+}$ and CCL17$^{E/+}$ mice revealed no differences of lymphocyte (c), monocyte / macrophage (d), and microglia (e) populations. Diagrams show mean ± SEM. Data analysis: Student's t-test. (n = 3-4 mice/group)

As shown by gates (blue ovals) three different main cellular populations can be distinguished: (1) Lymphocytes as CD45^{high}CD11b$^-$ cells, (2) macrophages as CD45^{high} CD11b^{high} cells, and (3) microglia as CD45^{low}CD11b^{high} cells. The numbers within the

gates are representative percentaged distribution of the cells. The analysis of intracerebral lymphocytes, macrophages, and microglial cells revealed no differences between APP/PS1-CCL17$^{E/+}$ and CCL17$^{E/+}$ mice (Fig.5.13.c, d, and e).

In addition, the activation status of ICL by CD40 expression was assessed. Enhanced CD40 levels by microglia are linked to chronic inflammation as it occurs in AD progression [128]. Flow cytometric analysis of CD40 expression by CD45/CD11b pre-gated lymphocytes, monocytes / macrophages, and microglia in the CNS of APP/PS1-CCL17$^{E/+}$ and CCL17$^{E/+}$ reporter mice revealed an increase of mean fluorescence intensity (MFI) of CD40 by microglia and macrophages, but not by lymphocytes isolated from the CNS of APP/PS1-CCL17$^{E/+}$ mice compared to healthy controls, as shown in Fig.5.14. Furthermore, lymphocytes possess the lowest CD40 geometric MFI in both mouse strains, while microglia have the highest geometric MFI.

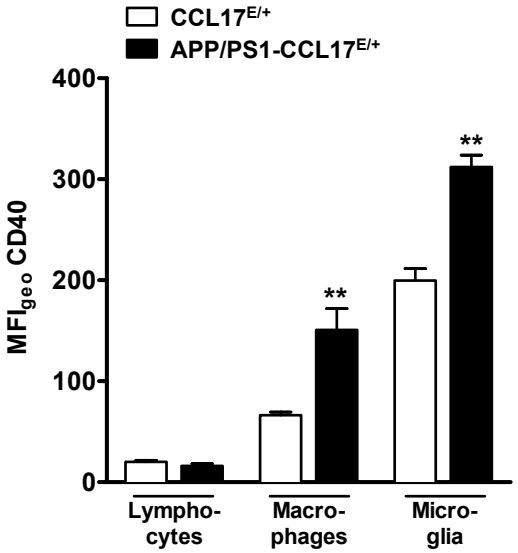

Figure 5.14: **Increased CD40 expression on macrophages and microglia in the CNS of APP/PS1-CCL17$^{E/+}$ reporter mice**
Enhanced geometric mean fluorescence intensity (MFI$_{geo}$) of CD40$^+$ microglia and macrophages in the CNS of APP/PS1-CCL17$^{E/+}$ mice compared to CCL17$^{E/+}$ controls. Lymphocytes showed the lowest CD40 MFI$_{geo}$. Diagram shows mean ± SEM. Data analysis: Student's t-test; **p <0.01. (n = 3-4 mice/group)

Altogether, no alteration in the numbers of myeloid and lymphoid cells in peripheral and brain tissue due to APP/PS1 transgene expression could be detected in 10-12 months-old APP/PS1-CCL17$^{E/+}$ mice compared to CCL17$^{E/+}$ mice. However, microglia and macrophages isolated from brains of APP/PS1-CCL17$^{E/+}$ mice revealed a higher activation status as indicated by CD40 expression compared to their CCL17$^{E/+}$ controls. Interestingly, eGFP expressing CD11c$^+$ cells were equivalent in spleen and LN, and not found in the brain or blood in both mouse strains.

5.1.5 Characterization of inflammatory CNS responses in APP/PS1-CCL17$^{E/E}$ mice

Neuroinflammation is characterized by the activation and proliferation of astrocytes (astrocytosis) and microglial cells (microgliosis), which is accompanied by morphological changes and altered gene transcription [28]. Astrocytosis is marked by an extensive upregulation of the intermediate filament protein GFAP (glial fibrillary acidic protein) and in context of AD, GFAP expression is correlated with Aβ accumulation [135]. Microgliosis in turn, is characterized by an increased CD11b expression by microglial cells upon activation [136]. To assess the inflammatory profile in the CNS of APP/PS1-CCL17$^{E/E}$ mice during robust plaque progression, the amount of GFAP$^+$ and CD11b$^+$ cells was determined in aged mice within cortex and hippocampus (HC) by immunofluorescence (Fig.5.15).

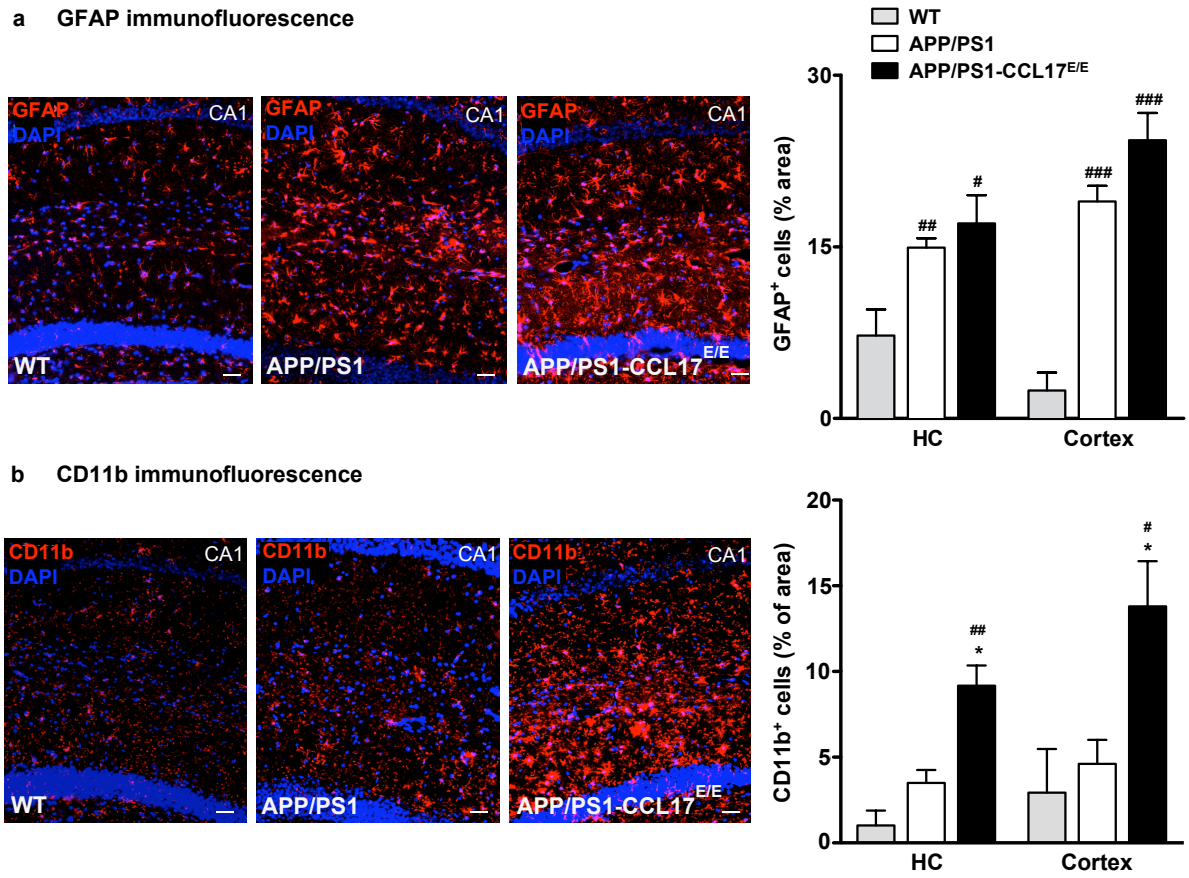

Figure 5.15: **Enhanced GFAP expression in aged APP/PS1-CCL17$^{E/E}$ and APP/PS1 mice** (a) Representative images of hippocampal CA1 region of GFAP immunoreactive brain slices of APP/PS1-CCL17$^{E/E}$, APP/PS1, and WT mice (scale bar = 50 μm). (b) Quantitative analysis of cortex and HC revealed increased number GFAP$^+$ cells in APP/PS1-CCL17$^{E/E}$ (black bar) and APP/PS1 (white bar) compared to WT controls (light grey bar). Diagram shows mean area fraction ± SEM. Data analysis: 1-way-ANOVA with Bonferroni *post-hoc*, $^*p < 0.05$ (APP/PS1-CCL17$^{E/E}$ *vs.* APP/PS1), $^{\#}p < 0.05$, $^{\#\#}p < 0.01$, $^{\#\#\#}p < 0.001$ (tg *vs.* WT). (n = 3 / group); (Fig.5.15: Christina Müller)

Representative images of GFAP and CD11b staining in CA1 region of HC are shown

in Fig.5.15.a, b. A marked increase of GFAP immunoreactive cells were found in the cortex and HC of APP/PS1 mice compared to WT mice. However, APP/PS1-CCL17$^{E/E}$ mice showed similar GFAP staining pattern like APP/PS1 mice (Fig.5.15.a). In contrast, the quantitative analysis of CD11b immunoreactive cells in brain tissue slices revealed an increase of CD11b immunoreactive cells in the cortex and HC of aged APP/PS1-CCL17$^{E/E}$ mice compared to APP/PS1 and WT mice (Fig.5.15.b).

Next, CD11b expression within the CNS of young, middle-aged, and aged mice were assessed to investigate whether there is an age-dependent alteration of microgliosis in the CNS of APP/PS1-CCL17$^{E/E}$ mice. Therefore, ICL of young, middle-aged, and aged APP/PS1-CCL17$^{E/E}$ and APP/PS1 mice were isolated and flow cytometric analysis of CD11b$^+$ cells was performed.

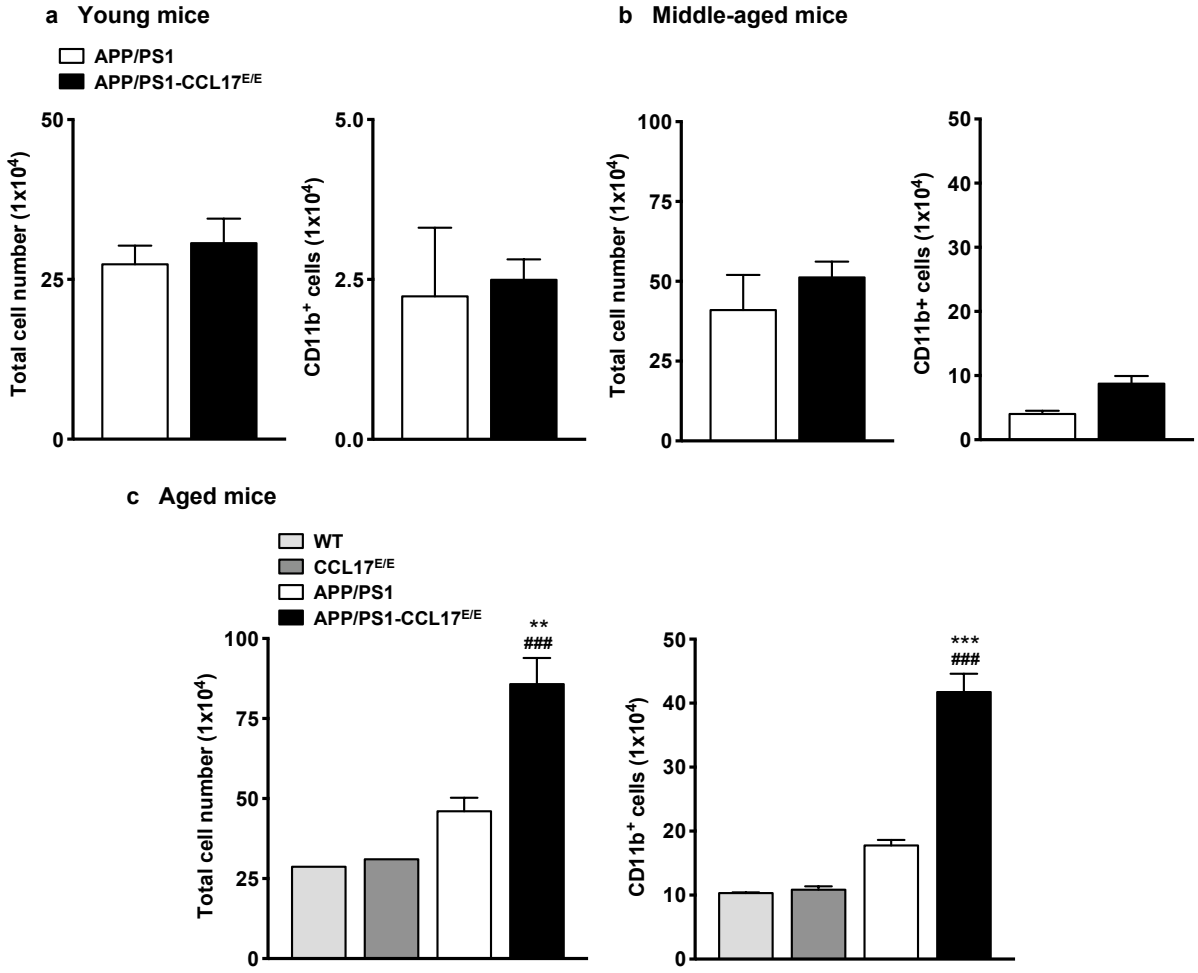

Figure 5.16: **Equivalent CD11b expression in young, but enhanced expression in the CNS of aged APP/PS1-CCL17$^{E/E}$ mice**
(a-c) Diagrams show mean ± SEM of total cell numbers (left) and numbers of CD11b$^+$ cells (right) in the CNS of young (a), middle-aged (b), and aged (c) APP/PS1-CCL17$^{E/E}$ (black bars) and APP/PS1 (white bars) mice. Total cell numbers and numbers of CD11b$^+$ cells are equivalent in young and middle-aged mice, but increased in aged APP/PS1-CCL17$^{E/E}$ mice. (c) Pooled CNS of WT (light grey bar) and CCL17$^{E/E}$ (dark grey bar) mice were used as non-tg controls. Total cell numbers and percentaged CD11b$^+$ cells were decreased in non-tg mice compared to both gt mouse strains. Data analysis: Student's t-test or 1-way-ANOVA with Bonferroni *post-hoc*, **p < 0.01, ***p < 0.001 (APP/PS1 *vs.* APP/PS1-CCL17$^{E/E}$), ###p < 0.001 (tg *vs.* WT). (n = 3-4 mice/group)

peptides and plaques [43, 70]. One key marker characterizing these cells, is the expression of the chemokine receptor CCR2 and the monocytic marker Ly6C [73]. As enhanced immigrating macrophages were found in the CNS of aged APP/PS1-CCL17$^{E/E}$ mice, it was investigated whether these cells express CCR2 and Ly6C. First, the expression levels of *ccr2* mRNA in the cortex of young, middle-aged, and aged APP/PS1-CCL17$^{E/E}$ mice were analyzed. Indeed, significant higher *ccr2* expression levels were found in the cortex of young (Fig.5.18.a) and middle-aged (Fig.5.18.b) APP/PS1-CCL17$^{E/E}$ mice compared to APP/PS1 controls. However, *ccr2* mRNA expression analysis of aged mice revealed no differences (Fig.5.18.c).

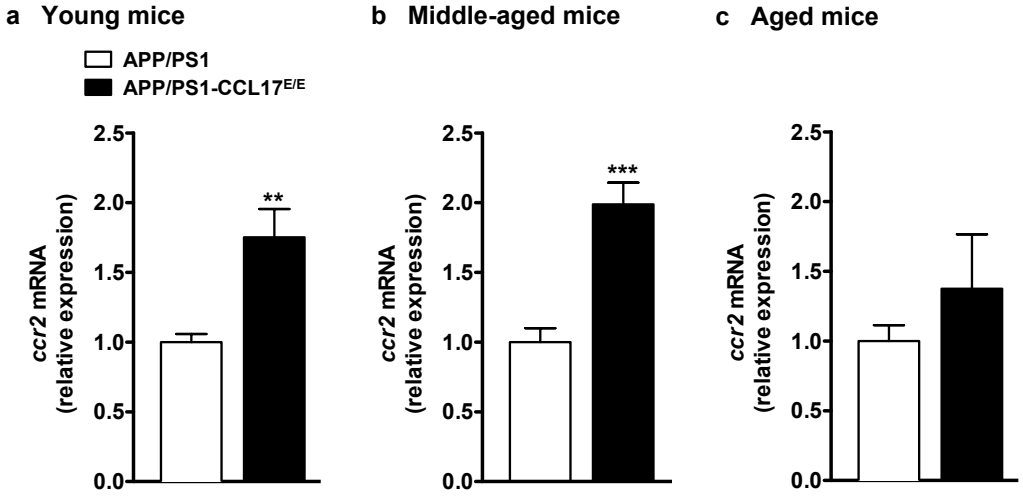

Figure 5.18: **Enhanced *ccr2* mRNA in the CNS of APP/PS1-CCL17$^{E/E}$ mice**
(a-c) qRT-PCR analysis of *ccr2* mRNA in the cortex of APP/PS1-CCL17$^{E/E}$ (black bar) and APP/PS1 (white bar) mice. Enhanced *ccr2* mRNA levels were found in young (a) and middle-aged (b) APP/PS1-CCL17$^{E/E}$ mice compared to APP/PS1 mice, but not in aged mice (c). Data analysis: Student's t-test, **p <0.01, ***p < 0.001. (n = 8-10 mice/group)

Next, in order to identify the CCR2^{+} cells in the CNS of APP/PS1-CCL17$^{E/E}$ and APP/PS1 mice, flow cytometric analysis were assessed on ICL. Interestingly, in line with mRNA data of the younger mice, but in contrast to the aged mice, a significant higher number of CCR2^{+} cells were found in the CNS of APP/PS1-CCL17$^{E/E}$ mice compared to APP/PS1 mice (Fig.5.19.a). In contrast, WT and CCL17$^{E/E}$ mice exhibit low numbers of CCR2^{+} cells. Moreover, as shown in Fig.5.19.b, CCR2 is most expressed by invading macrophages, at a lower level by microglial cells, and nearly absent on lymphocytes. Further, CCR2 expression is significant higher in both AD mouse groups than in healthy control groups. Representative CCR2 histograms of WT, CCL17$^{E/E}$, APP/PS1, and APP/PS1-CCL17$^{E/E}$ lymphocytes (light grey solid curve), macrophages (black line), and microglia (grey line) are shown in Fig.5.19.c. Furthermore, a significantly higher number of Ly6C^{high}CCR2^{+} macrophages was found in the CNS of APP/PS1-CCL17$^{E/E}$ mice compared to APP/PS1 mice (Fig.5.20.a, b). Interestingly, the Ly6C^{high}CCR2^{+} macrophage population is absent in non-tg mice, indicating an immigration of peripheral macrophages due to Aβ overexpression in both APP/PS1 tg mouse groups (Fig.5.20.a, b).

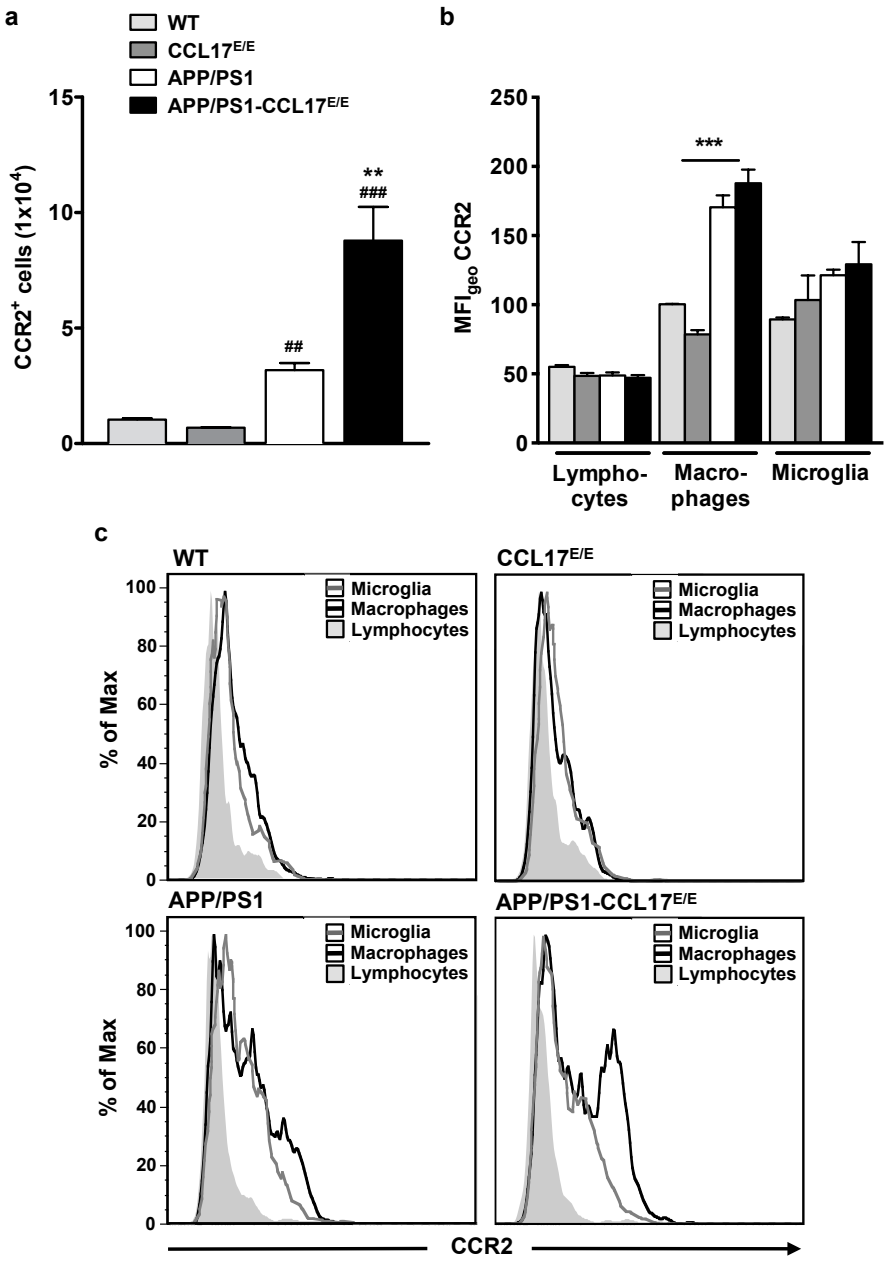

Figure 5.19: **Increased numbers of CCR2$^+$ cells in the CNS of aged APP/PS1-CCL17$^{E/E}$ mice** (a) Flow cytometric analysis of CCR2$^+$ cells in the CNS of aged APP/PS1-CCL17$^{E/E}$ (black bar), APP/PS1 (white bar), WT (light grey bar), and CCL17$^{E/E}$ (dark grey bar) mice. Diagram shows mean ± SEM. (b) Geometric mean fluoresence intensity (MFI$_{geo}$) of CCR2$^+$ macrophages is increased in APP/PS1-CCL17$^{E/E}$ and APP/PS1 mice compared to non-tg mice. Diagram shows mean MFI$_{geo}$ ± SEM. (c) Representative CCR2 histogram overlays of lymphocytes (light grey solid curve), macrophages (black line), and microglia (grey line) are shown of WT, CCL17$^{E/E}$, APP/PS1, and APP/PS1-CCL17$^{E/E}$ mice. % of Max = number of events normalized according to the FlowJo algorithms. Data analysis: 1-way-ANOVA with Bonferroni *post-hoc*, **p <0.01, ***p < 0.001 (APP/PS1 *vs.* APP/PS1-CCL17$^{E/E}$); ##p <0.01, ###p < 0.001 (tg *vs.* WT). (n = 3-4 mice/group)

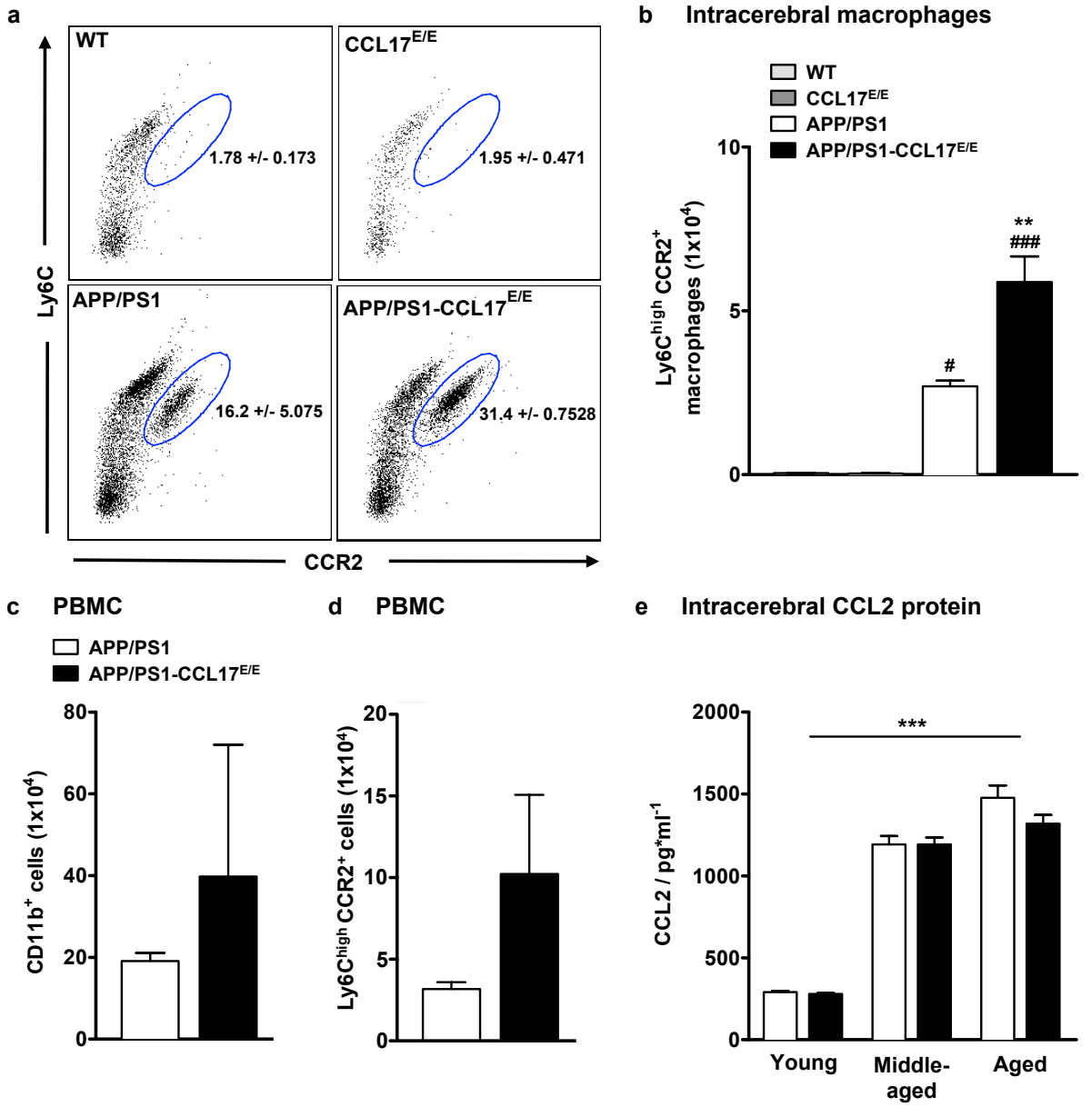

Figure 5.20: **Enhanced Ly6C^{high}CCR2^{+} cell immigration into the CNS of APP/PS1-CCL17$^{E/E}$ mice**
(a) Representative dot plots of Ly6C^{high}CCR2^{+} macrophages (blue gates) (CD45^{+}CD11b^{+} pre-gated) are shown of WT, CCL17$^{E/E}$, APP/PS1, and APP/PS1-CCL17$^{E/E}$ mice. (b) Significant higher numbers of Ly6C^{high}CCR2^{+} macrophages were found in the CNS of aged APP/PS1-CCL17$^{E/E}$ compared to APP/PS1. Diagrams show mean ± SEM. (c, d) Equivalent levels of CD11b^{+} and Ly6C^{high}CCR2^{+} PBMC of aged APP/PS1-CCL17$^{E/E}$ and APP/PS1 mice. Diagrams show mean ± SEM . (e) Diagram shows mean ± SEM of CCL2 protein level in the CNS of young, middle-aged, and aged APP/PS1-CCL17$^{E/E}$ and APP/PS1 mice. CCL2 concentrations showed an age-dependent increase, but equivalent levels between age-matched mouse groups. Data analysis: Student's t-test and 1-way-ANOVA with Bonferroni *post-hoc*, **p <0.01, ***p < 0.001 (APP/PS1 *vs.* APP/PS1-CCL17$^{E/E}$); ###p < 0.001 (tg *vs.* WT). (a-d: n = 3-4 mice/group; e: n = 7-9 mice/group)

Next, the amount of Ly6C^{high} CCR2^{+} monocytes in the peripheral blood of aged APP/PS1-CCL17$^{E/E}$ mice was assayed, to test whether an increase of intracerebral Ly6C^{high}CCR2^{+} macrophages is accompanied by an increase of peripheral blood Ly6C^{high} CCR2^{+} monocytes. However, the amount of CD11b^{+} PBMC and Ly6C^{high}CCR2^{+} mono-

cytes is equivalent in both mouse groups (Fig.5.20.c, d). To determine, whether increased invasion of peripheral Ly6C^{high}CCR2^{+} macrophage is related to an increase of intracerebral CCR2 ligand CCL2 expression, CCL2 concentration was measured in the CNS of young, middle-aged, and aged APP/PS1-CCL17$^{E/E}$ mice. However, although an age-dependent increase of intracerebral CCL2 level could be detected, differences in CCL2 expression between APP/PS1-CCL17$^{E/E}$ and APP/PS1 mice were not found (Fig.5.20.e).

Altogether, the analysis of intracerebral leukocytes of aged APP/PS1-CCL17$^{E/E}$ mice revealed an increase of CNS-resident microglia cells and a higher infiltration of peripheral monocytes / macrophages, which express high levels of Ly6C and CCR2 cell surface markers. Interestingly, this is not accompanied by an increase of CCL2 within the CNS of these mice. In addition, the amount of Ly6C^{high}CCR2^{+} PBMC were equivalent in APP/PS1-CCL17$^{E/E}$ and APP/PS1 mice.

5.1.7 Analysis of CCL17 (eGFP) expression in APP/PS1 transgenic mice

Recently, *ccl17* mRNA was found to be overexpressed in the frontal cortex of APPswe mice after intranasal Tat exposure modeling cerebral HIV-1 infection, suggesting a possible role of CCL17 during neuroinflammation and -degeneration [116]. However, similar to the heterozygous mice intracerebral localized eGFP^{+} cells could not be detected by either confocal microscopy (data not shown) or flow cytometry (Fig.5.21) in APP/PS1-CCL17$^{E/E}$ mice and CCL17$^{E/E}$ controls. Representative dot plots of CD11b and eGFP (Fig.5.21.a), and representative eGFP histograms of intracerebral macrophages and microglial cells (Fig.5.21.b) are shown. To investigate, whether CCL17 expression is altered due to APP/PS1 expression in the CNS of tg mice, the *ccl17* mRNA level in the hippocampus of aged APP/PS1 and WT mice was determined. Indeed, CCL17 expression is upregulated in APP/PS1 mice compared to healthy WT mice (Fig.5.22.a). To unravel the cellular source of intracerebral CCL17, ICL of aged APP/PS1 and WT mice were isolated and CCL17 expression was evaluated by qRT-PCR. As seen in Fig.5.22.b, it was found that adult microglia isolated from aged APP/PS1 and WT mice express *ccl17* mRNA. mRNA analysis of cortical tissue of CCL17$^{E/E}$ mice exhibit no *ccl17* expression, in contrast to WT mice, indicating no false-positive signal for RT-PCR analysis (Fig.5.22.c).

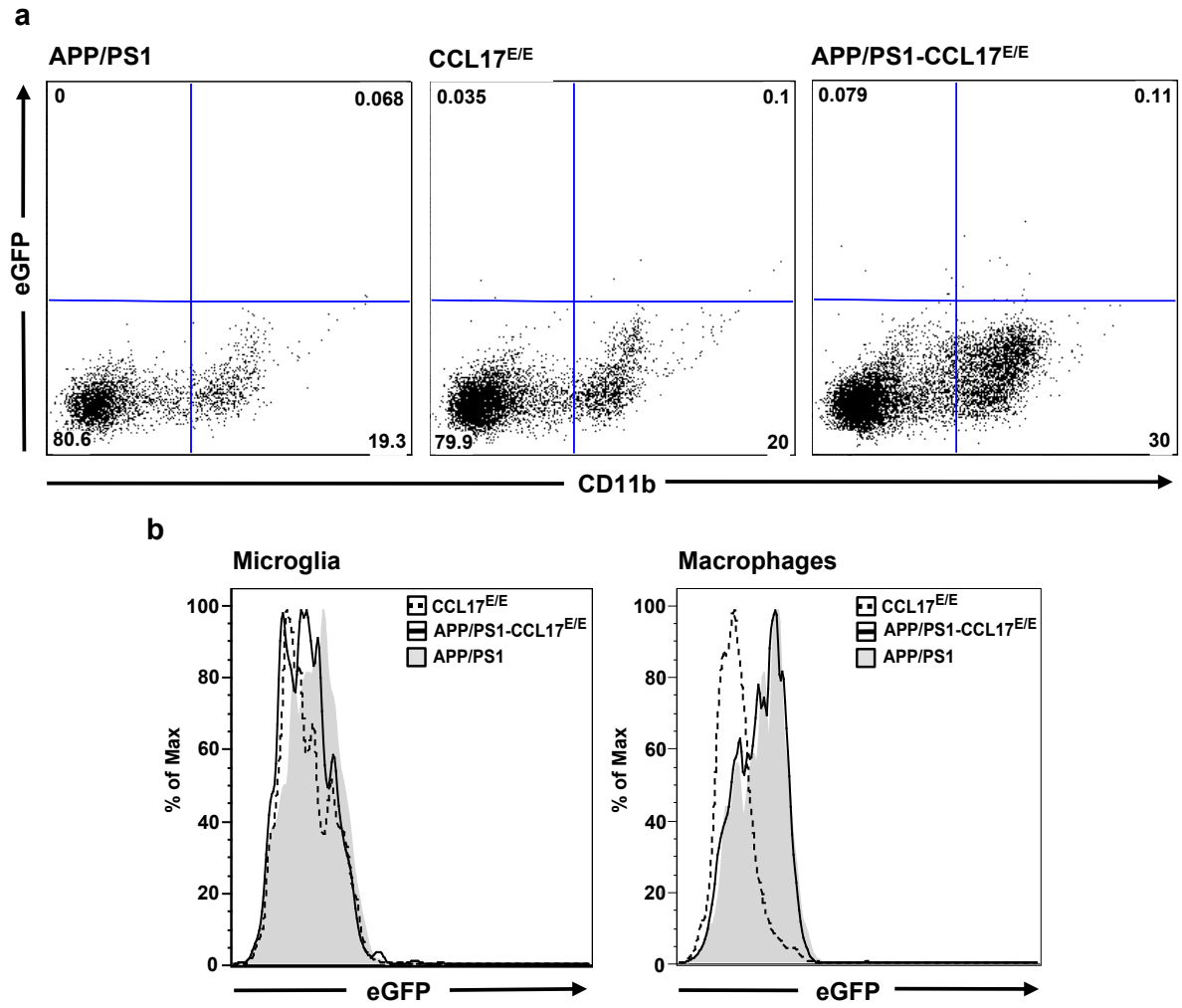

Figure 5.21: **eGFP$^+$ cells are absent in the CNS of APP/PS1-CCL17$^{E/E}$ and CCL17$^{E/E}$ mice** (a) Representative dot plots of CD11b eGFP expression of ICL of aged APP/PS1-CCL17$^{E/E}$ mice (right) and CCL17$^{E/E}$ mice (middle). ICL of aged APP/PS1 mice (left) served as eGFP negative control. (b) Representative eGFP histograms of CD45$^+$CD11b+ gated microglia (left) and macrophages (right) of APP/PS1-CCL17$^{E/E}$ mice (black line) and CCL17$^{E/E}$ mice (black dashed line). APP/PS1 mice (light grey solid curve) served as eGFP negative control.

The cognate receptor CCR4 is predominantly found on Th2 cells, but also on DCs, macrophages, NK cells and other cell types [137]. In addition, CCR4 expression was found in human astrocytes and microglial cells [138] and rat hippocampal neurons [139]. To investigate whether mouse microglia also express CCR4, primary neonatal microglial cells, isolated from WT and CCL17$^{E/E}$ mice were analyzed for *ccr4* mRNA without and after LPS stimulation. RNA from LPS stimulated BM-derived WT DCs served as positive control. LPS stimulated microglia present an extensive upregulation of *ccr4* mRNA compared to unstimulated controls, although CCR4 expression was much more higher in BM-differentiated DCs (Fig.5.22.b).

Beside CCL17, the other known ligand of CCR4 is CCL22. The analysis of *ccl22* mRNA in the hippocampus of APP/PS1-CCL17$^{E/E}$ and CCL17$^{E/E}$ mice revealed an enhanced expression of CCL22 compared to APP/PS1 and WT mice. Interestingly, the CCL22

expression is not changed by APP/PS1 transgene expression (Fig.5.23.a).

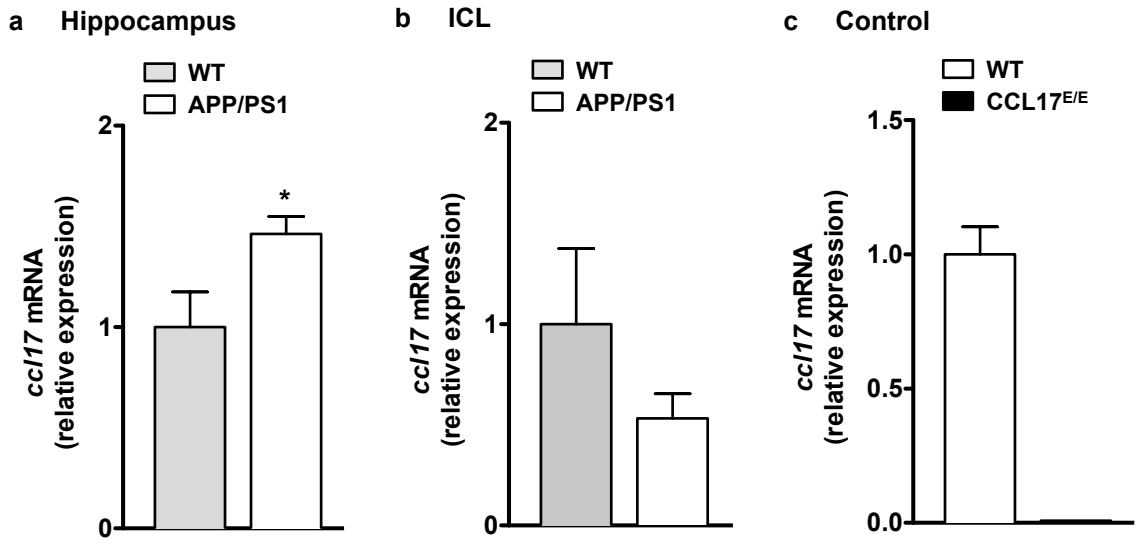

Figure 5.22: **Microglia are a potential source for elevated CCL17 expression in APP/PS1 mice**
(a) Enhanced *ccl17* mRNA expression level in the hippocampus of APP/PS1 mice (grey bar) compared to WT mice (white bar). (b) Isolated ICL of aged APP/PS1 and WT express *ccl17* mRNA. (c) Cortex of CCL17$^{E/E}$ mice did not show *ccl17* mRNA expression in contrast to cortical tissue of WT mice (c). Diagrams show mean relative expression ± SEM. Data analysis: Student's t-test; *p <0.05. (n = 4-9 mice/group)

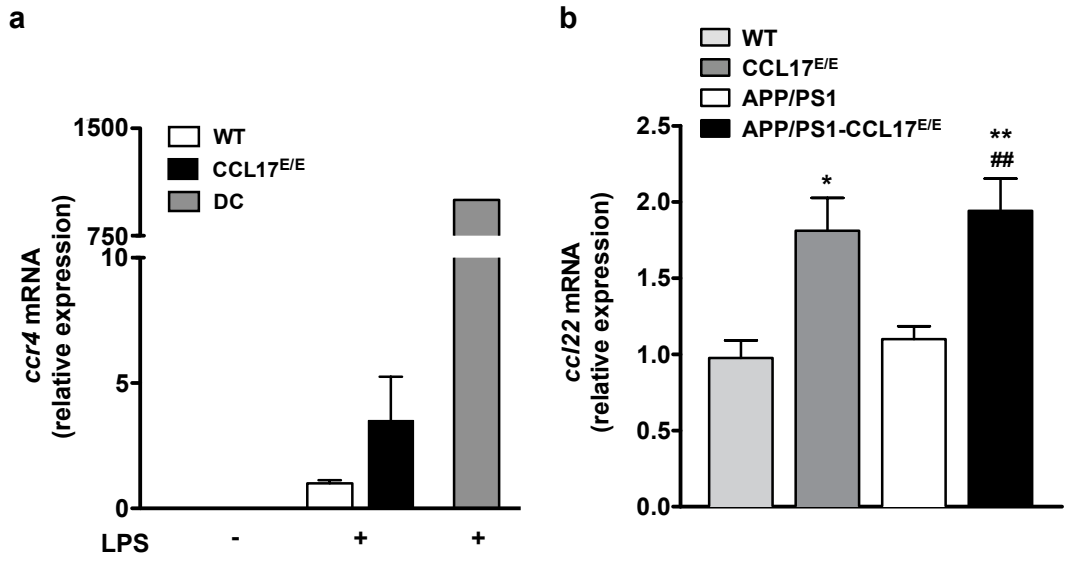

Figure 5.23: **CCR4 is expressed by neonatale microglia after LPS stimulation**
(a) Microglia of WT (white bar) and CCL17$^{E/E}$ (black bar) express *ccr4* mRNA after LPS stimulation, but to a lesser extent than DCs (dark grey bar). (b) Enhanced *ccl22* mRNA expression level in the hippocampus of APP/PS1-CCL17$^{E/E}$ mice (black bar) and CCL17$^{E/E}$ (dark grey) compared to APP/PS1 (white bar) and WT mice (light grey bar). Diagrams show mean relative expression ± SEM. Data analysis: 1-way-ANOVA with Bonferroni *post-hoc*; *p <0.05, **p <0.01 (APP/PS1 *vs.* APP/PS1-CCL17$^{E/E}$), ##p <0.01 (tg *vs.* WT). (a: n = 3 wells / mouse / group; b: n = 4-9 mice/group)

These data clearly show, although eGFP^{+} cells are absent in the CNS of APP/PS1-CCL17$^{E/E}$ and CCL17$^{E/E}$ mice, CCL17 expression is upregulated in the CNS of APP/PS1

mice. Further, microglia cells can express both CCR4 and its ligand CCL17. Interestingly, CCL22 expression is upregulated in the hippocampus of CCL17-deficient mice, but not in APP/PS1 mice.

5.1.8 Upregulation of alternative activation marker MMR and the anti-inflammatory cytokine IL-10 in APP/PS1-CCL17$^{E/E}$ mice

Neuroinflammation in AD is accompanied by the expression of several cytokines such as TNF, IL-6, and IL-1 [21]. In order to investigate the inflammatory profile in APP/PS1-CCL17$^{E/E}$ mice, the expression level of pro-inflammatory cytokines and iNOS, which are often found to be enhanced in AD [22], was analyzed in the hippocampus of aged APP/PS1-CCL17$^{E/E}$ mice compared to age-matched APP/PS1. qRT-PCR analysis revealed equivalent levels of *inos* and *il-1β* (Fig.5.24.a), while *tnf* mRNA (Fig.5.24.a) is not significantly increased (p (*tnf*) = 0.0799). However, the interleukin IL-6 is increased in the hippocampus of aged APP/PS1-CCL17$^{E/E}$ animals (Fig.5.24.a). IL-6 is a pleiotropic cytokine, with pro- and anti-inflammatory properties [140]. It is expressed by microglial cells isolated from the CNS of AD mice [141] and is found to be elevated in AD patients [21], although its role in AD remains unclear [142]. However, after LPS/IFNγ stimulation of neonatal microglial cells, IL-6 protein expression is increased to an equivalent level in the supernatant of both, WT and CCL17$^{E/E}$ microglia (Fig.5.24.b).

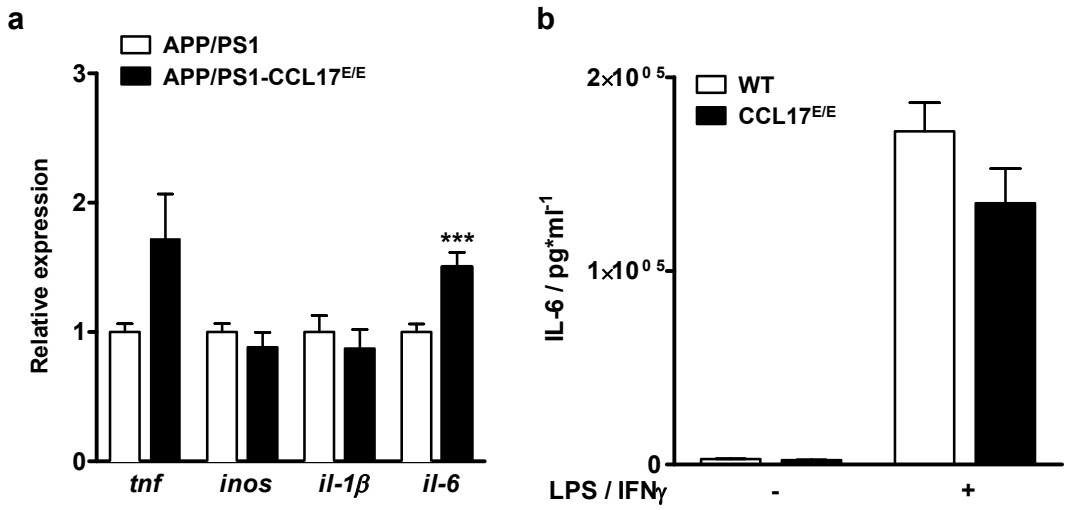

Figure 5.24: **Enhanced IL-6 expression in APP/PS1-CCL17$^{E/E}$ mice**
(a) Analysis of pro-inflammatory cytokines revealed an upregulation of *il-6* mRNA in the hippocampus of aged APP/PS1-CCL17$^{E/E}$ mice (black bar) compared to APP/PS1 mice (white bar). Diagram shows mean relative expression ± SEM. (b) Equivalent IL-6 protein expression by LPS-stimulated WT (white bar) and CCL17$^{E/E}$ (black bar) neonatal microglia. Diagram shows mean ± SEM. Data analysis: Student's t-test, ***p < 0.001. (a: n = 6-9 mice/group; b: n = 3 wells/mouse/group); (Fig.5.24.b: Ramona Göhrs)

Next, the anti-inflammatory profile of aged APP/PS1-CCL17$^{E/E}$ mice was evaluated. Upregulation of anti-inflammatory proteins are often related to an enhanced phagocytic

phenotype of macrophages and microglial cells [64]. qRT-PCR analysis of markers associated with anti-inflammatory functions of macrophages such as YM-1, Arg1, TGF-β, and IL-10 revealed equivalent levels of *ym-1*, *tgf-β*, and *arg1* mRNA in the hippocampus of APP/PS1-CCL17$^{E/E}$ and APP/PS1 mice (Fig.5.25.a). However, the expression of *il-10* is increased in aged APP/PS1-CCL17$^{E/E}$ mice compared to age-matched APP/PS1 mice (Fig.5.25.a). IL-10 is a prototypical anti-inflammatory cytokine, involved in M2 activation of macrophages and enhanced phagocytosis [52].

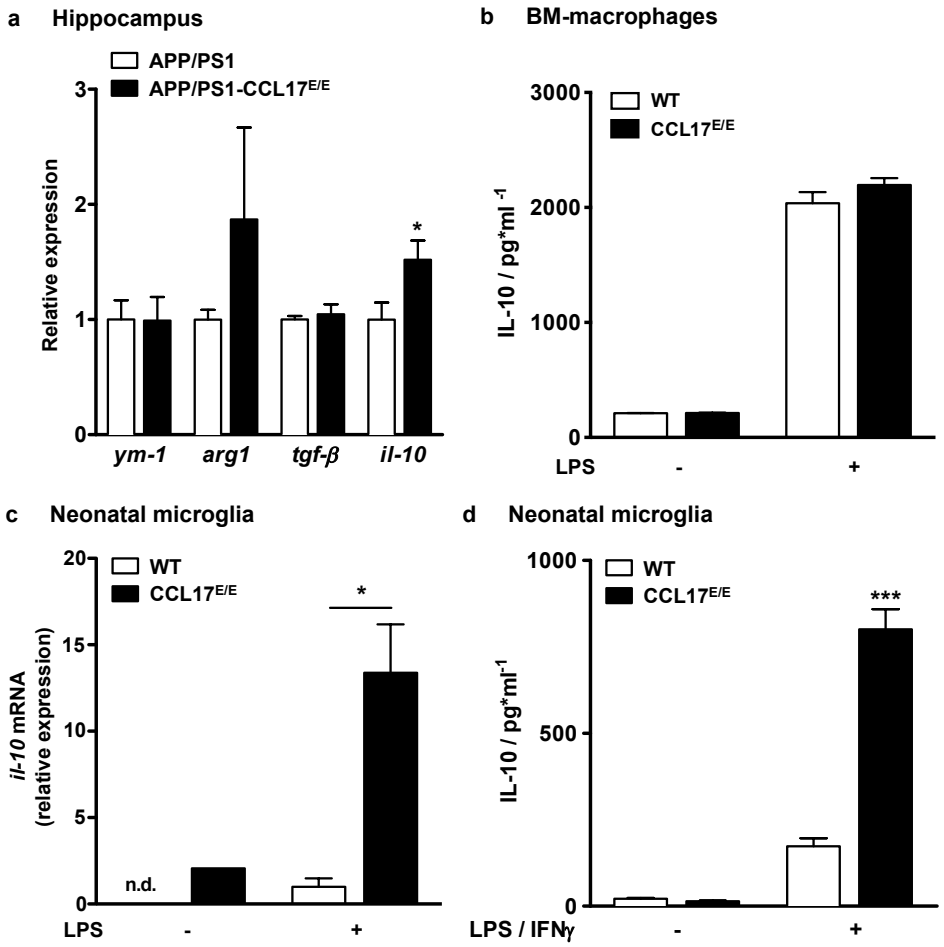

Figure 5.25: **Enhanced IL-10 expression in CCL17-deficient mice**
(a) Analysis of anti-inflammatory cytokines revealed an upregulation of *il-10* (a) in the hippocampus of aged APP/PS1-CCL17$^{E/E}$ mice (black bar) compared to APP/PS1 mice (white bar). Diagram shows mean relative expression ± SEM. (b) Equivalent IL-10 protein expression by LPS-stimulated WT (white bar) and CCL17$^{E/E}$ (black bar) BM-macrophages. Diagram shows mean ± SEM. (c-d) Increased IL-10 mRNA (c) and protein (d) expression by LPS-stimulated WT and CCL17$^{E/E}$ neonatal microglia. Diagrams show mean ± SEM. Data analysis: Student's t-test, *p < 0.05, ***p < 0.001. (a: n = 6-9 mice/group; b-d: n = 3 wells/mouse/group); (Fig.5.25.d: Ramona Göhrs)

To investigate whether macrophages or microglia are the cellular source for IL-10 expression, supernatant of BM-derived macrophages and neonatal microglial cells from WT and CCL17$^{E/E}$ mice were analyzed for IL-10 production. Interestingly, BM-macrophages of WT and CCL17$^{E/E}$ mice showed increased IL-10 protein secretion after LPS stimulation, but differences between both strains were not detected (Fig.5.25.b). In contrast,

neonatal microglial cells of CCL17$^{E/E}$ mice exhibit enhanced IL-10 mRNA and protein expression level compared to WT cells (Fig.5.25.c, d).

The higher expression of IL-6 in the HC of APP/PS1-CCL17$^{E/E}$ mice indicates a higher activation state in these mice compared to APP/PS1 mice. Further, the expression of IL-10 indicates a shift towards a more alternative activation state in these cells, which is often accompanied by enhanced macrophage mannose receptor (MMR) expression [63, 66]. In order to further characterize the ICL of APP/PS1-CCL17$^{E/E}$ and APP/PS1 mice, the expression of CD40 and MMR of intracerebral microglia and macrophages was assessed by flow cytometric analysis.

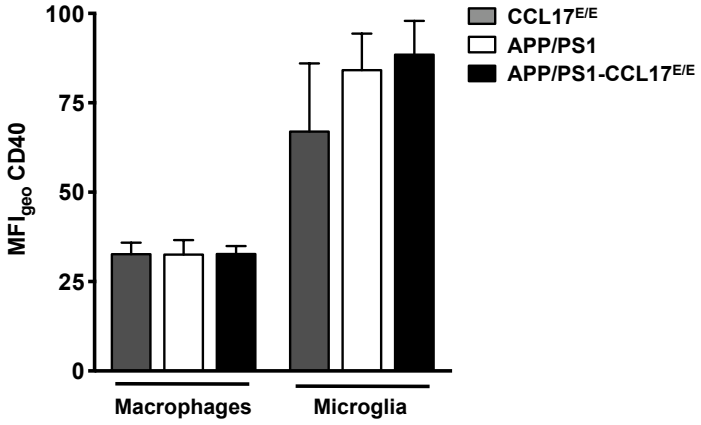

Figure 5.26: **Equivalent CD40 expression by microglia**
Flow cytometric analysis of surface expression of CD40 in aged APP/PS1-CCL17$^{E/E}$ mice compared to APP/PS1 mice. Equivalent mean fluorescence intensity of CD40^{+} microglia and macrophages in aged APP/PS1-CCL17$^{E/E}$ mice compared to APP/PS1 mice. Diagram shows mean MFI$_{geo}$ ± SEM. Data analysis: Student's t-test. (n = 3-4 mice/group)

The co-stimulatory molecule CD40 is often used as a marker for activated microglial cells in AD [128]. The analysis of the geometric mean fluoresence intensity of CD40 (MFI$_{geo}$ CD40) of macrophages and microglial cells from the CNS of APP/PS1-CCL17$^{E/E}$, APP/PS1, and CCCL17$^{E/E}$ mice revealed an increased CD40 expression by microglial cells in APP/PS1-CCL17$^{E/E}$, APP/PS1, and CCL17$^{E/E}$ mice, whereas macrophages showed a lower expression of CD40. Unexpectedly, CCL17$^{E/E}$ mice exhibit similar MFI$_{geo}$ CD40 like both AD mouse strains, although increased CD40 expression were found in the CNS of APP/PS1-CCL17$^{E/+}$ mice compared to CCL17$^{E/+}$ mice. However, APP/PS1-CCL17$^{E/E}$ mice present increased numbers of MMR^{+} macrophages and microglia isolated from the CNS compared to APP/PS1 mice (Fig.5.27). Interestingly, the amount of MMR^{+} microglia was much higher ($\sim$ 6x10^{4}) (Fig.5.27.b) than MMR^{+} macrophages ($<$ 1x10^{4}) (Fig.5.27.c).

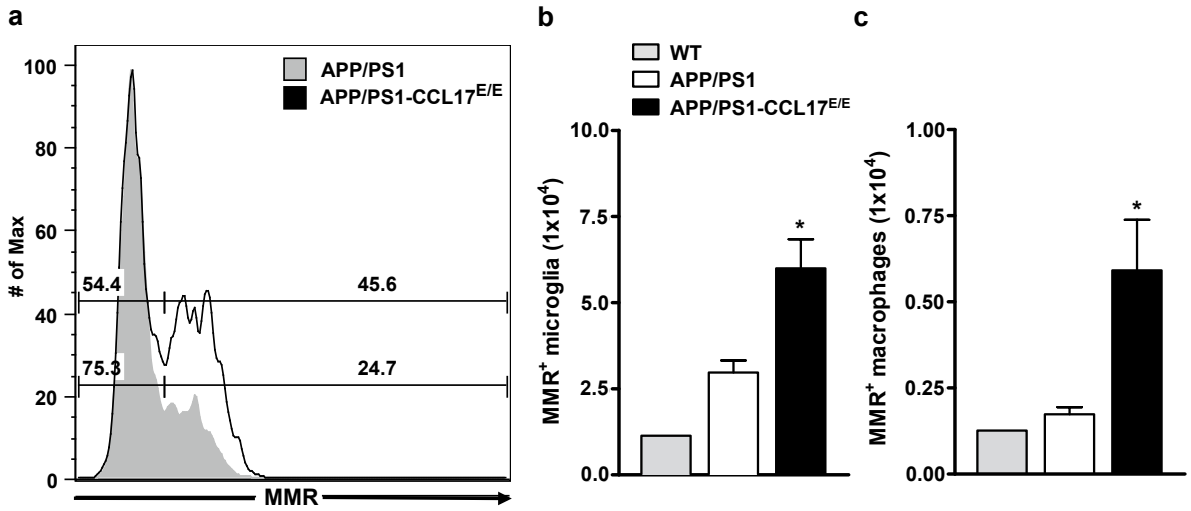

Figure 5.27: **Enhanced MMR expression in APP/PS1-CCL17$^{E/E}$ mice**
(a) Representative overlays of MMR histogram of microglia isolated from the CNS of aged APP/PS1-CCL17$^{E/E}$ (black line) and APP/PS1(light grey solid curve) mice. (b-c) Enhanced numbers of MMR$^+$ microglia (b) and macrophages (c) in the CNS of aged APP/PS1-CCL17$^{E/E}$ mice (black bar) compared to APP/PS1 (white bar) mice. Diagrams show mean ± SEM. Data analysis: Student's t-test, *p <0.05. (n = 4 mice/group, 1 WT)

Altogether, these data show an altered inflammatory milieu in the CNS of APP/PS1-CCL17$^{E/E}$ mice compared to APP/PS1 mice as given by enhanced IL-6 and IL-10 production together with increased numbers of MMR$^+$ macrophages and microglial cells indicating a shift of intracerebral microglia and macrophages towards an alternative activation or M2 type.

5.1.9 Phagocytosis and degradation of Aβ

Alternative activation is related to a supressor phenotype of macrophages and enhanced phagocytic ability of these cells [52, 66]. In order to investigate, whether CCL17$^{E/E}$ microglia or macrophages show enhanced Aβ uptake, phagocytosis assays of fluorescently-labeled Aβ1-42 peptides by BM-derived macrophages and neonatal microglia were performed. First, the internalization and degradation rate of Aβ_{42}-DyeLight649 *in vitro* by BM-derived macrophages of CCL17$^{E/E}$ and WT mice was measured. For this, Aβ_{42}-DyeLight649 peptides were added to BM-macrophages for 15 min in which the internalization process takes place. Intracellular localization of Aβ was verified by EEA-1 / Aβ double positive cells and analysis of z-stack images of Aβ_{42}-DyeLight649$^+$ cells was performed. Representative z-stack images of Aβ_{42}-DyeLight649$^+$ cells are depicted in Fig.5.28.a. As shown in Fig.5.28.b, the internalization rate given by counted particles within the cells is equivalent in both CCL17$^{E/E}$ and WT macrophages. Flow cytometric analysis of Aβ_{42}-DyeLight649$^+$ BM-macrophages after 15 min of internalization confirmed this showing an equivalent MFI$_{geo}$ of Aβ_{42}-DyeLight649$^+$ BM-macrophages, although a relatively high background for the 4°C controls were found (Fig.5.28.c).

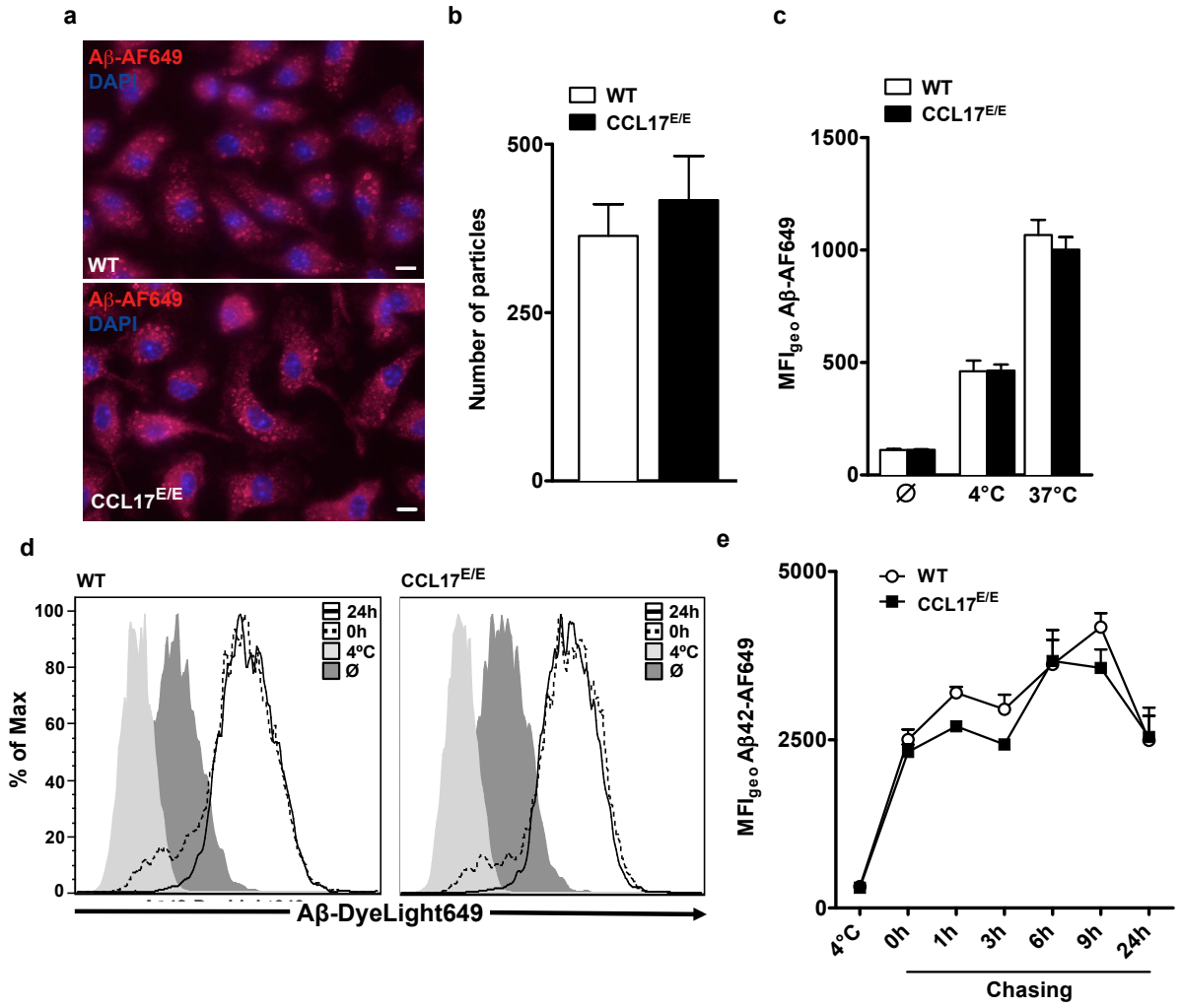

Figure 5.28: **Equivalent Aβ phagocytosis by CCL17$^{E/E}$ and WT macrophages**
(a-c) Internalization assay of Aβ_{42}-DyeLight649 by BM-derived macrophages. (a) Representative z-stack images of BM-macrophages of WT (upper panel) and CCL17$^{E/E}$ (lower panel) (scale bar = 15 μm). (b) Equivalent number of particles of internalized Aβ_{42}-DyeLight649 in BM-macrophages of CCL17$^{E/E}$ (black bar) and WT (white bar). Diagrams show mean ± SEM. (c) Flow cytometric analysis of MFI$_{geo}$ of Aβ_{42}-DyeLight649^{+} BM-derived macrophages of CCL17$^{E/E}$ and WT mice. Diagram shows mean ± SEM. (d-e) Degradation assay of Aβ_{42}-DyeLight649 by BM-derived macrophages. (d) Representative overlays of Aβ_{42}-DyeLight649 histograms of unstimulated (light grey solid curve) samples, at 4◦C (dark grey solid curve), at chasing time point 0 h (black dashed line), and after 24 h of chasing (black line) are shown for WT (left) and CCL17$^{E/E}$ (right) BM-macrophages. (e) Equivalent MFI$_{geo}$ of Aβ_{42}-DyeLight649^{+} BM-derived macrophages of CCL17$^{E/E}$ (black square) and WT (open circle) mice. Curves represent mean MFI$_{geo}$ ± SEM of samples taken within 24 h at different time points after medium exchange and 4°C sample as phagocytosis negative control. Data analysis: 1-way-ANOVA with Bonferroni *post-hoc*. (n = 3 wells/mouse/group)

It was also reported that BM-derived macrophages are able to degrade Aβ *in vitro* [143]. In a second approach, Aβ_{42}-DyeLight649 petides were incubated with the BM-macrophages for 1 h and after medium exchange with Aβ_{42}-DyeLight649-free medium, chasing of the degradation of intracellular localized Aβ_{42}-DyeLight649 within 24 h was achieved by flow cytometry (Fig.5.28d-e). Fig.5.28.e shows degradation curves of MFI$_{geo}$ of Aβ_{42}-DyeLight649^{+} BM-macrophages of several time points within 24 h. However, a

degradation of Aβ_{42}-DyeLight649 as given by MFI$_{geo}$, was not found. In addition, the MFI$_{geo}$ of Aβ_{42}-DyeLight649 was equivalent in both groups for 24 h.

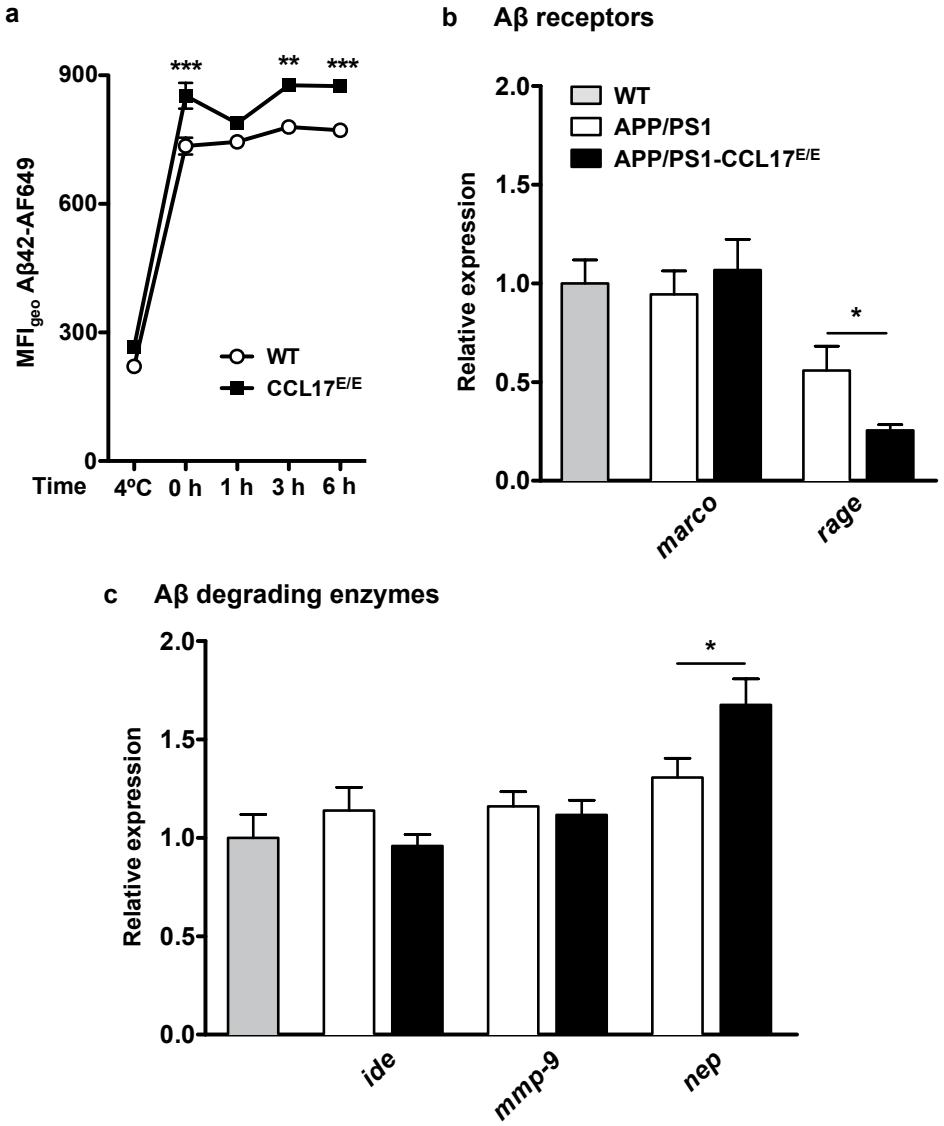

Figure 5.29: **Enhanced Aβ uptake by CCL17$^{E/E}$ microglia, reduced RAGE and enhanced neprilysin expression levels**
(a) Curves represent mean MFI$_{geo}$ ± SEM of Aβ_{42}-DyeLight649^{+} neonatal microglia of CCL17$^{E/E}$ and WT mice within 6 h of chasing after medium exchange. Neonatal microglia derived from CCL17$^{E/E}$ mice showed enhanced Aβ phagocytosis compared to WT microglia. (b-c) Diagrams show mean relative expression ± SEM of Aβ receptors (b) and Aβ degrading enzymes (c). Equivalent hippocampal expression of *marco* (b), *ide* (c), and *mmp-9* mRNA (c) in the hippocampus of aged APP/PS1-CCL17$^{E/E}$ and APP/PS1 mice. APP/PS1-CCL17$^{E/E}$ mice exhibit reduced *rage* (b) and increased *nep* mRNA expression (c) in the hippocampus compared to APP/PS1 mice. Data analysis: 1-way-ANOVA with Bonferroni *post-hoc* (a) and Student's t-test (b, c), *p < 0.05, **p < 0.01, ***p < 0.001. (n = 3 wells/mouse/group). (Fig.5.29.a: Ramona Göhrs)

Then, the phagocytosis capacity of neonatal microglia for Aβ_{42}-DyeLight649 was also performed. Here, flow cytometric analysis revealed that chasing of Aβ degradation for 6 h did not lead to a decrease of MFI$_{geo}$ of Aβ_{42}-AF649^{+} microglia. But, a significant higher uptake of Aβ_{42}-DyeLight649 by CCL17$^{E/E}$ microglial cells compared to WT microglia

was found (Fig.5.29.a).

Decreased soluble Aβ levels in the CNS of aged APP/PS1-CCL17$^{E/E}$ mice together with a higher Aβ uptake by CCL17$^{E/E}$ microglial cells raised the question, whether the expression levels of receptors and enzymes involved in the uptake and degradation of Aβ peptides are altered in APP/PS1-CCL17$^{E/E}$ mice. Major Aβ receptors are the receptor for advanced glycation end products (RAGE) and the macrophage receptor with collagenous structure (MARCO), whereas important degradation enzymes are insulin-degrading enzyme (IDE), matrix-metalloprotease-9 (MMP-9), and neprilysin (NEP) [38, 144, 145]. To adress this, qRT-PCR analysis of mRNA levels of the Aβ receptors RAGE and MARCO, as well as the Aβ degrading enzymes IDE, MMP-9, and NEP in the hippocampus of APP/PS1-CCL17$^{E/E}$ and APP/PS1 mice was assessed. Equivalent levels of *marco*, *ide*, and *mmp-9* mRNA were measured in the HC of aged APP/PS1-CCL17$^{E/E}$ and APP/PS1 mice (Fig.5.29.b, c). However, RAGE expression level is decreased in APP/PS1-CCL17$^{E/E}$ mice compared to APP/PS1, while NEP expression level is increased (Fig.5.29.b, c). These data suggest a reduced Aβ-RAGE signaling in APP/PS1-CCL17$^{E/E}$ mice, together with a probably enhanced Aβ degradation due to enhanced NEP expression.

These data show that CCL17$^{E/E}$ deficient microglia, but not macrophages exhibit an enhanced phagocytic capacity of Aβ *in vitro*, but differences in degradation were not detected. In addition, aged APP/PS1-CCL17$^{E/E}$ mice present reduced RAGE, but enhanced NEP expression in the hippocampus, indicating an altered Aβ signaling and processing compared to age-matched APP/PS1 mice.

5.2 Determination of human CCL17 protein level in plasma samples of elderly patients

CCL17 is an inducible chemokine found to be involved in several human diseases. So, it was found at higher concentrations in the serum of patients with atopic dermatitis [112] and in cerebrospinal fluid (CSF) and serum of multiple sclerosis (MS) patients [117, 146]. In order to investigate a possible role of CCL17 as a biomarker for Alzheimer's disease, CCL17 concentrations in CSF and plasma samples of AD patients should be determined.

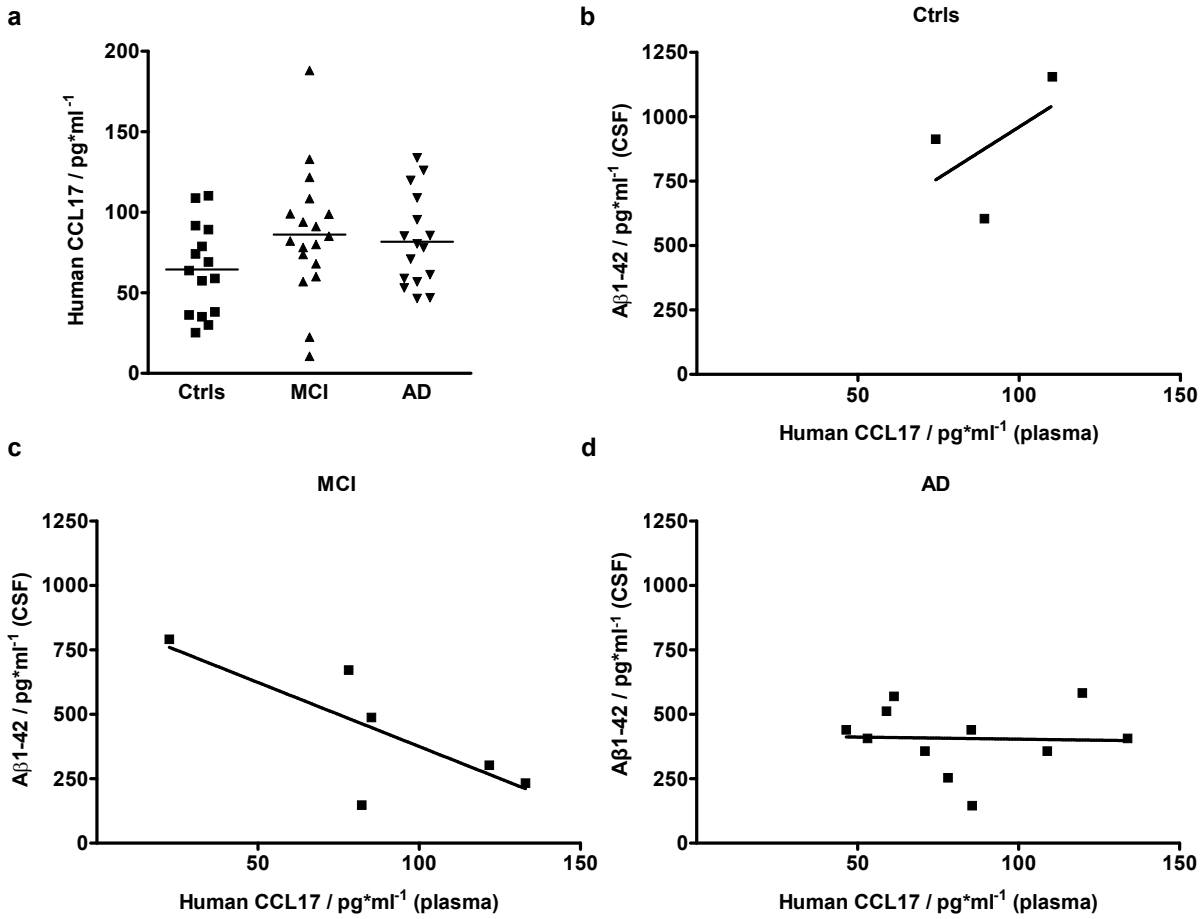

Figure 5.30: **Analysis of human plasma CCL17 protein**
Pretest for human plasma CCL17 concentration and its correlation with Aβ concentration in cerebrospinal fluids (CSF) of elderly patients. (a) Diagram shows mean ± SEM of CCL17 protein concentration in Ctrls, MCI, and AD patients. Each dot represent one value. (b-d) Diagrams show CSF Aβ *vs.* CCL17 concentration. Each dot represent one subject. Ctrls = healthy for MCI or AD, MCI = mild cognitive impairment, AD group = Alzheimer's disease. Data analysis: 1-way-ANOVA with Bonferroni *post-hoc* (a), Pearson correlation assay, p = 0.6500, r = 0.5225 (b); p = 0.0814, r = -0.7570 (c); p = 0.9167, r = -0.03585 (d). (n = 15-18 (a); n = 3 (b), 6 (c), and 11 (d))

First, the concentration of CCL17 in CSF samples were evaluated using human CCL17 ELISA. However, the detection of CCL17 protein failed in samples of AD patients and in healthy controls (data not shown).

Then, the analysis of plasma CCL17 levels of healthy controls, patients with mild cog-

nitive impairment (MCI), and AD patients was performed. In healthy controls a concentration of 64.48 pg/ml ± 7.201 was found, whereas in both, MCI and AD, concentrations of 86.21 pg/ml ± 9.334 and 81.75 pg/ml ± 7.086 were measured (Fig.5.30.a). Next, correlation assays for plasma CCL17 concentrations, found in these patients, with the respective CSF Aβ1-42 levels were performed for all three groups. As shown in Fig.5.30.d, a correlation between plasma CCL17 and CSF Aβ of AD patients could not be found. Nevertheless, a negative correlation curve was found in MCI patients, although it is not significant (Fig.5.30.c). The Pearson coefficient (r = -0.7570) showed a tendency to -1, indicating a correlation for CCL17 and Aβ1-42 in these patients. To verify this, the experiment for MCI patients were repeated with a higher number of samples. However, performing the correlation assay for serum CCL17 and CSF Aβ1-42 revealed a Pearson coefficient of r = -0.06714 and thereby not confirming the initial result (Fig.5.31).

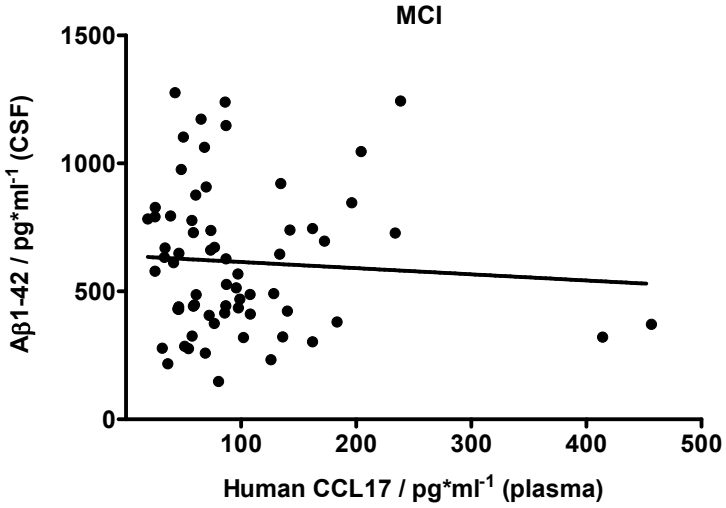

Figure 5.31: **Human plasma CCL17 did not correlate with CSF Aβ levels in MCI patients**
Correlation assay was performed for human plasma CCL17 levels with CSF Aβ levels in MCI patients. Diagram show CSF Aβ *vs.* CCL17 concentration. Each dot represent one patient. Data analysis: Correlation assay with Pearson, p = 0.5922, Pearson coefficient r = -0.06714. (n= 66)

6 Discussion

In the Alzheimer's disease international (ADI) World Alzheimer's report it was estimated that 2010 more than 36 million people worldwide would suffer from dementia. Around US$604 billion were calculated by ADI for dementia care worldwide. Without a breakthrough in the treatment, due to the higher life expectancy, the number of AD patients will be doubled in twenty years [147].

Although the biochemical cause for Aβ generation is well-researched, the principal reason for developing AD is totally unclear and is controversially discussed since more than 100 years. New insights by basic experimental and clinical studies using new and sophisticated technicological approaches visualize a more complex view of causes for developing AD. Genetical studies have identified more than hundred different gene mutations leading to familial AD. Results of epidemiological studies took into account environmental stress factors, smoking, diabetes and other risk factors. And at last, many post mortem studies and experiments using animal models of AD featured chronic or acute inflammation at least as a bystander if not as a cause for AD development [21, 25, 148]. The purpose of this work was to unravel a potential role of the chemokine CCL17 in inflammatory mechanisms occuring in AD using a CCL17-deficient APP/PS1 mouse strain, APP/PS1-CCL17$^{E/E}$.

6.1 Analysis of APP/PS1-CCL17$^{E/E}$ mice

6.1.1 APP/PS1-CCL17$^{E/E}$ mice exhibit improved cognitive performance, reduced neuronal loss and sAβ burden

First, the phenotypic behavior of APP/PS1-CCL17$^{E/E}$ mice in a survival paradigm and in the Morris water maze test was assessed. For the investigation of the survival rate, mice were weekly controlled from three to nine months of age, and fatalities were noted. Survival analysis revealed a death rate of 15 % for APP/PS1-CCL17$^{E/E}$ mice within this time, whereas 25 % of APP/PS1 mice did not survive. WT mice had a death rate of 11 %. A previous study reported a pre-mature death rate of approximately 35 % for APP/PS1 mice before six months of age, whereas after six months of age death events were less common [129].

Cognitive deficits of APP/PS1 mice were shown at 12 months of age [17, 130] using Morris water maze (MWM), and at six months of age using a radial arm water maze [129]. Here, in this study, aged APP/PS1-CCL17$^{E/E}$ mice had a similar escape latency

like WT during the acquisition trial, and they spent a similar time period in the target quadrant during probe trial. In contrast, APP/PS1 mice showed a significant impaired cognitive behavior in both tasks, as described earlier [19]. These data clearly show a WT-like learning and memory ability of aged APP/PS1-CCL17$^{E/E}$ mice in contrast to age-matched APP/PS1 mice.

The overexpression of APP together with presenilin-1 leads to remarkable Aβ production even in young [129] and with a strong correlation effect on cognitive functions in aged mice [130]. Most studies showed that modulation of inflammatory responses influencences cerebral amyloidosis and behavioral phenotype of AD mice in the same manner [40, 60, 91]. Therefore, the amount of extracellular deposits, soluble Aβ oligomers and soluble Aβ_{40} and Aβ_{42} peptides in aged APP/PS1-CCL17$^{E/E}$ mice was evaluated. In addition, the amount of soluble Aβ_{40} and Aβ_{42} in the CNS and serum Aβ_{42} level of young and middle-aged mice were assayed in order to investigate age-dependent alterations in APP/PS1-CCL17$^{E/E}$ mice compared to APP/PS1 mice.

Interestingly, although intracerebral Aβ_{40} and Aβ_{42} levels were significant higher in young APP/PS1-CCL17$^{E/E}$ mice compared to age-matched APP/PS1 controls, in the middle-aged group differences between APP/PS1-CCL17$^{E/E}$ and APP/PS1 mice were not found. Further, serum levels of Aβ_{42} were significant reduced in young APP/PS1-CCL17$^{E/E}$ mice compared to APP/PS1 mice, equivalent serum levels were found in middle-aged mice. However, these data indicate an age-dependent remarkable increase of intracerebral and serum Aβ level in both, APP/PS1-CCL17$^{E/E}$ and APP/PS1 mice between six and nine months of age.

The determination of Thioflavin-stained amyloid plaques in the cortex and the hippocampus of aged APP/PS1-CCL17$^{E/E}$ and APP/PS1 mice revealed no differences neither in the precentaged area occupied by extracellular deposits nor in the mean size of these plaques, indicating the good cognitive performance of aged APP/PS1-CCL17$^{E/E}$ mice is not due to a reduced deposition of fibrillary Aβ. In a previous study it was shown, soluble Aβ, but not amyloid plaques and insoluble Aβ, correlates with cognitive deficits of 12-months-old APP/PS1 mice [130]. In line with this data, aged APP/PS1-CCL17$^{E/E}$ mice present significant reduced soluble Aβ oligomers as shown by western blot analysis, while middle-aged mice did not show differences in oAβ levels. Additionally, although soluble Aβ_{40} levels were equivalent, soluble Aβ_{42} levels were reduced in the CNS of these mice compared to APP/PS1 mice, indicating a detrimental effect on neuronal survival and cognitive functions for Aβ_{42} and soluble Aβ oligomers rather than Aβ_{40} and extracellular deposits. Several *in vitro* studies featured a higher neurotoxicity of Aβ_{42} monomers than Aβ_{40} [9]. Except for Aβ clearance by phagocytosis and degradation, a reduction of intracerebral Aβ levels can be due to several reasons. Increased insoluble Aβ deposits reduces the soluble Aβ concentration isolated from the brain. Also, diminished plasma Aβ concentrations have been correlated to increase brain Aβ levels pointing to the importance of Aβ efflux from the CNS into the periphery [43]. However, aged APP/PS1-CCL17$^{E/E}$

mice did not show enhanced serum Aβ_{42} levels. Also, increased plaque deposition was not found in the CNS of aged APP/PS1-CCL17$^{E/E}$ mice, therefore increased Aβ uptake and / or degradation could be one possibility. In generally, serum Aβ_{42} and soluble Aβ_{40} levels increased remarkable during aging in both strains, while soluble Aβ_{42} concentration increased in APP/PS1 mice, but remained nearly constant in APP/PS1-CCL17$^{E/E}$ mice.

Previously it was suggested that the principal cause for cerebral dystrophy and cognitive decline in AD patients and AD mice are extracellular deposits and Aβ fibrils [9, 150, 133]. However, based on recent data the hypothesis raised that Aβ monomers, especially Aβ_{42}, and Aβ oligomers are the neurotoxic compounds in the CNS rather than Aβ deposits [132, 151, 152, 153]. AD patients show successive cognitive impairments and severe neuronal dysfunction [154, 150]. In mouse models of AD, this frank neuronal loss is not observed [1, 19], but many strains exhibit neuritic dystrophies [15, 155], hippocampal interneuron loss [156], or decreased neuronal activity in plaque environment [157]. The neuronal integrity of aged APP/PS1-CCL17$^{E/E}$ mice were determined for NeuN$^+$ mature neurons. APP/PS1 displayed a marked loss of NeuN$^+$ CA3 neurons, whereas APP/PS1-CCL17$^{E/E}$ showed WT-like NeuN pattern. Some studies revealed diminished neurogenesis as shown by BrdU$^+$/NeuN$^+$ [158] or DCX$^+$ labeled neurons [159] within the hippocampal region of these APP/PS1 mice, although a general reduction of NeuN$^+$ neurons was not reported. On the other hand, in these studies, mice were analyzed at an age of eight [158] and nine [159] months, respectively, hence a progressively impaired neurogenesis with aging potentially can be manifested by a loss of NeuN$^+$ cells in aged APP/PS1 mice. In another approach, the authors found a significant reduction of NeuN expression in the brain of 8-months-old APP/PS1 mice lacking the hematopoetic cell marker CD45 (PSAPP/CD45 (-/-)), but not in age-matched CD45-sufficient PSAPP littermates, indicating an increased neurotoxic environment due to CD45 ablation [43]. Further investigation is needed to examine, whether diminished neuronal loss in APP/PS1-CCL17$^{E/E}$ mice compared to APP/PS1 mice is due to increased neurogenesis or decreased cell death. In addition, an increased *bdnf* expression was found in the hippocampus of APP/PS1 mice, whereas APP/PS1-CCL17$^{E/E}$ mice exhibit equivalent levels like control mice. BDNF levels were found increased in MCI and patients with mild AD, whereas it was decreased in patients with severe AD, suggesting a kind of compensatory mechanism in earlier stages, but probably absent in later stages [123]. These data suggest an altered neuronal environment in aged APP/PS1 mice in which the growth factor BDNF is upregulated in response to an increased neuronal loss.

6.1.2 Analysis of APP/PS1-CCL17$^{E/+}$ reporter mice

The overexpression of APP/Aβ in AD mice results in a massive accumulation of Aβ deposits and simultaneously severe neuroinflammation within the CNS. In AD patients and in mouse models of AD several studies showed an enhanced intracerebral inflammatory response as given by enhanced cell activation, particularly glia cells (gliosis), as well as

expression of inflammatory mediators by these cells, e.g. inducible nitric oxide synthetase (iNOS), TNF-α, IL-1β, or CCL2 [21, 50]. Moreover, an alteration of several peripheral inflammation markers, mostly enhanced serum or plasma levels of cytokines and chemokines, are detectable in AD patients and mouse models of AD [93, 121]. In spleen and blood of 3xTg-AD mice increased percentages of $CD8^+$ memory T cells and $CCR6^+$ B cells were found compared to WT mice [93]. Also, the perivascular drainage of Aβ from the CNS to cervical lymph nodes (LN_{cerv}) was discussed for humans [125, 126] and further it has been shown that a DC-mediated $CD4^+$ T cell entry into the CNS in response to Aβ accumulation around cerebral blood vessels occur in mice [149]. Indeed, own observations confirmed the hypothesis that peripheral circulating Aβ can be phagocytosed by $CD11c^+$ DCs and possibly presented to T cells by upregulation of MHC II-Aβ antigen complex [127]. Here, the influence of APP/PS1 expression on peripheral immune cells of heterozygous APP/PS1-$CCL17^{E/+}$ mice after disease onset was investigated. For this, flow cytometric analysis of $CD11b^+$, $CD11c^+$ myeloid cells, or TCR^+ T cells in the spleen, lymph nodes (LN), and blood of 10-12 months old APP/PS1-$CCL17^{E/+}$ was performed. In addition, cerebral immune responses were assayed by flow cytometric analysis of intracerebral leukocytes (ICL) for CNS-resident microglia ($CD45^{low}CD11b^{high}$), invading monocytes / macrophages ($CD45^{high}CD11b^{high}$), and invading lymphocytes ($CD45^{high}CD11b^-$). The activation status of ICL was assessed by their CD40 expression. The analysis of immune cells in peripheral lymphoid organs, spleen, LN, and blood of APP/PS1-$CCL17^{E/+}$ mice revealed no alterations in numbers of myeloid or lymphoid cells compared to $CCL17^{E/+}$ controls. These initial findings indicate that peripheral immune cells were not affected by the overexpression of APP/Aβ in $CCL17^{E/+}$ mice. However, it is possible that a more detailed analysis of specific activation markers like CD40 and MHC II could reveal inflammatory changes in the periphery of these mice. The date of analysis was selected for marked plaque progression, as reported for APP/PS1 mice older than six months of age [129]. Except of increased CD40 expression, which is always linked to microglial activation in AD mouse models [43, 128], increased microgliosis was not detectable in these mice, though analysis at a later date could possibly disclose an enhanced inflammatory response in brain or periphery.

Furthermore, eGFP/CCL17 expression in spleen, LN, blood, and brain was investigated using flow cytometry. It has been shown, using $CCL17^{E/+}$ and $CCL17^{E/E}$ mice that CCL17 is expressed by mature DCs found in lung, lymph nodes, and skin, and upregulated upon TLR-ligand stimulation [101]. Although normally absent in spleen [101], $eGFP^+$ DCs were found in spleen after NKT cell-mediated licensing to be crucial for cross presentation [113]. However, eGFP expressing DCs in $LN_{ax,mes}$, LN_{cerv}, and spleen were equivalent for APP/PS1-$CCL17^{E/+}$ and $CCL17^{E/+}$ mice. The expression of eGFP in the spleen was below 0.1 %, as it was previously reported [101]. In addition, $eGFP^+$ cells were not found in brain or blood in both APP/PS1-$CCL17^{E/+}$ and $CCL17^{E/+}$ mice. However, previous analysis of brain slices of APP/PS1-$CCL17^{E/+}$ and $CCL17^{E/+}$ mice by confocal

microscopy support these findings [127].

6.1.3 Increased microgliosis and infiltration of peripheral macrophages in APP/PS1-CCL17$^{E/E}$ mice

Inflammation in AD brains of patients and mouse models are characterized by a marked astrocytosis and microgliosis [150]. Astrocytosis is marked by increased GFAP surface expression, while microgliosis can be measured by CD11b expression [136]. Diminished neuronal loss was found in aged APP/PS1-CCL17$^{E/E}$ mice in contrast to age-matched APP/PS1 mice. Neuronal loss is often accompanied by reactive astrocytes or microglial cells that are either cause or defense for neuronal degeneration [160, 161]. Investigation of GFAP^{+} astrocytes and CD11b^{+} microglial cells within the CNS of aged APP/PS1-CCL17$^{E/E}$ mice revealed equivalent astrocytosis in APP/PS1-CCL17$^{E/E}$ and APP/PS1 mice, whereas microgliosis is enhanced in APP/PS1-CCL17$^{E/E}$ mice. These data indicate an enhanced neuroinflammatory response in APP/PS1-CCL17$^{E/E}$ mice, without neurotoxic effects in these mice. Furthermore, flow cytometric analysis of CD11b^{+} cells in young and middle-aged groups revealed an age-dependent increase of microgliosis in both mouse strains, which is more pronounced in APP/PS1-CCL17$^{E/E}$ mice.

Increased microgliosis can be due to enhanced proliferation of CNS-resident microglial cells or due to infiltration of peripheral monocytes that proliferate into tissue-macrophages and can renew microglia population [162, 163]. The origin of CD11b^{+} cells in the CNS of APP/PS1-CCL17$^{E/E}$ mice was investigated by analysis of CD45 and CD11b phenotype of intracerebral leukocytes (ICL). Small numbers of lymphocytes, but increased numbers of macrophages and microglial cells were found in APP/PS1-CCL17$^{E/E}$ mice compared to APP/PS1 mice. Invading monocytes / macrophages in AD brains are often characterized by the expression of CCR2 surface expression. Further, it has been shown that CCR2^{+} macrophages are critical in plaque clearance and cognitive performance in APP/PS1 mice [42, 164]. The investigation of CCR2 expression within the CNS of APP/PS1-CCL17$^{E/E}$ mice revealed an increase of *ccr2* mRNA in young and middle-aged APP/PS1-CCL17$^{E/E}$ mice compared to APP/PS1 mice, although it was not significant in aged mice. However, flow cytometric analysis of ICL revealed the highest CCR2 expression on invading macrophages in aged mice, and it was enhanced on macrophages derived from the CNS of APP/PS1-CCL17$^{E/E}$ and APP/PS1 mice compared to non-tg controls. Additionally, total numbers of CCR2^{+} cells were increased in aged APP/PS1-CCL17$^{E/E}$ mice compared to APP/PS1 mice. Furthermore, phenotypically characterization of intracerebral Ly6C^{high}CCR2^{+} macrophages showed that they were enhanced in APP/PS1-CCL17$^{E/E}$ mice compared to APP/PS1 mice, but totally absent in non-tg controls. In generally, Ly6C^{+}CCR2^{+} monocytes, derived from adult bone marrow, circulate in the peripheral blood until they immigrate into tissue where they proliferate into DCs, macrophages, or in case of inflamed CNS into microglial cells [71, 163]. It has also been shown in

CCR2-deficient mice that CCR2 expression is critical for the intracerebral localization of Ly6C^{high}CCR2^{+} monocytes in the context of EAE (experimental autoimmune encephalomyelitis) development [165]. Our data support the hypothesis of beneficial effects of CCR2^{+} cells in AD-like pathology and suggest a potential role of CCL17-mediated inhibitory mechanism for CCR2^{+} macrophage recruitment into the brain of APP/PS1 mice.

The main ligand of CCR2 is CCL2, which has been shown to be upregulated in AD brains and serum [75, 87]. Interestingly, overexpression of CCL2 mediates Aβ oligomer formation and worsened cognitive perfomance in AD mice [97, 166]. Investigation of intracerebral CCL2 level in APP/PS1-CCL17$^{E/E}$ mice revealed an age-dependent increase, but equivalent protein level in both APP/PS1-CCL17$^{E/E}$ and age-matched APP/PS1 mice. These data exclude CCL2 as the sole factor for Ly6C^{high}CCR2^{+} macrophage recruitment in APP/PS1-CCL17$^{E/E}$ mice.

6.1.4 CCL17 expression in aged APP/PS1 mice

CCL17 expression was evaluated in aged APP/PS1 and WT mice to see whether CCL17 expression is altered by APP/PS1 transgene expression. Indeed, *ccl17* mRNA is increased in the hippocampus of APP/PS1 mice when plaque development and cognitive impairment is fully developed. Since the detection of eGFP^{+} cells in the CNS failed in APP/PS1-CCL17$^{E/E}$ and CCL17$^{E/E}$ mice, ICL were isolated from aged APP/PS1 and WT mice to unravel the intracerebral source for CCL17 expression. In fact, *ccl17* mRNA was found in both mouse strains, indicating intracerebral CCL17, but not eGFP expression by macrophages or microglial cells in this model. Full eGFP protein expression and subsequent correct self-folding is needed for fluorescence emission [167]. In CCL17$^{E/+}$ and CCL17$^{E/E}$ mice eGFP fluorescence is described for Langerhans cells and mature DCs [101]. Although macrophages are found to express CCL17 [103, 168], up to now eGFP^{+} macrophages are not reported to be found in CCL17$^{E/E}$ mice. It is possible that full eGFP expression is somehow disturbed at the transcription or translation level, or posttranslational modifications different from that in DCs inhibit correct protein folding that eGFP fluorescence is suppressed. A former cloning study for the mouse CX3CL1/fractalkine gene revealed an unexpected alternative splicing variant of CCL17/TARC containing the signal sequence of CX3CL1 and protein encoding sequence of CCL17 [169]. The authors found that the fracTARC mRNA expression under the control of fractalkine promotor is tissue-specific in mouse kidney and brain, while normal CCL17 is expressed in thymus, lung, and with low amount in spleen.

The cognate receptor for CCL17 is CCR4. Several immune cells like DCs and T cells, but also macrophages express CCR4. It has also been shown that CHME3 cells, a human microglia cell line, and also primary human astrocytes express CCR4 [138]. Here, it was found that neonatal mouse microglia express *ccr4* mRNA upon LPS stimulation, although the expression level is lower than that of LPS stimulated DCs. However, a potential

auto- or paracrine signaling mechanism of microglial CCL17-CCR4 pathway is possibly involved in AD-linked neuroinflammation. On the other hand, a former study reported a Ca^{2+} increase in $CCR4^+$ hippocampal neurons stimulated with CCL17 [139], indicating a direct signaling between microglia and neurons via the CCL17-CCR4 axis. The principal function of CCL17 is the chemotactic recruitment of cells expressing its cognate receptor CCR4. Previous data of our group showed that $Ly6C^+CCR2^+$ monocytes express CCR4 [115]. Since increased recruitment of peripheral macrophages into the CNS is apparent in APP/PS1-CCL17$^{E/E}$ mice, the question raised whether CCL22, the other CCR4 ligand is altered in APP/PS1-CCL17$^{E/E}$ mice. Expression analysis revealed that *ccl22* mRNA is upregulated in the hippocampus of both CCL17$^{E/E}$ and APP/PS1-CCL17$^{E/E}$ mice compared to WT and APP/PS1. Interestingly, in contrast to CCL17, CCL22 is not altered by APP/Aβ overexpression. A potential synergistic working mechanism for CCL22 and CCL2 in the recruitment of $Ly6C^{high}CCR2^+CCR4^+$ monocytes into the CNS of aged APP/PS1-CCL17$^{E/E}$ is possible.

6.1.5 M2 shift and enhanced phagocytosis ability by CCL17-deficient microglial cells

The increased microgliosis and infiltration of peripheral macrophages suggest an alteration in the inflammatory milieu indicated by an altered expression of inflammatory mediators. While TNF, iNOS, IL-1β, YM-1, Arg1, and TGF-β present an equivalent expression level, increased *il-6* and *il-10* mRNA levels were found in the hippocampus of APP/PS1-CCL17$^{E/E}$ mice compared to APP/PS1 controls. IL-6 mediates, depending on the soluble or membrane-bound form of IL-6 receptor, pro- or anti-inflammatory signaling [170]. Indeed, in a previous study it has been shown that viral-mediated IL-6 overexpression in a mouse model of AD decreases plaque deposition, which is accompanied by enhanced astrocytosis and microgliosis [142]. *In vitro* studies of LPS-stimulated astrocytes showed neurotrophic functions of IL-6 by increasing the survival of dopaminergic neurons in a dose-dependent manner [160]. IL-10 is a prototypic anti-inflammatory cytokine blocking pro-inflammatory cytokine production and downregulating MHC II and co-stimulatory molecules on DCs and macrophages [171]. IL-10 can be expressed in the CNS by microglia, astrocytes, and oligodendrocytes and supports neuronal survival indirectly by the suppression of a pro-inflammatory phenotype of CNS-derived glia cells or directly on neurons via IL-10R signaling [172, 173]. Overexpression of IL-10 in APP/PS1 mice improved cognitive function and increased neurogenesis while reducing astrocytosis and microgliosis in APP/PS1 mice [159]. In addition, stimulation of macrophages or microglia with IL-10 *in vitro* shifts these cells towards an alternative activated phenotype. Furthermore, flow cytometric analysis of surface expression of CD40, a co-stimulatory molecule expressed by reactive microglia, and MMR, which is expressed by M2 macrophages revealed that CD40 is equivalently expressed by microglia of APP/PS1-CCL17$^{E/E}$, APP/PS1 mice, and

CCL17$^{E/E}$, but nearly absent on invading macrophages. However, increased numbers of MMR^{+} microglia and macrophages are found in APP/PS1-CCL17$^{E/E}$ mice, indicating that these cells possess a more alternatively activated phenotype in the CNS of aged APP/PS1-CCL17$^{E/E}$ mice.

Alternative activation of macrophages or microglial cells may lead to enhanced phagocytosis of Aβ peptides [50, 63, 174]. The phagocytosis ability of BM-dervied macrophages and neonatal microglia was assayed by using fluorescence-labeled Aβ1-42 peptide. Internalization and degradation assays revealed equivalent phagocytosis of Aβ peptides by CCL17$^{E/E}$ and WT macrophages. Intracellular Aβ peptides retain in macrophages for several hours, equivalent degradation probably takes place after 24 h of chasing. In contrast to the data found here in this model, it was reported that macrophages degrade Aβ within 24 h of incubation [175], Other authors also showed an effective reduction of intracellular Aβ by macrophages only after 64 h of incubation [143], hence a longer chasing period for Aβ degradation by CCL17$^{E/E}$ macrophages and microglia is required to assay the complete degradation process. However, neonatal CCL17$^{E/E}$ microglia exhibit enhanced Aβ uptake compared to WT mice, although Aβ degradation was not seen in the first 6 hours after medium exchange similar to BM-derived macrophages. Although microglia potentially degrade Aβ peptides when cultured on AD brain sections [44], other data indicate that microglia degrade internalized Aβ only after M-CSF stimulation leading to the acidification of lysosomes [48]. Nevertheless, these data support a potential Aβ clearance mechanism by CNS-resident microglial cells leading to the reduced soluble Aβ levels found in the CNS of aged APP/PS1-CCL17$^{E/E}$ mice.

The expression of MARCO and RAGE was examined by qRT-PCR, and an equivalent expression level of *marco* mRNA, but reduced expression of *rage* mRNA was detected in the hippocampus of APP/PS1-CCL17$^{E/E}$ mice. RAGE binds soluble Aβ monomers or oligomers and mediates on the one hand the transport of Aβ peptides from the periphery into the CNS leading to Aβ accumulation [133]. On the other hand Aβ-induced RAGE signaling results in several activation incidents. In APP/PS1 mice activation of RAGE via Aβ induces overactivation of autophagy, hence promoting neurodegeneration by the accumulation of autophagolysosomes [176]. Further, it has been shown that microglial RAGE-signaling in mouse models of AD increases the production of TNF-α and IL-1β, Aβ accumulation, and cognitive deficits [177]. Interestingly, it was found that RAGE was decreased in the hippocampus of 18-month-old APP/PS1 mice [178]. However, this is accompanied by a switch of alternatively activated microglia in young to classically activated microglia in old mice. In contrast to these data, in the CNS of aged APP/PS1-CCL17$^{E/E}$ mice decreased *rage* expression is accompanied by a M2 shift of microglial cells, indicating a potential beneficial effect by a reduced RAGE signaling in this model. The expression analysis of Aβ-degrading enzymes revealed equivalent levels of *ide* and *mmp-9*. However, *nep* mRNA level is enhanced in APP/PS1-CCL17$^{E/E}$ mice compared to APP/PS1 mice, indicating a potentially enhanced neprilysin protein expression leading

to enhanced Aβ monomer and oligomer degradation. These data are in line with the reduced soluble Aβ concentration found in APP/PS1-CCL17$^{E/E}$ mice. However, the enzymatic activity of MMP-9, IDE, and NEP proteins needs further investigation, to determine whether their Aβ degradation ability is altered in APP/PS1-CCL17$^{E/E}$ mice.

Our data indicate enhanced Aβ clearance in the CNS of APP/PS1-CCL17$^{E/E}$ by microglia, but not macrophages. Although increased infiltration of peripheral macrophages into the CNS of APP/PS1-CCL17$^{E/E}$ mice were found, which has been shown to be more effective in Aβ clearance [40, 48], phagocytosis assay with BM-derived macrophages failed to show enhanced uptake and degradation. These data suggest a possibly synergistic effect of increased Aβ uptake by CNS-resident microglia together with enhanced numbers of infiltrating macrophages leading to decreased soluble Aβ in the CNS of APP/PS1-CCL17$^{E/E}$ mice. Another explanation could be that *in vivo* CNS-invading macrophages potentially adopt an CNS-related microglial phenotype differently from that of *in vitro* cultured and matured BM-derived macrophages.

6.2 Determination of human CCL17 protein level in plasma of elderly patients

The chemokine CCL17 suggest a functional role in the progression of Alzheimer's disease as shown by enhanced expression in the hippocampus of aged APP/PS1 mice compared to age-matched WT mice. And breeding APP/PS1 mice with CCL17$^{E/E}$-deficient mice revealed beneficial effects on learning and memory performance in MWM, neuronal loss, and soluble Aβ burden due to CCL17 deficiency. To investigate, whether CCL17 is altered in the CSF of AD patients and patients with mild cognitive impairment (MCI), CCL17 concentration was determined in pre-test samples of healthy, MCI, and AD subjects by human CCL17 ELISA. However, CCL17 protein content was indetectable in these samples. Although some studies found CCL17 protein concentrations at 10-15 pg/ml in the CSF of relapsing neuromyelitis optica (RNMO) and MS patients measured by ELISA, others also reported that CCL17 concentration is under the detection limit of the used ELISA [179, 180, 146]. Since the minimum detectable concentration of CCL17 using comercial avaible ELISA is around 7 pg/ml, another detection system, for example a fluorescence-based protein-assay (with higher detection sensitivity) or analysis by mass spectrometry, seems to be reasonable.

Nevertheless, others showed measurable levels of CCL17 in plasma samples of MS patients using comercial available ELISA [146]. Plasma proteins as biomarkers for AD are highly desirable because of the easier and less painful way of sample-taking for the patients. CCL17 protein concentration was analyzed in plasma samples of all three groups. Although good detectable levels of plasma CCL17 were found, all groups present equivalent CCL17 content. Pre-test correlation assays for plasma CCL17 and CSF-Aβ_{42} found indications for a correlation in MCI patients. Since the test group size of this pre-test was

relatively low, the experiment was repeated with increased group size. However, there was no correlation found between plasma CCL17 and CSF-Aβ_{42} concentrations. Since the date of sample-taking ranges from 2000 to 2010, it is possible that some samples had lowered CCL17 concentrations due to degradation processes, although samples were stored at -80°C. Nevertheless, further investigation of CCL17 as a possible biomarker for Alzheimer's disease might be promising.

7 Summary and conclusion

The purpose of this project was to investigate the potential effect of CCL17 in the neuroinflammatory response occuring in AD. For this, a CCL17$^{E/E}$-deficient mouse model for AD was used (APP/PS1-CCL17$^{E/E}$). APP/PS1-CCL17$^{E/E}$ showed a WT-like learning and memory performance in Morris water maze together with reduced levels of soluble Aβ oligomers and Aβ_{42} peptides at 12-14 months of age, when cognitive deficits and plaque deposition are fully developed in normal APP/PS1 [17, 130]. Surprisingly, APP/PS1-CCL17$^{E/E}$ mice exhibit equivalent reactive GFAP^{+} astrocytes, but enhanced microgliosis. CD11b^{+} microglial cells derive from CNS-resident microglia and from peripheral Ly6C^{high}CCR2^{+} monocytes / macrophages infiltrating the CNS of APP/PS1-CCL17$^{E/E}$ mice. Increased CCL22, but not CCL2 expression was found in the hippocampus of APP/PS1-CCL17$^{E/E}$ mice, suggesting a potential convergent recruitment mechanism of Ly6C^{high}CCR2^{+}CCR4^{+} monocytes. For the first time it could be demonstrated that microglia isolated from the CNS of APP/PS1 mice express CCL17. The cognate receptor CCR4 is expressed by neonatal microglia upon LPS stimulation, indicating a para- or autocrine signaling. As indicated by increased hippocampal IL-6 and IL-10 expression, APP/PS1-CCL17$^{E/E}$ mice showed an altered inflammatory reponse in the CNS. Furthermore, CCL17$^{E/E}$microglia, but not macrophages, show enhanced expression of IL-10 *in vitro* and MMR expression *in vivo*. Phagocytosis assay of fluorescence-labeled Aβ_{1-42} peptide revealed an increased uptake by neonatal microglia, but not by BM-derived macrophages of CCL17$^{E/E}$ mice. Analysis of hippocampal expression levels of Aβ receptors and degrading enzymes revealed an increase of neprilysin, accompanied by a decrease of RAGE supporting the hypothesis of enhanced Aβ degradation within the CNS of APP/PS1-CCL17$^{E/E}$ mice, but reduced detrimental signaling. Fig.7.1 summarizes the potential mechanisms and effects of CCL17 deficiency in APP/PS1 mice. The underlying mechanism possibly involves the recruitment of peripheral macrophages into the CNS, accompanied by a more anti-inflammatory and neurotrophic milieu. Furthermore, enhanced Aβ clearance is indicated by increased uptake and enhanced neprilysin expression level.

These data clearly demonstrate a crucial role of CCL17 in the development of AD-like phenotypes in a double transgenic APP/PS1 mouse model. However, the exact working mechanism of the chemokine CCL17 in AD needs further investigation.

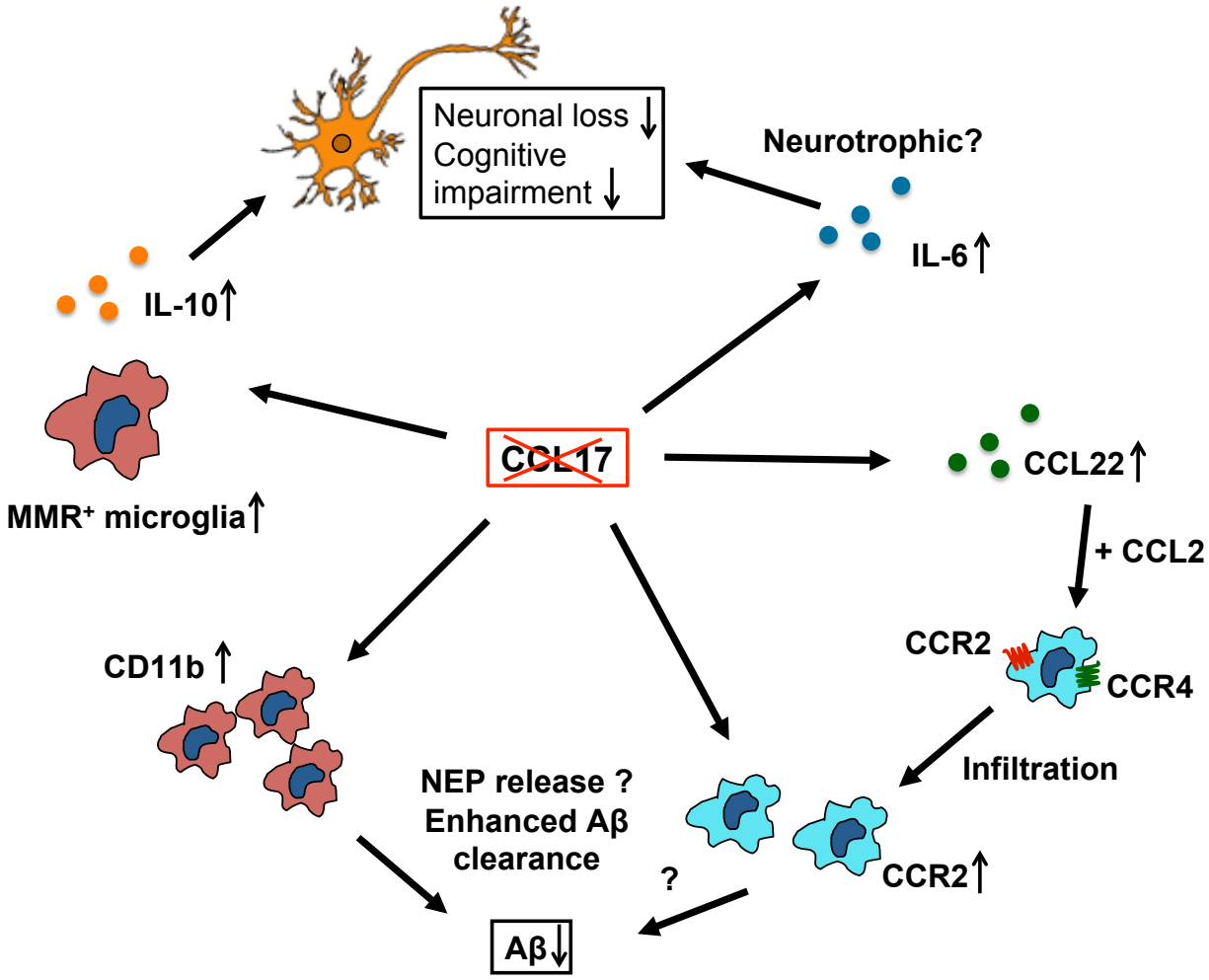

Figure 7.1: **CCL17 deficiency in APP/PS1 mice**
CCL17 deficiency results in reduced cognitive impairment, neuronal loss, and soluble Aβ burden. Microgliosis is enhanced due to increased CNS-resident microglial cells, which exhibit increased M2 phenotype and increased uptake of Aβ peptides *in vitro*, and due to increased infiltration of beneficial peripheral Ly6C^{high}CCR2^{+}CCR4^{+} monocytes. IL-6 can act as a potential neurotrophic factor. Increased CCL22 in concert with CCL2 possibly recruits Ly6C^{high}CCR2^{+}CCR4^{+} monocytes, which may contribute to renew of microglial population.

8 Acknowledgement

Zuallererst möchte ich mich bei Dr. med. Judith Alferink und Prof. Andreas Zimmer ganz herzlich bedanken für die Bereitstellung dieses fantastischen Projekts, dem wissenschaftlichen Rat und der andauernden Unterstützung bei der Fertigstellung dieser Arbeit. Ich habe während dieser Zeit unglaublich viel gelernt.

Bei Prof. Waldemar Kolanus möchte ich mich für die freundliche Übernahme der Zweitkorrektur sehr bedanken.

I also have to thank PD Dr. Andras Bilkei-Gorzo and Dr. Önder "Now we are real colleagues" Albayram for the behavioral analysis and especially for all the help and fascinating discussions we had.

Further, I would like to thank Prof. Jochen Walter, Dr. Sathish Kumar, Ilka Karaca and Sonya Tosheva for their cooperation work, scientific discussions concerning Alzheimer's disease, and especially Ilka for the WB analysis and Sonya for helping me with the phagocytosis analysis!

Dem gesamten Institut für Molekulare Psychiatrie und besonders der AG Alferink gilt mein Dank für die grossartige Arbeitsatmosphäre (nicht zuletzt gefördert durch diverse Lab retreats, Instituts- und Sommerpartys: Danke Andreas und Anne Zimmer), die immer gute fachliche Hilfe, und die moralische Unterstützung bei kleinen und grossen Problemen! Insbesondere möchte ich mich hier bei Kerstin Michel, Anastasia Piyanova, Anne Schmöle, Bruno Pradier, Astrid Becker und Ildikó Rácz bedanken für die wissenschaftlichen und unwissenschaftlichen, aber immer sehr hilfreichen Diskussionen und Ratschläge.

Karola Poppensieker: für ihre geduldige Einarbeitung insbesondere mit den Mäusen!

Christina Müller & Ramona Göhrs: Es war mir eine Ehre mit euch zu arbeiten!

Svenja Ternes: Und in weiteren 20 Jahren werden wir bei einem Schnaps zusammen sitzen und darüber lachen!!!

Ganz besonders bedanke ich mich bei meinen Eltern, Manfred und Jutta Neitzert, und bei meinen Geschwistern Kai und Kris Neitzert, bei Bastian Reupke, Tina Esch, Christian Franke und nicht zuletzt bei Daniel Kutscher für die unglaubliche Unterstützung und Geduld in diesen Jahren.

9 Appendix

Bibliography

[1] J. Götz and L. M. Ittner, "Animal models of Alzheimer's disease and frontotemporal dementia," *Nat Rev*, vol. 9, pp. 532–544, 2008.

[2] R. A. Stelzmann, H. N. Schnitzlein, and F. R. Murtagh, "An English Translation of Alzheimer's 1907 Paper, "Ueber eine eigenartige Erkrankung der Hirnrinde"," *Clin Anatomy*, vol. 8, pp. 429–431, 1995.

[3] N. I. on Aging and N. I. of Health, "Alzheimer's disease: Unraveling the mystery," *Alzheimer's Disease Education and Referral (ADEAR) Center*, Silver Spring, MD, U.S.

[4] M. Citron, "Alzheimer's disease: strategies for disease modification," *Nat Rev Drug Disc*, vol. 9, pp. 387–398, 2010.

[5] L. Bertram and R. E. Tanzi, "Thirty years of Alzheimer's disease genetics: the implications of systematic meta-analyses," *Nat Rev Neurosci*, vol. 9, pp. 768–778, 2008.

[6] G. Bu, "Apolipoprotein E and its receptors in Alzheimer's disease: pathways, pathogenesis and therapy," *Nat Rev Neurosci*, vol. 10, pp. 333–344, 2009.

[7] "www.advancedpsy.com."

[8] G. Thinakaran and E. H. Koo, "Amyloid precursor protein trafficking, processing, and function," *J Biol Chem*, vol. 283, pp. 29615–9, 2008.

[9] R. J. O'Brien and P. C. Wong, "Amyloid precursor protein processing and Alzheimer's disease," *Annu Rev Neurosci*, vol. 34, pp. 185–204, 2011.

[10] S. Rivest, "Regulation of innate immune responses in the brain," *Nat Rev Immunol*, vol. 10, pp. 429–439, 2009.

[11] X. Xu, "y-Secretase catalyzes sequential cleavages of the APP transmembrane domain," *J Alzheimers Dis*, vol. 16, pp. 211–224, 2009.

[12] S. L. Cole and R. Vassar, "The role of amyloid precursor protein processing by BACE1, the β-secretase, in Alzheimer's disease pathophysiology," *J Biol Chem*, vol. 283, pp. 29621–25, 2008.

[13] P. Hortschansky, V. Schroeckh, T. Christopeit, G. Zandomeneghi, and M. Fändrich, "The aggregation kinetics of Alzheimer's β-amyloid peptide is controlled by stochastic nucleation," *Protein Sci*, vol. 14, pp. 1753–59, 2005.

[14] S. Kumar and J. Walter, "Phosphorylation of amyloid beta (Aβ) peptides trigger for formation of toxic aggregates in Alzheimer's disease," *Aging*, vol. 3, pp. 1–10, 2011.

[15] C. Sturchler-Pierrat, D. Abramowski, M. Duke, K. H. Wiederhold, C. Mistl, S. Rothacher, *et al.*, "Two amyloid precursor protein transgenic mouse models with Alzheimer disease-like pathology," *PNAS*, vol. 94, pp. 13287–92, 1997.

[16] K. Hsiao, P. Chapman, S. Nilsen, C. Eckman, Y. Harigaya, S. Younkin, *et al.*, "Correlative memory deficits, Abeta elevation, and amyloid plaques in transgenic mice," *Science*, vol. 274, pp. 99–102, 2009.

[17] J. L. Jankowsky, D. J. Fadale, J. Anderson, G. M. Xu, V. Gonzales, N. A. Jenkins, N. G. Copeland, *et al.*, "Mutant presenilins specifically elevate the levels of the 42 residue beta-amyloid peptide in vivo: evidence for augmentation of a 42-specific gamma secretase," *Hum Mol Genet*, vol. 13, pp. 159–170, 2004.

[18] O. Wirths and T. A. Bayer, "Neuron loss in transgenic mouse models of Alzheimer's disease," *Int J Alzheimer's disease*, vol. 2010, pp. 6–11, 2010.

[19] T. Malm, J. Koistinaho, and K. Kanninen, "Utilization of APPswe/PS1dE9 Transgenic Mice in Research of Alzheimer's Disease: Focus on Gene Therapy and Cell-Based Therapy Applications," *Int J Alzheimer's Disease*, vol. 2011, p. 8, 2011.

[20] K. M. Lucin and T. Wyss-Coray, "Immune activation in brain aging and neurodegeneration: Too much or too little?," *Neuron*, vol. 64, pp. 1–11, 2009.

[21] J. Rogers, "The inflammatory response in Alzheimer's disease," *J Periodontol*, vol. 79, pp. 1535–43, 2008.

[22] J. Rogers, S. Webster, L.-F. Lue, L. Brachova, W. H. Civin, M. Emmerling, *et al.*, "Inflammation and Alzheimer's Disease Pathogenesis," *Neurobiol Aging*, vol. 17, pp. 681–686, 1996.

[23] P. L. McGeer, J. Rogers, and E. G. McGeer, "Inflammation, antiinflammatory agents and Alzheimer disease: the last 12 years," *J Alzheimer's disease*, vol. 9, pp. 271–276, 2006.

[24] R. B. Maccioni, L. E. Rojo, J. a. Fernández, and R. O. Kuljis, "The role of neuroimmunomodulation in Alzheimer's disease," *Ann N Y Acad Sci*, vol. 1153, pp. 240–246, 2009.

[25] M. T. Heneka and M. K. O'Banion, "Inflammatory processes in Alzheimer's disease," *J Neuroimmunology*, vol. 184, pp. 69–91, 2007.

[26] P. L. McGeer, S. Itagaki, and E. G. McGeer, "Expression of the histocompatibility glycoprotein HLA-DR in neurological disease," *Acta Neuropathol*, vol. 76, pp. 550–557, 1988.

[27] J. Rogers, J. Luber-Narod, S. D. Styren, and W. H. Civin, "Expression of immune system-associated antigens by cells of the human central nervous system: Relationship to the pathology of Alzheimer's disease," *Neurobiol Aging*, vol. 9, pp. 339–349, 1988.

[28] T. Wyss-Coray and J. Rogers, "Inflammation in Alzheimer disease-a brief review of the basic science and clinical literature," *Cold Spring Harb Perspec Med*, vol. 2, 2012.

[29] U.-K. Hanisch and H. Kettenmann, "Microglia: active sensor and versatile effector cells in the normal and pathologic brain," *Nat Neurosci*, vol. 10, pp. 1387–94, 2007.

[30] R. M. Ransohoff and A. E. Cardona, "The myeloid cells of the central nervous system parenchyma," *Nat Rev*, vol. 468, pp. 253–262, 2010.

[31] A. Nimmerjahn, F. Kirchhoff, and F. Helmchen, "Resting microglial cells are highly dynamic surveillants of brain parenchyma in vivo," *Science*, vol. 308, pp. 1314–8, 2005.

[32] H. M. Wisniewski, M. Barcikowska, and E. Kida, "Phagocytosis of beta-amyloid fibrils of the neuritic neocortical plaques," *Acta Neuropathol*, vol. 81, pp. 588–590, 1991.

[33] M. Stalder, a. Phinney, a. Probst, B. Sommer, M. Staufenbiel, and M. Jucker, "Association of microglia with amyloid plaques in brains of APP23 transgenic mice," *Am J Pathol*, vol. 154, pp. 1673–84, 1999.

[34] C. Y. D. Lee and G. E. Landreth, "The role of microglia in amyloid clearance from the AD brain," *J Neural Transm*, vol. 117, pp. 949–960, 2010.

[35] D. M. Paresce, R. N. Ghosh, and F. R. Maxfield, "Microglial cells internalize aggregates of the Alzheimer's disease amyloid beta-protein via a scavenger receptor," *Neuron*, vol. 17, pp. 553–565, 1996.

[36] R. Pluta, M. Barcikowski, A. Misicka, A. W. Lipkowski, S. Spisacka, and S. Januszewski, "Ischemic rats as a model in the study of the neurobiological role of human beta-amyloid peptide," *Neuroreport*, vol. 10, pp. 3615–19, 1999.

[37] T. Bolmont, F. Haiss, D. Eicke, R. Radde, C. A. Mathis, W. E. Klunk, *et al.*, "Dynamics of the microglial/amyloid interaction indicate a role in plaque maintenance," *J Neurosci*, vol. 28, pp. 4283–92, 2008.

[38] S. E. Hickman, E. K. Allison, and J. El Khoury, "Microglial dysfunction and defective beta-amyloid clearance pathways in aging Alzheimer's disease mice," *J Neurosci*, vol. 28, pp. 8354–60, 2008.

[39] S. Shaftel, S. Kyrkanides, J. Olschowka, J. Miller, R. Johnson, and M. O'Banion, "Sustained hippocampal IL-1β overexpression mediates chronic neuroinflammation and ameliorates Alzheimer plaque pathology," *J Clin Invest*, vol. 117, pp. 1595–04, 2007.

[40] T. Town, Y. Laouar, C. Pittenger, T. Mori, C. A. Szekely, J. Tan, *et al.*, "Blocking TGF-beta-Smad2/3 innate immune signaling mitigates Alzheimer-like pathology," *Nat Med*, vol. 14, pp. 681–687, 2008.

[41] K. Takata, Y. Kitamura, D. Yanagisawa, S. Morikawa, M. Morita, T. Inubushi, *et al.*, "Microglial transplantation increases amyloid-beta clearance in Alzheimer model rats," *FEBS Lett.*, vol. 581, pp. 475–478, 2007.

[42] J. El Khoury, M. Toft, S. E. Hickman, T. K. Means, K. Terada, C. Geula, *et al.*, "Ccr2 deficiency impairs microglial accumulation and accelerates progression of Alzheimer-like disease," *Nat Med*, vol. 13, pp. 432–438, 2007.

[43] Y. Zhu, H. Hou, K. Rezai-Zadeh, B. Giunta, A. Ruscin, C. Gemma, *et al.*, "CD45 deficiency drives amyloid-β peptide oligomers and neuronal loss in Alzheimer's disease mice," *J Neurosci*, vol. 31, pp. 1355–65, 2011.

[44] F. Bard, C. Cannon, R. Barbour, R. Burke, D. Games, H. Grajeda, *et al.*, "Peripherally administered antibodies against amyloid β-peptide enter the central nervous system and reduce oathology in a moue model of Alzheimer disease," *Nat Med*, vol. 6, pp. 616–619, 2000.

[45] S. Gratwohl, R. Kalin, T. Bolmont, S. Prokop, G. Winkelmann, S. Kaeser, *et al.*, "Formation and maintenance of Alzheimer's disease beta-amyloid plaques in the absence of microglia," *Nat Neurosci*, vol. 12, pp. 812–822, 2009.

[46] D. M. Paresce, H. Chung, and F. R. Maxfield, "Slow degradation of aggregates of the Alzheimer's disease amyloid beta-protein by microglial cells," *J Biol Chem*, vol. 272, pp. 29390–97, 1997.

[47] D. Walker and L. Lue, "Investigations with cultured human microglia on pathogenic mechanisms of Alzheimer's disease and other neurodegenerative diseases," *J Neurosci*, vol. 81, pp. 412–425, 2005.

[48] A. Majumdar, D. Cruz, N. Asamoah, A. Buxbaum, I. Sohar, P. Lobel, *et al.*, "Activation of Microglia Acidifies Lysosomes and Leads to Degradation of Alzheimer Amyloid Fibrils," *Mol Biol Cell*, vol. 18, pp. 1490–96, 2007.

[49] J. Koenigsknecht-Talboo and G. E. Landreth, "Microglial phagocytosis induced by fibrillar beta-amyloid and IgGs are differentially regulated by proinflammatory cytokines," *J Neurosci*, vol. 25, pp. 8240–9, 2005.

[50] J. Rogers and L.-f. Lue, "Microglial chemotaxis , activation , and phagocytosis of amyloid b-peptide as linked phenomena in Alzheimer's disease," *Neurochem Intern*, vol. 39, pp. 333–340, 2001.

[51] J. Rogers, R. Strohmeyer, C. J. Kovelowski, and R. Li, "Microglia and inflammatory mechanisms in the clearance of amyloid beta peptide," *Glia*, vol. 40, pp. 260–269, 2002.

[52] J. D. Sokolowski and J. W. Mandell, "Phagocytic clearance in neurodegeneration," *Am J Pathol*, vol. 178, 2011.

[53] K. Tahara, H. Kim, J. Jin, J. Maxwell, L. Li, and K. Fukuchi, "Role of toll-like receptor signalling in Abeta uptake and clearance," *Brain*, vol. 129, pp. 3006–19, 2006.

[54] K. Fassbender, S. Walter, S. Kühl, R. Landmann, K. Ishii, T. Bertsch, *et al.*, "The LPS receptor (CD14) links innate immunity with Alzheimer's disease," *FASEB J*, vol. 18, pp. 203–205, 2004.

[55] S. Walter, M. Letiembre, H. Liu, H. Heine, B. Penke, W. Hao, *et al.*, "Role of the toll-like receptor 4 in neuroinflammation in Alzheimer's disease," *Cell Physiol Biochem*, vol. 20, pp. 947–956, 2007.

[56] M. Jana, C. Palencia, and K. Pahan, "Fibrillar amyloid-beta peptides activate microglia via TLR2: implications for Alzheimer's disease," *J Immunol*, vol. 181, pp. 7254–62, 2008.

[57] K. Richard, M. Filiali, P. Prefontaine, and S. Rivest, "Toll-like receptor 2 acts as a natural innate immune receptor to clear amyloid beta 1-42 and delay the cognitive decline in a mouse model of Alzheimer's disease," *J Neurosci*, vol. 28, pp. 5784–93, 2008.

[58] E. Reed-Geaghan, Q. Reed, P. Cramer, and G. Landreth, "Deletion of CD14 attenuates Alzheimer's disease pathology by influencing the brain's inflammatory milieu," *J Neurosci*, vol. 30, pp. 15369–73, 2010.

[59] S. Liu, Y. Liu, W. Hao, L. Wolf, A. J. Kiliaan, B. Penke, *et al.*, "TLR2 is a primary receptor for Alzheimer's amyloid β peptide to trigger neuroinflammatory activation," *J Immunol*, vol. 188, pp. 1098–107, 2012.

[60] M. Song, J. Jin, J.-E. Lim, J. Kou, A. Pattanayak, J. A. Rehman, *et al.*, "TLR4 mutation reduces microglial activation, increases Abeta deposits and exacerbates cognitive deficits in a mouse model of Alzheimer's disease," *J Neuroinflamm*, vol. 8, p. 92, 2011.

[61] D. Farfara, V. Fishitz, and D. Frenkel, "Neuroprotective and neurotoxic properties of glial cells in the pathogenesis of Alzheimer's disease," *J Cell Mol Med*, vol. 12, pp. 762–780, 2008.

[62] C. K. Combs, J. C. Karlo, S. C. Kao, and G. E. Landreth, "beta-Amyloid stimulation of microglia and monocytes results in TNFalpha-dependent expression of inducible nitric oxide synthase and neuronal apoptosis," *J Neurosci*, vol. 21, pp. 1179–88, 2001.

[63] C. A. Colton, "Heterogeneity of microglial activation in the innate immune response in the brain," *J Neuroimm Pharmacol*, vol. 4, pp. 399–418, 2009.

[64] B. Cameron and G. E. Landreth, "Inflammation, microglia, and Alzheimer's disease," *Neurobiol Dis*, vol. 37, pp. 503–509, 2010.

[65] S. David and A. Kroner, "Repertoire of microglial and macrophage responses after spinal cord injury," *Nat Rev Neurosci*, vol. 12, pp. 388–399, 2011.

[66] D. Mosser, "The many faces of macrophage activation," *Leukoc Biol*, vol. 73, pp. 209–212, 2003.

[67] C. Schwab, A. Klegeris, and P. L. McGeer, "Inflammation in transgenic mouse models of neurodegenerative disorders," *Biochim Biophys Acta*, vol. 1802, pp. 889–902, 2010.

[68] J. El Khoury and A. D. Luster, "Mechanisms of microglia accumulation in Alzheimer's disease: therapeutic implications," *Trends Pharmacol Sci*, vol. 13, pp. 626–623, 2008.

[69] T. M. Malm, M. Koistinaho, M. Pärepalo, T. Vatanen, A. Ooka, S. Karlsson, *et al.*, "Bone-marrow-derived cells contribute to the recruitment of microglial cells in response to beta-amyloid deposition in APP/PS1 double transgenic Alzheimer mice," *Neurobiol Dis*, vol. 18, pp. 134–142, 2005.

[70] A. R. Simard, D. Soulet, G. Gowing, J.-P. Julien, and S. Rivest, "Bone marrow-derived microglia play a critical role in restricting senile plaque formation in Alzheimer's disease," *Neuron*, vol. 49, pp. 489–502, 2006.

[71] S. Gordon and P. R. Taylor, "Monocyte and macrophage heterogeneity," *Nat Rev Immunol*, vol. 5, pp. 953–964, 2005.

[72] R. M. Ransohoff, "Chemokines and chemokine receptors: standing at the crossroads of immunobiology and neurobiology," *Immunity*, vol. 31, pp. 711–721, 2009.

[73] M. Prinz and J. Priller, "Tickets to the brain: role of CCR2 and CX3CR1 in myeloid cell entry in the CNS," *J Neuroimmunol*, vol. 224, pp. 80–84, 2010.

[74] M. Jutila, F. Kroese, K. Jutila, A. Stall, S. Fiering, L. Herzenberg, *et al.*, "Ly-6C is a monocyte/macrophage and endothelial cell differentiation antigen regulated by interferon-gamma," *Eur J Immunol*, vol. 18, pp. 1819–26, 1988.

[75] L. Cartier, O. Hartley, M. Dubois-Dauphin, and K.-H. Krause, "Chemokine receptors in the central nervous system: role in brain inflammation and neurodegenerative diseases," *Brain Res Rev*, vol. 48, pp. 16–42, 2005.

[76] A. Mildner, H. Schmidt, M. Nitsche, D. Merkler, U.-K. Hanisch, M. Mack, *et al.*, "Microglia in the adult brain arise from Ly-6ChiCCR2+ monocytes only under defined host conditions," *Nat Neurosci*, vol. 10, pp. 1544–53, 2007.

[77] A. Mildner, B. Schlevogt, K. Kierdorf, C. Böttcher, D. Erny, M. P. Kummer, *et al.*, "Distinct and non-redundant roles of microglia and myeloid subsets in mouse models of Alzheimer's disease," *J Neurosci*, vol. 31, pp. 11159–71, 2011.

[78] G. Naert and S. Rivest, "Hematopoietic CC-chemokine receptor 2 (CCR2) competent cells are protective for the cognitive impairments and amyloid pathology in a transgenic mouse model of Alzheimer's disease," *Mol Med*, vol. 18, pp. 297–313, 2012.

[79] M. Sofroniew and H. Vinters, "Astrocytes: Biology and pathology," *Acta Neuropathol*, vol. 119, pp. 7–35, 2010.

[80] J. Rodriguez, M. Olabarria, A. Chvatal, and V. A, "Astroglia in dementia and Alzheimer's disease," *Cell Death Differ*, vol. 16, pp. 378–385, 2009.

[81] J. White, A. Manelli, K. Holmberg, L. Van Eldik, and M. Ladu, "Differential effects of oligomeric and fibrillar amyloid-β 1-42 on astrocyte-mediated inflammation," *Neurobiol Dis*, vol. 18, pp. 459–465, 2005.

[82] A. Abramov, L. Canevari, and M. Duchen, "β-amyloid peptides induce mitochondrial dysfunction and oxidative stress in astrocytes and death of neurons through activation of NADPH oxidase," *J Neurosci*, vol. 24, pp. 565–575, 2004.

[83] A. Cardona, E. Pioro, M. Sasse, V. Kostenko, S. Cardona, I. Dijkstra, *et al.*, "Control of microglial neurotoxicity by the fractalkine receptor," *Nat Neurosci*, vol. 9, pp. 917–924, 2006.

[84] A. Roth, G. Ramirez, R. Alarcon, and R. von Bernhardi, "Oligodendrocytes damage in Alzheimer's disease: Beta amyloid toxicity and inflammation," *Biol Res*, vol. 38, pp. 381–387, 2005.

[85] S. J. Allen, S. E. Crown, and T. M. Handel, "Chemokine: Receptor structure, interactions, and antagonism," *Annu Rev Immunol*, vol. 25, pp. 787–820, 2007.

[86] M. Li and R. Ransohoff, "Multiple roles of chemokine CXCL12 in the central nervous system: A migration from immunology to neurobiology," *Progr Neurobiol*, vol. 84, pp. 116–131, 2008.

[87] I. Blasko, W. Lederer, H. Oberbauer, T. Walch, G. Kemmler, H. Hinterhuber, *et al.*, "Measurement of thirteen biological markers in CSF of patients with Alzheimer's disease and other dementias," *Dement Geriatr Cogn Disord*, vol. 21, pp. 9–15, 2006.

[88] D. Galimberti, N. Schoonenboom, E. Scarpini, and P. Scheltens, "Chemokines in serum and cerebrospinal fluid of Alzheimer's disease patients," *Ann Neurol*, vol. 53, pp. 547–548, 2003.

[89] D. Galimberti, C. Fenoglio, C. Lovati, E. Venturelli, I. Guigi, B. Corra, *et al.*, "Serum MCP-1 levels are increased in mild cognitive impairment and mild Alzheimer's disease," *Neurobiol Aging*, vol. 27, pp. 1763–68, 2006.

[90] L. Lue, R. Rydel, B. EF, L. Yang, H. Hampel, M. J. GM, *et al.*, "Inflammatory repertoire of Alzheimer's disease and nondemented elderly microglia in vitro," *Glia*, vol. 35, pp. 72–79, 2001.

[91] Y. K. Lee, D. H. Kwak, K. W. Oh, S.-Y. Nam, B. J. Lee, Y. W. Yun, *et al.*, "CCR5 deficiency induces astrocyte activation, Abeta deposit and impaired memory function," *Neurobiol Learn Memory*, vol. 92, pp. 356–63, 2009.

[92] J. Skuljec, H. Sun, R. Pul, K. Bénardais, D. Ragancokova, D. Moharregh-Khiabani, *et al.*, "CCL5 induces a pro-inflammatory profile in microglia in vitro," *Cell Immunol*, vol. 270, pp. 164–171, 2011.

[93] S. Subramanian, P. Ayala, T. L. Wadsworth, and C. J. Harris, "CCR6: A biomarker for Alzheimer's-like disease in a triple trasngenic mouse model," *J Alzheimers Dis*, vol. 22, pp. 619–629, 2011.

[94] S. Lee, N. H. Varvel, M. E. Konerth, G. Xu, A. E. Cardona, R. M. Ransohoff, *et al.*, "CX3CR1 deficiency alters microglial activation and reduces beta-amyloid deposition in two Alzheimer's disease mouse models," *Am J Pathol*, vol. 177, pp. 2549–62, 2010.

[95] M. Fuhrmann, T. Bittner, C. K. E. Jung, S. Burgold, R. M. Page, G. Mitteregger, *et al.*, "Microglial Cx3cr1 knockout prevents neuron loss in a mouse model of Alzheimer's disease," *Nat Neurosci*, 2010.

[96] S.-H. Cho, B. Sun, Y. Zhou, T. M. Kauppinen, B. Halabisky, P. Wes, *et al.*, "CX3CR1 signaling modulates microglial activation and protects against plaque-independent cognitive deficits in an mouse model of Alzheimer's disease," *J Biol Chem*, vol. 286, pp. 32713–22, 2011.

[97] T. Kiyota, M. Yamamoto, H. Xiong, M. P. Lambert, W. L. Klein, H. E. Gendelman, *et al.*, "CCL2 accelerates microglia-mediated Abeta oligomer formation and progression of neurocognitive dysfunction," *PLoS one*, vol. 4, p. e6197, 2009.

[98] T. Mizuno, J. Kawanokuchi, K. Numata, and A. Suzumura, "Production and neuroprotective functions of fractalkine in the central nervous system," *Brain Res*, vol. 979, pp. 65–70, 2003.

[99] V. Zujovic, J. Benavides, X. Vige, C. Carter, and V. Taupin, "Fractalkine modulates TNF-alpha secretion and neurotoxicity induced by microglial activation," *Glia*, vol. 29, pp. 305–315, 2000.

[100] T. Imai, T. Yoshida, M. Baba, M. Nishimura, M. Kakizaki, and O. Yoshie, "Molecular cloning of a novel T cell-directed CC chemokine expressed in thymus by signal sequence trap using Epstein-Barr virus vector," *J Biol Chemistry*, vol. 271, pp. 21514–21, 1996.

[101] J. Alferink, I. Lieberam, W. Reindl, a. Behrens, S. Weiss, N. Huser, *et al.*, "Compartmentalized production of CCL17 in vivo: Strong inducibility in peripheral dendritic cells contrasts selective absence from the spleen," *J Exp Med*, vol. 197, pp. 585–599, 2003.

[102] T. Katakura, M. Miyazaki, M. Kobayashi, D. N. Herndon, and F. Suzuki, "CCL17 and IL-10 as effectors that enable alternatively activated macrophages to inhibit the generation of classically activated macrophages," *J Immunol*, vol. 172, pp. 1407–13, 2004.

[103] K. Liddiard, J. S. Welch, J. Lozach, S. Heinz, C. K. Glass, and D. R. Greaves, "Interleukin-4 induction of the CC chemokine TARC (CCL17) in murine macrophages is mediated by multiple STAT6 sites in the TARC gene promoter," *BMC Mol Biol*, vol. 7, p. 45, 2006.

[104] B. Yu, T. Koga, K. Urabe, Y. Moroi, S. Maeda, Y. Yanagihara, and M. Furue, "Differential regulation of thymus- and activation-regulated chemokine induced by IL-4, IL-13, TNF-alpha and IFN-gamma in human keratinocyte and fibroblast," *J Dermatol Sci*, vol. 30, pp. 29–36, 2002.

[105] O. Yoshie, T. Imai, and H. Nomiyama, "Novel lymphocyte-specific CC chemokines and their receptors," *J Leukoc Biol*, vol. 62, pp. 634–644, 1997.

[106] I. F. Charo and R. M. Ransohoff, "The many roles of chemokines and chemokine receptors in inflammation," *New Engl J Med*, vol. 354, pp. 610–621, 2006.

[107] G. Bernardini, J. Hedrick, S. Sozzani, W. Luini, G. Spinetti, M. Weiss, *et al.*, "Identification of the CC chemokine TARC and macrophage inflammatory protein-1 beta as novel functional ligands for the CCR8 receptor," *Eur J Immunol*, vol. 28, pp. 582–588, 1998.

[108] C. Garlisi, H. Xiao, F. Tian, J. Hedrick, M. Billah, R. Egan, *et al.*, "The assignment of chemokine-chemokine receptor pairs: TARC and MIP-1 beta are not ligands for human CC-chemokine receptor 8," *Eur J Immunol*, vol. 29, pp. 3210–3215, 1999.

[109] P. Vijayanand, K. Durkin, G. Hartmann, J. Morjaria, G. Seumois, K. J. Staples, *et al.*, "Chemokine receptor 4 plays a key role in T cell recruitment into the airways of asthmatic patients," *J Immunol*, vol. 184, pp. 4568–74, 2010.

[110] S. Specht, J. K. Frank, J. Alferink, B. Dubben, L. E. Layland, G. Denece, *et al.*, "CCL17 controls mast cells for the defense against filarial larval entry," *J Immunol*, vol. 186, pp. 4845–52, 2011.

[111] S. Stutte, T. Quast, N. Gerbitzki, T. Savinko, N. Novak, J. Reifenberger, *et al.*, "Requirement of CCL17 for CCR7- and CXCR4- dependent migration of cutaneous dendritic cells," *PNAS*, vol. 107, pp. 8736–41, 2010.

[112] H. Saeki and K. Tamaki, "Thymus and activation regulated chemokine (TARC)/CCL17 and skin diseases," *J Dermatol Sci*, vol. 43, pp. 75–84, 2006.

[113] V. Semmling, V. Lukacs-Kornek, C. A. Thaiss, T. Quast, K. Hochheiser, U. Panzer, *et al.*, "Alternative cross-priming through CCL17-CCR4-mediated attraction of CTLs toward NKT cell-licensed DCs," *Nat Immunol*, vol. 11, pp. 313–20, 2010.

[114] C. Weber, S. Meiler, Y. Döring, M. Koch, M. Drechsler, R. T. A. Megens, *et al.*, "CCL17-expressing dendritic cells drive atherosclerosis by restraining regulatory T cell homeostasis in mice," *J Clin Invest*, vol. 121, pp. 2898–2910, 2011.

[115] K. Poppensieker, D.-M. Otte, B. Schürmann, A. Limmer, P. Dresing, E. Drews, *et al.*, "CC chemokine receptor 4 is required for experimental autoimmune encephalomyelitis by regulating GM-CSF and IL-23 production in dendritic cells," *PNAS*, vol. 109, pp. 3897–902, 2012.

[116] L. Pulliam, B. Sun, H. Rempel, P. M. Martinez, J. D. Hoekman, R. J. Rao, *et al.*, "Intranasal tat alters gene expression in the mouse brain," *J Neuroimm Pharmacol*, vol. 2, pp. 87–92, 2007.

[117] K. Narikawa, T. Misu, K. Fujihara, I. Nakashima, S. Sato, and Y. Itoyama, "CSF chemokine levels in relapsing neuromyelitis optica and multiple sclerosis," *J Neuroimmunol*, vol. 149, pp. 182–186, 2004.

[118] J. Haas, L. Schopp, B. Storch-Hagenlocher, B. Fritzsching, C. Jabobi, L. Milkova, *et al.*, "Specific recruitment of regulatory T cells into the CSF in lymphomatous and carcinomatous meningitis," *Blood*, vol. 111, pp. 761–766, 2008.

[119] T. Bussiere, F. Bard, R. Barbour, H. Grajeda, T. Guido, K. Khan, *et al.*, "Morphological characterization of Thioflavin-S-positive amyloid plaques in transgenic Alzheimer mice and effect of passive Abeta immunotherapy on their clearance," *AJP*, vol. 165, pp. 987–995, 2004.

[120] R. Khurana, C. Coleman, C. Ionescu-Zanetti, S. A. Carter, V. Krishna, R. K. Grover, *et al.*, "Mechanism of thioflavin T binding to amyloid fibrils," *J Struct Biol*, vol. 151, pp. 229–238, 2005.

[121] M. Reale, C. Iarlori, C. Feliciani, and D. Gambi, "Peripheral Chemokine Receptors, Their Ligands, Cytokines and Alzheimer's Disease," *J Alzheimers Dis*, vol. 14, pp. 147–159, 2008.

[122] A. Monsonego, V. Zota, A. Karni, J. I. Krieger, A. Bar-or, G. Bitan, *et al.*, "Increased T cell reactivity to amyloid β protein in older humans," *J Clin Invest*, vol. 112, no. 3, pp. 415–422, 2003.

[123] E. Mossello, E. Ballini, A. Mello, F. Tarantini, D. Simoni, S. Baldasseroni, *et al.*, "Biomarkers of ALzheimer's disease: From central nervous system to periphery?," *Int J Alzheimers Dis*, vol. 2011, p. 7, 2011.

[124] A. Ciaramella, F. Bizzoni, F. Salani, D. Vanni, G. Spalletta, N. Sanarico, *et al.*, "Increased pro-inflammatory responses by dendritic cells from patients with Alzheimer's disease," *J Alzheimers Dis*, vol. 19, pp. 559–572, 2010.

[125] R. Weller, A. Massey, T. Newman, M. Hutchings, Y.-M. Kuo, and A. Roher, "Cerebral amyloid angiopathy: Amyloid β accumulates in putative interstitial fluid drainage pathways in Alzheimer's disease," *Am J Pathol*, vol. 153, pp. 725–733, 1998.

[126] R. Weller, M. Subash, S. Preston, I. Mazanti, and C. RO, "Perivascular drainage of amyloid-beta peptides from the brain and its failure in cerebral amyloid angiopathy and Alzheimer's disease," *Brain Pathol*, vol. 18, pp. 253–266, 2008.

[127] M. Cron, "Charakterisierung der Interaktion von β-Amyloid mit professionellen Antigen-präsentierenden Zellen," *Diploma thesis, Friedrich-Wilhelm-Universität Bonn*, 2007.

[128] B. Giunta, K. Rezai-Zadeh, and J. Tan, "Impact of the CD40-CD40L Dyad in Alzheimer's Disease," *CNS Neurol Disord Drug Targets*, vol. 9, pp. 149–155, 2010.

[129] H. Xiong, D. Callaghan, J. Wodzinska, J. Xu, M. Premyslova, Q.-Y. Liu, *et al.*, "Biochemical and behavioral characterization of the double transgenic mouse model (APPswe/PS1dE9) of Alzheimer's disease," *Neurosci Bull*, vol. 27, pp. 221–232, 2011.

[130] W. Zhang, J. Hao, R. Liu, Z. Zhang, G. Lei, C. Su, *et al.*, "Soluble Aβ levels correlate with cognitive deficits in the 12-month-old APPswe/PS1dE9 mouse model of Alzheimer's disease," *Behav Brain Res*, vol. 222, pp. 342–350, 2011.

[131] O. Albayram, J. Alferink, J. Pitsch, A. Piyanova, K. Neitzert, K. Poppensieker, *et al.*, "Role of CB1 cannabinoid receptors on GABAergic neurons in brain aging," *PNAS*, vol. 108, pp. 11256–61, 2011.

[132] J. P. Cleary, D. M. Walsh, J. J. Hofmeister, G. M. Shankar, M. A. Kuskowski, D. J. Selkoe, *et al.*, "Natural oligomers of the amyloid-beta protein specifically disrupt cognitive function," *Nat Neurosci*, vol. 8, pp. 79–84, 2005.

[133] R. Deane, S. Du Yan, R. K. Submamaryan, B. LaRue, S. Jovanovic, E. Hogg, *et al.*, "RAGE mediates amyloid-beta peptide transport across the blood-brain barrier and accumulation in brain," *Nat Med*, vol. 9, pp. 907–913, 2003.

[134] T. Kiyota, M. Yamamoto, B. Schroder, M. T. Jacobsen, R. J. Swan, M. P. Lambert, *et al.*, "AAV1/2-mediated CNS gene delivery of dominant-negative CCL2 mutant suppresses gliosis, beta-amyloidosis, and learning impairment of APP/PS1 mice," *Mol Ther*, vol. 17, pp. 803–809, 2009.

[135] T. Wyss-Coray, J. Loike, T. Brionne, E. Lu, R. Anankov, and F. Yan, "Adult mouse astrocytes degrade amyloid-beta in vitro and in situ," *Nat Med*, vol. 9, pp. 453–457, 2003.

[136] A. Roy, Y. K. Fung, X. Liu, and K. Pahan, "Up-regulation of microglial CD11b expression by nitric oxide," *J Biol Chem*, vol. 281, pp. 14971–80, 2006.

[137] T. L. Ness, J. L. Ewing, C. M. Hogaboam, and S. L. Kunkel, "CCR4 is a key modulator of innate immune responses," *J Immunol*, vol. 177, pp. 7531–9, 2006.

[138] G. Flynn, S. Maru, J. Loughlin, I. A. Romero, and D. Male, "Regulation of chemokine receptor expression in human microglia and astrocytes," *J Neuroimmunol*, vol. 136, pp. 84–93, 2003.

[139] O. Meucci, a. Fatatis, a. a. Simen, T. J. Bushell, P. W. Gray, and R. J. Miller, "Chemokines regulate hippocampal neuronal signaling and gp120 neurotoxicity," *PNAS*, vol. 95, pp. 14500–5, 1998.

[140] J. Scheller, A. Chalaris, D. Schmidt-Arras, and S. Rose-John, "The pro- and anti-inflammatory properties of the cytokine interleukin-6," *Biochim Biophys Acta*, vol. 1813, pp. 878–888, 2011.

[141] E. G. Njie, E. Boelen, F. R. Stassen, H. W. M. Steinbusch, D. R. Borchelt, and W. J. Streit, "Ex vivo cultures of microglia from young and aged rodent brain reveal age-related changes in microglial function," *Neurobiol Aging*, 2010.

[142] P. Chakrabarty, K. Jansen-West, A. Beccard, C. Ceballos-Diaz, Y. Levites, C. Verbeeck, *et al.*, "Massive gliosis induced by interleukin-6 suppresses Abeta deposition in vivo: evidence against inflammation as a driving force for amyloid deposition," *FASEB J*, vol. 24, pp. 548–559, 2010.

[143] M. Yamamoto, T. Kiyota, S. M. Walsh, and T. Ikezu, "Kinetic analysis of aggregated amyloid-beta peptide clearance in adult bone-marrow-derived macrophages from APP and CCL2 transgenic mice," *J Neuroimm Pharmacol*, vol. 2, pp. 213–21, 2007.

[144] J. S. Miners, N. Barua, P. G. Kehoe, S. Gill, and S. Love, "Aβ-degrading enzymes: potential for treatment of Alzheimer disease," *J Neuropathol Exp Neurol*, vol. 70, pp. 944–959, 2011.

[145] V. Srikanth, A. Maczurek, T. Phan, M. Steele, B. Westcott, D. Juskiw, *et al.*, "Advanced glycation endproducts and their receptor RAGE in Alzheimer's disease," *Neurobiol Aging*, vol. 32, pp. 763–77, 2011.

[146] A. Kalinowska-Lyszczarz, A. Szczucinski, M. A. Pawlak, and J. Losy, "Clinical study on CXCL13, CCL17, CCL20 and IL-17 as immune cell migration navigators in relapsing-remitting multiple sclerosis patients," *J Neurologic Sci*, vol. 300, pp. 81–85, 2011.

[147] "World Alzheimer report 2010," *Alzheimer's disease international*, 2010.

[148] B. Giunta, F. Fernandez, W. V. Nikolic, D. Obregon, E. Rrapo, T. Town, *et al.*, "Inflammaging as a prodrome to Alzheimer's disease," *J Neuroinflamm*, vol. 5, p. 51, 2008.

[149] Y. Fisher, A. Nemirovsky, R. Baron, and A. Monsonego, "Dendritic cells regulated amyloid-β-specific T-cell entry into the brain: The role of perivascular amyloid-β," *J Alzheimers Dis*, vol. 27, pp. 99–111, 2011.

[150] D. J. Selkoe, "Alzheimer's Disease : Genes, Proteins, and Therapy," *Physiological Reviews*, vol. 81, pp. 741–767, 2001.

[151] H. W. Querfurth and F. M. Laferla, "Alzheimer's Disease," *Clinical Trials*, pp. 329–344, 2010.

[152] D. M. Walsh, I. Klyubin, J. V. Fadeeva, W. K. Cullen, R. Anwyl, M. S. Wolfe, M. J. Rowan, *et al.*, "Naturally secreted oligomers of amyloid beta protein potently inhibit hippocampal long-term potentiation in vivo," *Nature*, vol. 416, pp. 535–539, 2002.

[153] C. Casas, N. Sergeant, J.-M. Itier, V. Blanchard, O. Wirths, N. van der Kolk, *et al.*, "Massive CA1/2 neuronal loss with intraneuronal and N-terminal truncated Aβ42 accumulation in a novel Alzheimer transgenic model," *Am J Pathol*, vol. 165, pp. 1289–1300, 2004.

[154] R. Baron, I. Harpaz, A. Nemirovsky, H. Cohen, and A. Monsonego, "Immunity and neuronal repair in the progression of Alzheimer's disease: a brief overview," *Exp Gerontol*, vol. 42, pp. 64–69, 2007.

[155] M. Garcia-Alloza, E. Robbins, Z.-N. SX, P. SM, B. RA, *et al.*, "Characterization of amyloid deposition in the APPswe/PS1dE9 mouse model of Alzheimer's disease," *Neurobiol Dis*, vol. 24, pp. 516–524, 2006.

[156] H. Takahashi, I. Brasnjevic, B. P. Rutten, and N. Van Der Kolk, "Hippocampal interneuron loss in an APP/PS1 double mutant mouse and in Alzheimer's disease," *Brain Struct Funct*, vol. 214, pp. 145–160, 2010.

[157] M. Meyer-Luehmann, M. Mielke, T. L. Spires-Jones, W. Stoothoff, P. Jones, B. J. Bacskai, *et al.*, "A reporter of local dendritic translocation shows plaque- related loss of neural system function in APP-transgenic mice," *J Neurosci*, vol. 29, pp. 12636–40, 2009.

[158] O. Butovsky, M. Koronyo-hamaoui, G. Kunis, E. Ophir, G. Landa, H. Cohen, *et al.*, "Glatiramer acetate fights against Alzheimer's disease by inducing dendritic-like microglia expressing insulin-like growth factor 1," *PNAS*, vol. 103, pp. 11784–11789, 2006.

[159] T. Kiyota, K. L. Ingraham, R. J. Swan, M. T. Jacobsen, S. J. Andrews, and T. Ikezu, "AAV serotype 2/1-mediated gene delivery of anti-inflammatory interleukin-10 enhances neurogenesis and cognitive function in APP+PS1 mice," *Gene Ther*, vol. 19, pp. 724–733, 2012.

[160] X.-z. Li, L.-m. Bai, Y.-p. Yang, W.-f. Luo, W.-d. Hu, J.-p. Chen, *et al.*, "Effects of IL-6 secreted from astrocytes on the survival of dopaminergic neurons in lipopolysaccharide-induced inflammation," *Neurosci Res*, vol. 65, pp. 252–258, 2009.

[161] U. Neniskyte, J. J. Neher, and G. C. Brown, "Neuronal death induced by nanomolar amyloid beta is mediated by primary phagocytosis of neurons by microglia," *J Biol Chem*, pp. 1–18, 2011.

[162] K. Rezai-Zadeh, D. Gate, G. Gowing, and T. Town, "How to get from here to there: Macrophage recruitment in Alzheimer's disease," *Curr Alzheimer Res*, vol. 8, pp. 156–163, 2011.

[163] R. M. Ransohoff, "Microglia and monocytes: 'tis plain the twain meet in the brain," *Nat Neurosci*, vol. 14, pp. 1098–100, 2011.

[164] G. Naert and S. Rivest, "CC chemokine receptor 2 deficiency aggravates cognitive impairments and amyloid pathology in a transgenic mouse model of Alzheimer's disease," *J Neurosci*, vol. 31, pp. 6208–20, 2011.

[165] N. Saederup, A. E. Cardona, K. Croft, M. Mizutani, A. C. Cotleur, C.-L. Tsou, *et al.*, "Selective chemokine receptor usage by central nervous system myeloid cells in CCR2-red fluorescent protein knock-in mice," *PLoS one*, vol. 5, 2010.

[166] M. Yamamoto, M. Horiba, J. L. Buescher, D. Huang, H. E. Gendelman, and R. M. a. Ransohoff, "Overexpression of monocyte chemotactic protein-1/CCL2 in beta-amyloid precursor protein transgenic mice show accelerated diffuse beta-amyloid deposition," *Am J Pathol*, vol. 166, pp. 1475–85, 2005.

[167] G. Patterson, S. Knobel, W. Sharif, S. Kain, and P. DW, "Use of the green fluorescent protein and its mutants in quantitative fluorescence microscopy," *Biophys J*, vol. 73, pp. 2782–2790, 1997.

[168] C. El Chartouni and M. Rehli, "Comprehensive analysis of TLR4-induced transcriptional responses in interleukin 4-primed mouse macrophages," *Immunobiol*, vol. 215, pp. 780–787, 2010.

[169] T. Hiroyama, a. Iwama, Y. Nakamura, and H. Nakauchi, "Fractalkine shares signal sequence with TARC: gene structures and expression profiles of two chemokine genes," *Genomics*, vol. 75, pp. 3–5, 2001.

[170] J. Scheller, A. Chalaris, D. Schmidt-Arras, and S. Rose-John, "The pro- and anti-inflammatroy properties of the cytokine interleukine-6," *Biochim Biophys Acta*, vol. 1813, pp. 878–888, 2011.

[171] L. M. Williams, G. Ricchetti, U. Sarma, T. Smallie, and B. M. J. Foxwell, "Interleukin-10 suppression of myeloid cell activation: a continuing puzzle," *Immunology*, vol. 113, pp. 281–292, 2004.

[172] Z. Zhou, X. Peng, R. Insolera, D. J. Fink, and M. Mata, "Interleukin-10 provides direct trophic support to neurons," *J Neurochem*, vol. 110, pp. 1617–27, 2009.

[173] S. Sharma, B. Yang, X. Xi, J. C. Grotta, J. Aronowski, and S. I. Savitz, "IL-10 directly protects cortical neurons by activating PI-3 kinase and STAT-3 pathways," *Brain research*, vol. 1373, pp. 189–94, 2011.

[174] S. Gordon and F. O. Martinez, "Alternative activation of macrophages: mechanism and functions," *Immunity*, vol. 32, pp. 593–604, 2010.

[175] L. Zhao, S. Lin, K. R. Bales, V. Gelfanova, D. Koger, C. Delong, *et al.*, "Macrophage-mediated degradation of beta-amyloid via an apolipoprotein E isoform-dependent mechanism," *J Neurosci*, vol. 29, pp. 3603–12, 2009.

[176] S. M. Son, E. S. Jung, H. J. Shin, J. Byun, and I. Mook-Jung, "Aβ-induced formation of autophagosomes is mediated by RAGE-CaMKKβ-AMPK signaling," *Neurobiol Aging*, vol. 33, 2012.

[177] F. Fang, L.-F. Lue, S. Yan, H. Xu, J. S. Luddy, D. Chen, *et al.*, "RAGE-dependent signaling in microglia contributes to neuroinflammation, Abeta accumulation, and impaired learning/memory in a mouse model of Alzheimer's disease," *The FASEB J*, vol. 24, pp. 1043–55, 2010.

[178] S. Jimenez, D. Baglietto-Vargas, C. Caballero, I. Moreno-Gonzalez, M. Torres, R. Sanchez-Varo, *et al.*, "Inflammatory response in the hippocampus of PS1M146L/APP751SL mouse model of Alzheimers' disease: age-dependent switch in the microglial phenotype from alternative to classic," *J Neuroscience*, vol. 28, pp. 11650–61, 2008.

[179] H. Okamoto, Y. Katsumata, N. K, and N. Kamatani, "Interferon-inducible protein 10/CXCL19 is increased in he cerebrospinal fluid of patients with central nervous system lupus," *Arthritis Rheum*, vol. 50, pp. 3731–32, 2004.

[180] L. M. P. le Blanc, A. W. T. van Lieshout, G. J. Adema, P. L. C. M. van Riel, M. M. Verbeek, *et al.*, "CXCL16 is elevated in the cerebrospinal fluid versus serum and in inflammatory conditions with suspected and proved central nervous system involvement," *Neurosci Lett*, vol. 397, pp. 145–148, 2006.

List of Figures

List of Tables